

**QUANTITATIVE PETROGRAPHIC INVESTIGATIONS OF PORPHYRITIC
RHYOLITIC LACCOLITHS OF THE HALLE VOLCANIC COMPLEX, GERMANY**

Von der Fakultät für Geologie, Geotechnik und Bergbau
der Technischen Universität Bergakademie Freiberg genehmigte

DISSERTATION

zur Erlangung des akademischen Grades

doctor rerum naturalium

Dr. rer. nat.

vorgelegt

von Diplom-Geologe Alexander Mock
geboren am 06.12.1973 in Hannover

Gutachter: Prof. Dr. Christoph Breitzkreuz (Freiberg)

Dr. Dougal Jerram (Durham, UK)

Prof. Dr. Volker Lorenz (Würzburg)

Tag der Verleihung: 02.07.2004

Prologue

This cumulative dissertation consists of five parts. Each part deals with different aspects of the common topic: the application of quantitative petrographic methods to elucidate the evolution of a Permocarbiniferous felsic laccolith complex – part of the Halle Volcanic Complex in Germany. Each part is, is being or will be published in the following way:

- MOCK, A., EHLING, B.-C. & BREITKREUZ, C. (submitted): Anatomy of a laccolith complex - Geometry and texture of porphyritic rhyolites in the Permocarbiniferous Halle Volcanic Complex (Germany). - *Neues Jahrbuch für Geologie und Paläontologie, Abhandlungen*.
- MOCK, A., JERRAM, D. A. & BREITKREUZ, C. (2003): Using quantitative textural analysis to understand the emplacement of shallow level rhyolitic laccoliths - a case study from the Halle volcanic complex, Germany. - *Journal of Petrology*, **44(5)**: 833-849.
- MOCK, A. & JERRAM, D. A. (submitted): Crystal size distributions in three dimensions: insights from the 3D reconstruction of a highly porphyritic rock texture. - *Earth and Planetary Science Letters*.
- BREITKREUZ, C. & MOCK, A. (in press): Are laccolith complexes characteristic of transtensional basin systems? - Examples from Permocarbiniferous Central Europe. - *In: Breitkreuz, C. & Petford, N. (eds.) Physical geology of high-level magmatic systems. London (Geological Society London) Special Publications*.
- SCHAE BEN, H., BOOGAART, G. V. D., MOCK, A. & BREITKREUZ, C. (2002): Inherited Correlation in Crystal Size Distribution - Comment. - *Geology*, **30(3)**: 282-283.

The first part introduces the subject, gives a broad overview of the research history of the Halle Volcanic Complex and shows the state of the art of concepts of laccolith formation. The main part of data is presented here giving a detailed picture of the laccolith complex, its evolution and petrologic processes important during its formation.

The second part exemplifies in a drill core section through one of the laccoliths how quantitative petrographic methods (i.e. crystal size distribution and spatial distribution pattern analyses) can be employed to investigate and elucidate complex intrusive relationships.

The third part focuses on phenocryst populations of the felsic laccoliths in more detail and shows how methodologies of three dimensional reconstruction of geological material can be combined with techniques of quantitative petrography to reveal the history of crystal populations.

The fourth part deals with the tectonic framework of laccolith complexes and aims to establish new systematics of laccoliths by comparing two temporally and spatially different settings.

The last part is a comment on an article questioning the mainly used method of this study.

Affiliations of co-authors are mentioned in parts two and five, except for Bodo-Carlo Ehling of Landesamt für Geologie und Bergwesen, Sachsen-Anhalt, Köthener Str. 34, 06118 Halle (part one). A CD containing sample images, data files, figures of each part, parts as PDF-files and animations belonging to part III is attached to this thesis.

Acknowledgements

In addition to all the people thankfully acknowledged in each of the five parts of this thesis, I would like to express my sincerest gratitude towards my parents H. and W. Mock whose material and spiritual support strongly facilitated my work. Thank you to K. Nøklestad who listened patiently to many a weary complaint. Students and staff of Institut für Geologie and Fakultät 3 of TU Bergakademie Freiberg, namely M. Beyer, but also everyone whose names would fill more than this page, are thanked for making these last years as pleasant and successful as possible. Last but not least, my supervisors C. Breitzkreuz and D. Jerram who appear as authors on the dissertation's parts deserve a special thank you for their support and fruitful discussions. Anyone left out of this list: you are not forgotten.

If you can measure that of which you speak, and can express it by a number, you know something of your subject; but if you can not measure it, your knowledge is meagre and unsatisfactory.

William Thompson (Lord Kelvin)

Part I

Anatomy of a laccolith complex – Geometry and texture of porphyritic rhyolites in the Permocarboniferous Halle Volcanic Complex (Germany)

Alexander Mock, Bodo-Carlo Ehling, Christoph Breitzkreuz

Submitted to Neues Jahrbuch für Geologie und Paläontologie – Abhandlungen

Table of contents

Abstract.....	2
Introduction	2
Laccoliths	3
Geological setting and evolution of the HVC	4
Plate tectonic framework, stratigraphy, host rocks and large scale relationships	4
Internal structure, petrographic and petrologic studies	9
Laccoliths of the HVC	12
Wettin Laccolith	12
Löbejün Laccolith.....	13
Petersberg Laccolith	14
Landsberg and Schwerz Laccoliths	14
Dimensions of the laccoliths	14
Laccolith margin geometries and textures.....	15
Flow foliation	17
Quantitative petrography and small scale textures.....	17
Drill core and outcrop sample location	18
Sample preparation.....	18
Phenocryst petrography, feldspar mineral chemistry and melt inclusions.....	25
Crystal size distribution (CSD)	28
In general.....	28
In the Halle Laccoliths.....	30
Spatial distribution pattern (SDP)	32
Model calculations for cooling, filling and crystallization.....	34
Timescale of cooling and solidification (Tab. 3).....	34
Timescale of emplacement (Tab. 6)	36
Timescale of crystallization.....	37
Discussion.....	39
Lava flow or laccolith?	39
Different crystal populations and levels of emplacement	40
Conditions of crystallization.....	40
Magma viscosities	41
Magma densities.....	42
Details of crystal populations: magma batches and marginal effects.....	42
Ascent, emplacement, crystal growth: a volatile perspective.....	45
Conclusions	47
Acknowledgements	48
References	49

Abstract

New quantitative petrographic data of felsic phenocrysts (K-feldspar, plagioclase, quartz) of voluminous rhyolitic laccoliths of the Permocarboniferous Halle Volcanic Complex in Germany are presented. A comprehensive literature review of geology and evolution of this classic area of geological research is given. Crystal size distributions and spatial distribution patterns of phenocrysts were determined and supplemented with crystal scale geochemical and melt inclusion compositional data. Phenocrysts exhibit very straight size distributions with characteristic lengths ranging from 3.4 to 36 mm advocating simple growth histories, despite complicated phenocryst shapes. Textural coarsening possibly played a role in the crystallization history, but this interpretation is not unambiguous. Phenocrysts are generally randomly distributed and do not form touching frameworks. R-values range from 1.34 to 0.78. Phenocryst crystallinities range from 10 to 30% with some rare exceptions being more crystalline. Laccoliths intruded as distinct magma batches. Furthermore, more individual laccoliths can be distinguished with the methods of quantitative petrography than have been recognised so far. Different textural varieties developed late in the magmatic history between an upper crustal magma chamber and the level of emplacement. They differed in density (~1%) and viscosity and, thus, level of emplacement. Contacts of laccoliths appear brecciated with some indication for peperitic shallow level magma/unconsolidated-wet-sediment interaction and sometimes show magma and host sediment intercalated under conditions of ductile deformation on a cm-scale. Dimensions of laccoliths fall well within the field characteristic for such intrusions on a logarithmic width vs. thickness plot forming part of an S-shaped curve proposed for power law relationship for horizontal intrusions. According to crystal size distributions, phenocryst populations formed on a timescale between 10 days and a couple of 1000 years depending on assumed growth rates. Phenocryst growth during emplacement is negligible. Simple models for filling and cooling of laccoliths suggest timescales up to one order of magnitude higher than maximum crystallization timescales, but at least several hundred years.

Introduction

This study represents a comprehensive account of a long studied geological structure – a laccolith complex in the Permocarboniferous Halle Volcanic Complex (HVC), Germany (Laspeyres 1864, 1875; Schulz 1936; Haase 1938; Veltheim 1940; Gädeke 1960). State of the art quantitative petrographic methods provide useful insight into the internal structure of the laccoliths. They are supplemented by field observations from both natural and mining

outcrops and hundreds of drill cores providing a unique detailed three dimensional image of the whole laccolith complex. Previously unpublished geochemical data on the phenocryst scale and melt inclusion analyses complement the data set presented here.

This study builds on a large amount of published literature as well as previous own work on the laccoliths of the HVC dealing with the phenocryst textures of one particular laccolith (Mock et al. 2003), the 3D arrangement and shape of phenocrysts (Mock & Jerram submitted) and the tectonic setting and its influence on laccolith complex formation (Breitkreuz & Mock in press). It also builds on the multitude of field and modelling literature available on laccoliths. Therefore, the concept of laccoliths is now introduced.

Laccoliths

Corry (1988) following Bates and Jackson (1987) defines the laccolith as “*a concordant igneous intrusion with a known or assumed flat floor and a postulated dike-like feeder commonly thought to be beneath its thickest point. It is generally plano-convex in form and roughly circular in plan, less than five miles in diameter, and from a few feet to several hundred feet in thickness.* Laccoliths commonly have much greater dimensions than those given and they may have discordant floors and margins. Laccoliths are distinguished from sills by nonlinear, inelastic, large-scale deflection of the roof. I have used the arbitrary distinction between a sill and a laccolith as a thickness ≥ 30 m. No evidence is available to support Billings (1974) classification of a laccolith versus a sill based on a diameter to thickness ratio. The term may also be used in a generic sense for forcible intrusions of any final form that have domed the country rock above or below them and created a chamber.”

Laccoliths are initiated as sills and start to lift the overburden after reaching a critical width being in turn a function of the overburden thickness. Above the distinguishing thickness of 30 m, they vary in thickness. It is not uncommon for laccolithic intrusions to breach their roof and/or form subsidiary intrusions, multi-level Christmas tree laccoliths or emergent domes (Minakami et al. 1951; Corry 1988; Lorenz & Haneke in press).

Mechanics of laccolith intrusion are relatively well established by field studies, analogue and numerical experiments (Dixon & Simpson 1987; Corry 1988; Roman Berdiel et al. 1995; Zenzri & Keer 2001). Kerr and Pollard (1998) further develop and generalize analytical solutions for the evolution of laccoliths with a variable maximum width of the initial sill. Laccolith size and shape depend on the thickness of overburden and on the volume of magma intruded. The latter also determines lift-off width (maximum width).

If intrusions emplace at deeper levels, floor depression is preferred to roof lifting (Cruden 1998). A mechanical model built upon semianalytical elastic solutions for a pressurized horizontal crack buried between an overburden and a semi-infinite base exists for this case (Zenzri & Keer 2001): "For a given geometrical ratio ($2a/h$), licit ratios of the magma pressure averaged over the intrusion area to the lithostatic pressure are given. These ratios are greater than one for small geometrical ratios and smaller than one for large ratios. For small geometrical ratios a geological realistic material contrast can introduce an asymmetry in the vertical displacements above and below the intrusion. It is shown that for small ratios ($2a/h < 0.02$) and a substrate shear modulus which is 2 times that of the overburden (...), the depressing of the intrusion's floor is more important than the doming of its roof, and thus lopolithic shapes are favoured." The term lopolith should be applied to intrusions emplaced by floor depression.

Sills as initial intrusions of laccoliths often exhibit complicated geometries. They often step up and down stratigraphy as a function of differing lithology and complicated tectonics (e.g. McPhie 1993). If complicated sills inflate to become laccoliths, the condition of flat lower contacts might only be achieved locally and the overall geometry of the laccolith is complex.

Furthermore, intrusion into host rocks subject to a confining stress regime might lead to irregularly shaped discordant laccoliths without completely flat lower contact (Morgan et al. 1998). Thus, mega and macro scale geometries are often complex, but some general rules govern the shapes of magmatic intrusions on all scales (McCaffrey & Petford 1997; Petford et al. 2000).

In contrast to well established models for the mechanics of laccolith formation, quantitative studies of internal textures of laccoliths with a combination of scales and methods on a whole laccolith complex are scarce. Thus, the geology of the HVC shall now be introduced.

Geological setting and evolution of the HVC

Plate tectonic framework, stratigraphy, host rocks and large scale relationships

Laccolith complexes are an important feature of the magmatic inventory of basins developing in the wane of the Variscan orogenesis in Central Europe. In addition to the Saale basin hosting the HVC, the Oslo rift, Norway, the Midland Valley, Scotland, the Sudetic Mountains, Poland and the Saar-Nahe basin, Western Germany are regions within the orogen and its northern foreland with a similar history dominated by shallow, subvolcanic, intrusive

complexes (Sundvoll et al. 1990; Neumann et al. 1992; Stollhofen & Stanistreet 1994; Upton 1994; Awdankiewicz 1998; Stollhofen 1998).

The Saale Basin is a late Palaeozoic transtensional volcano-sedimentary basin in the area of the decaying Variscan orogen (Eigenfeld & Schwab 1974; Lorenz & Nicholls 1984). It formed on the Mid-German Crystalline Rise (Fig. 1) a structural unit of the orogen between the Saxothuringian and Rhenohercynian zones (Romer et al. 2001). Central Europe was subject to a dextral strike slip tectonic regime 20 Ma after culmination of the Variscan orogenesis (for more comprehensive reviews see Arthaud & Matte 1977; Henk 1997; Oncken 1997; Tait et al. 1997; Anthes & Reischmann 2001). This tectonic regime strongly influenced the development of laccolith complexes from magma genesis to final emplacement (Breitkreuz & Mock in press).

In the beginning of HVC evolution, magmatic activity consisted of trachybasaltic to trachyandesitic lavas and pyroclastics with minor intrusive activity (Haase 1943; Kampe et al. 1965; Siegert 1967b; Romer et al. 2001). One rhyolitic laccolith (Schwerz) intruded relatively early (307 ± 3 ma, 1σ error), followed around 5-10 Ma later by the main intrusive phase ($301-294 \pm 3$ Ma, 1σ error, ages after Breitkreuz & Kennedy 1999). Other SiO₂-rich porphyritic units, such as the Wieskau rhyolite (Fig. 2) considered to have formed early in the evolution of the HVC (Kunert 1995), whose intrusive vs. extrusive nature and, thus, stratigraphic position are not established.

The laccolith units have been mapped traditionally according to outcrop and drill core data as the Wettin, Löbejün, Petersberg, Landsberg and Schwerz units (Fig. 1). Wettin and Petersberg units consist of small crystal rhyolite; Löbejün and Landsberg units of large crystal rhyolite; the Schwerz laccolith is a smaller and more complex composite unit with a number of phases with differing phenocryst sizes – large, medium and small crystal – and groundmass colours (brown or black). The Schwerz laccolith has been intruded by younger rhyolite magma from the Landsberg laccolith (Löffler 1979; Löffler & Seydewitz 1983).

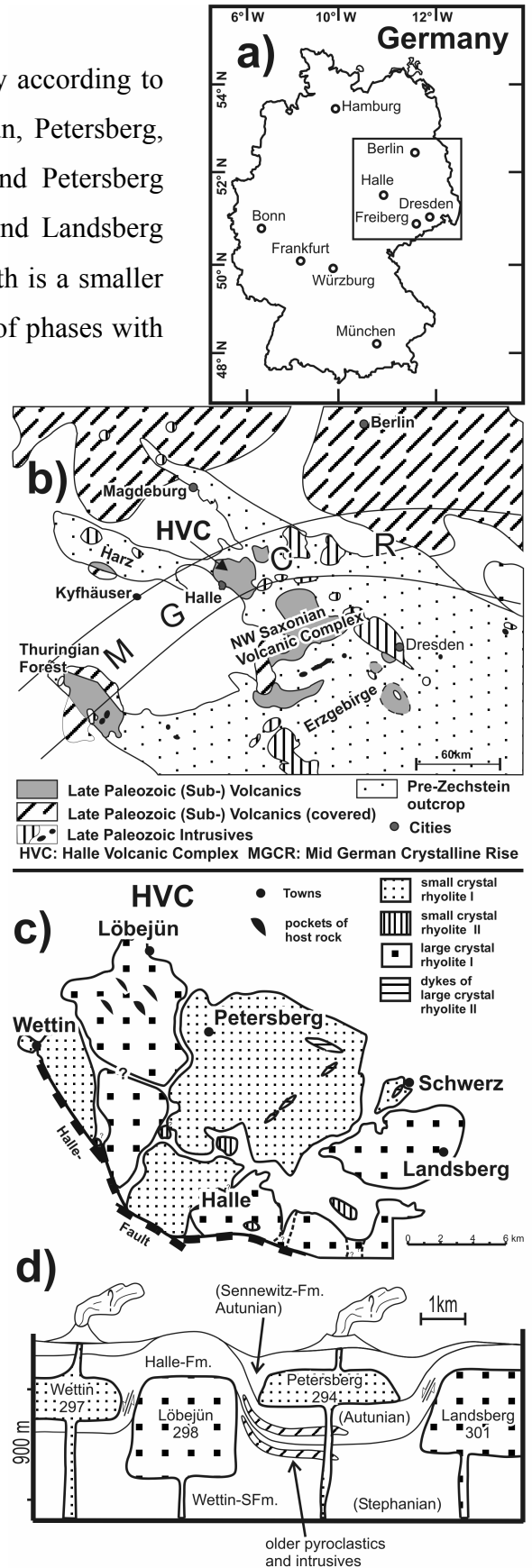


Fig. 1. a) Study area in Germany; b) Halle Volcanic Complex (HVC) and its geological context; c) subcrop pattern of HVC laccoliths and other relevant features; d) hypothetical E-W cross section through the HVC during time of laccolith emplacement with name and ages of laccoliths and formation names of host rocks (Breitkreuz & Kennedy, 1999).

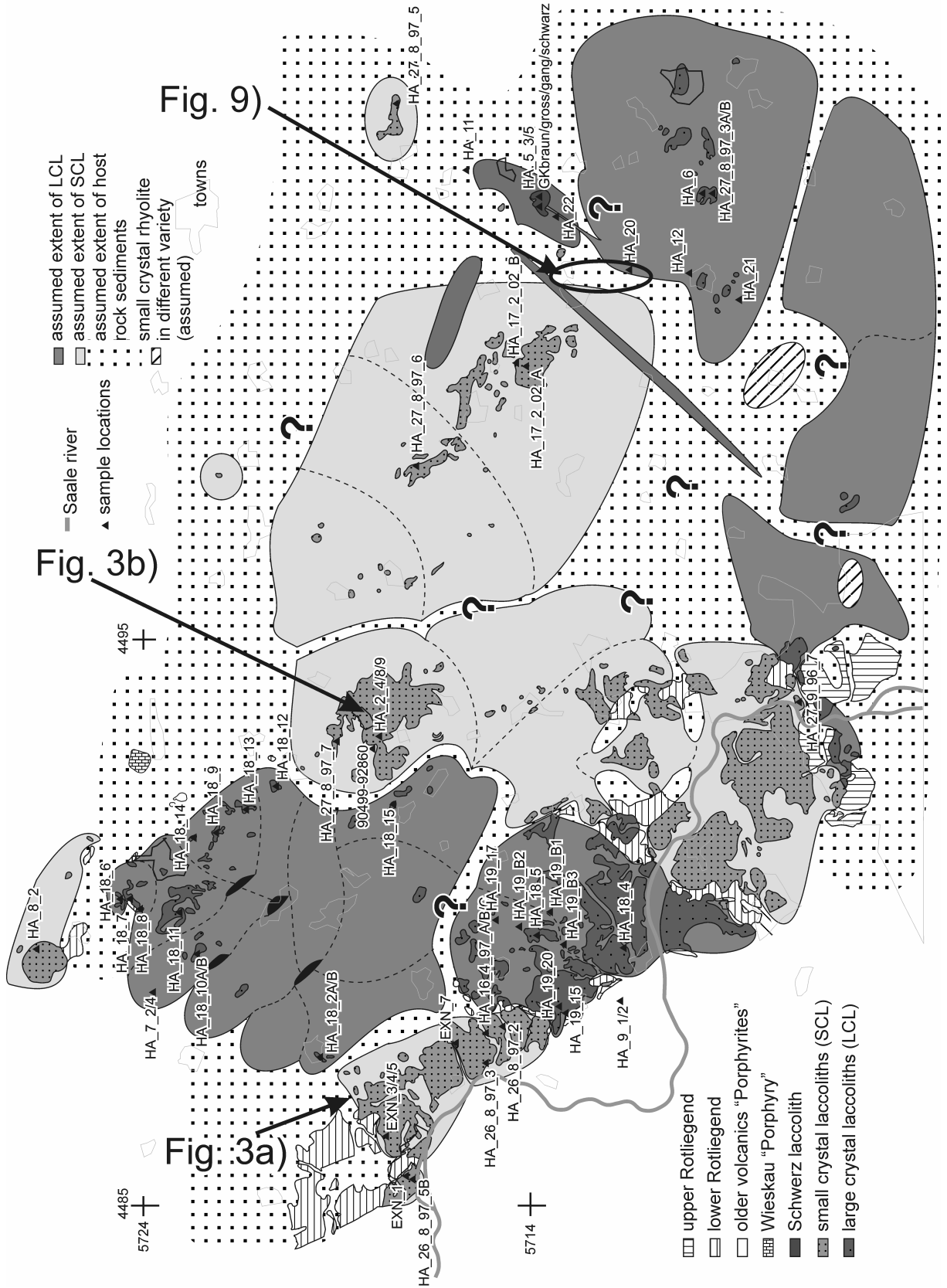


Fig. 2. Outcrop pattern and sample localities in the Halle Laccolith Complex.

Local and regional stratigraphy (Schneider et al. 1994; Kunert 1995; Knoth et al. 1998) and volcano-tectonic relationships (Schwab 1965, 1977) have been worked on. The eruptive equivalents of the laccoliths consist of tuffs with a varying degree of welding, lapilli tuffs, base surge and pyroclastic flow deposits. Rhyolitic compositions dominate, but, subordinately, more silicic or rhyodacitic to trachytic/trachydacitic rocks, respectively, can be found. Altered volcanic glass and perlitic structures occur frequently. Alteration to clay minerals is very common (Büchner & Kunert 1997).

The laccoliths are exposed today in numerous outcrops and have been intersected by a large number of drillings during coal and uranium exploration in the second half of the 20th century. In the late 19th century, a deep research drill hole was sunk in the area N of the city of Halle (Beyschlag & Fritsch 1899) intersecting large and small crystal rhyolites. These were then erroneously considered to be both lavas and, thus, stratigraphic relationships were wrongly established. More recently, the laccoliths were shown to be roughly contemporaneous by U/Pb-SHRIMP dating on zircons (Breitkreuz & Kennedy 1999 and above). After much debate (see references above), the intrusive character of the main units of porphyritic rhyolite of the HVC has been shown by the large thicknesses, the occurrence of sedimentary host rocks tilted during laccolith emplacement (Kampe et al. 1965; Breitkreuz & Mock in press), the architecture of the internal flow structures (Mock et al. 1999) and evidence from top contacts of both varieties (Klaus 1964). These aspects will also be discussed further in this contribution. In addition to laccoliths, rhyolitic porphyritic lavas have been observed in drill cores. They are less thick than the laccoliths and exhibit distinct carapace facies and top breccias (Plögert et al. 2001; Geißler 2002).

Sedimentary host rocks of the laccoliths (Fig. 2) consist of grey silt- and mudstones with several fine sandstone beds and coal seams (Mansfeld Subgroup, Wettin Sfm., German-Stratigraphic-Commission 2002) and a fluvio-limnic succession of reddish grey conglomerates, siltstones, clays and sandstones with abundant volcanoclastics (Halle Fm., German-Stratigraphic-Commission 2002) of lower Rotliegend age. Younger deposits have been lithostratigraphically interpreted and organized on the formation level into Sennewitz-, Hornburg-, Brachwitz- (not officially a formation), and Eisleben-Fm. comprising coarse grained debris from the (sub-)volcanics of the HVC as well as from other settings and equivalent fine grained deposits (Kunert 1995; German-Stratigraphic-Commission 2002). The stratigraphic relations in this highly complex continental setting are far from being completely understood (Schneider et al. 1994; Schneider 1996; Schneider et al. 1998).

The laccoliths were exhumed shortly after emplacement and deposited their own debris apron as alluvial fan and fluvial deposits intercalated with deposits of late volcanic activity. Aphanitic SiO₂-rich lavas and phreatomagmatic deposits overlying these erosional products indicate a continuation of volcanism after emplacement and partial exhumation of the laccoliths (Rüffer et al. 1998). In Jurassic times (~200 Ma), a thermal event (~250-280°C) of unknown origin overprinted the rocks in the Halle area weakly and led to authigenic growth of clay minerals (Brecht 1999; Jacobs & Breitskreuz 2003). Hydrothermal alteration coupled with advective heating related to block faulting and inversion of the European plate during the early stages of the Alpine orogenesis (~100 Ma) is revealed by apatite fission track analyses (Jacobs & Breitskreuz 2003). So, final cooling to below 100°C did not take place before late Early Cretaceous time. During Mesozoic and Tertiary times the area was subject to intensive tropical weathering, leading to formation of minor kaolin deposits in the rhyolites (Störr 1983). During the Pleistocene, the Halle area was either covered by ice or affected by periglacial processes (Knoth et al. 1998).

Internal structure, petrographic and petrologic studies

The laccoliths comprise around 210 km³ of rhyolitic magma (Breitskreuz & Mock in press). Phenocryst phases are quartz, K-feldspar, plagioclase and subordinately biotite and an Fe-oxide phase. Accessories are apatite, zircon and Fe-oxides. The rhyolite appears in two readily distinguishable size varieties, large and small feldspar phenocrysts, 21 mm and 11 mm in size on average, respectively (Schwab 1965; Kunert 1978; Breitskreuz & Kennedy 1999; Mock et al. 2003). Further subordinate varieties have been recognised according to colour and grain size of groundmass and state of alteration (Koch 1967b, 1979; Löffler 1979, 1983). Mainly, different groundmass colours stem from varying abundances of magnetite and hematite (unpublished magnetic data, Nowaczyk (GFZ-Potsdam), written comm.).

Some contact alteration has been described from the Petersberg laccolith. It is mainly propylitization and a change in colour to green, grey and black (Koch 1967a). Upper contacts of both the small and large crystal laccoliths have been found in drill cores and exploratory excavations in the southern part of the Löbejün laccolith (Fig. 2). They consist of mylonized and sheared rhyolite and host rock sediment. The rhyolite is strongly hydrothermally altered and propylitized at the contact on a decametre scale. Small (~5 cm) apophyses into the host rock are common. These observations favour an intrusive character of both varieties of rhyolite (Klaus 1964). Detailed studies of alteration of a rhyolite occurrence north of Löbejün and Petersberg (Fig. 2) are also available (Kelch 1963). Petrographic investigations of

minerals in the rhyolites estimated the P/T conditions of beginning magmatic crystallization at $>500^{\circ}\text{C}$ and $>10^9$ Pa (Löffler 1986). Contact metamorphic alteration of the host rock is manifested in coalification of coal measures in the area (Schwab 1962). Some host rock alteration is also described in conjunction with alteration of the rhyolite itself (Koch 1967a). Weak contact metamorphism has been mentioned especially from the large crystal rhyolite of Löbejün within the city limits of Halle. Many of the contacts might be faults either relating to intrusion of the rhyolite or of a later tectonic nature (Schulz 1936).

Flow structures have been measured before in the Petersberg laccolith, but misinterpretation, ambiguous representation as directional data on maps and dubious magnetic measurements led to erroneous reconstruction of rhyolitic flood lava (Koch 1966). Thin to absent contact aureoles and chilled margins advocate very shallow emplacement of the laccoliths. Perlitic cracks and abundant spherulites have been found in the groundmass of the small crystal Petersberg and Wettin laccoliths giving additional evidence for shallow emplacement of the bodies (Klaus 1964; Löffler 1979, 1983). Flow structures (Fig. 3) and carapace facies (Fig. 4) also indicate the level of erosion and roughly constrain a position within the intrusion (Klaus 1964).

Xenoliths of sedimentary and volcanic rocks are abundant especially in small crystal rhyolites, metamorphic – mainly amphibolite facies – and plutonic rocks occur less frequently (Steiner 1960). An example of a granite xenolith is given by Hafermalz et al. (1980). A gneiss xenolith from the Löbejün rhyolite has been described by Koch and Fischer (1961) who also summarize findings of xenoliths in intrusive and volcanic rocks of the HVC. Large xenoliths (several metres) within large crystal rhyolite in Halle might be roof and wall rock pendants. They consist of metamorphosed sedimentary rock (Koch 1981).

Geochemical results indicate the origin of the calc-alkaline slightly peraluminous low-Si rhyolites from late orogenic crustal anatexites with a subduction fingerprint (Siegert 1967a, b; Röllig & Schirmer 1978; Romer et al. 2001). Microprobe analyses of feldspar phenocrysts presented in this study reveal a degree of crystal scale chemical inhomogeneity in the Ba content. Apart from that, geochemistry could neither reveal internal structures of the laccoliths nor details of phenocryst populations' crystallization histories.

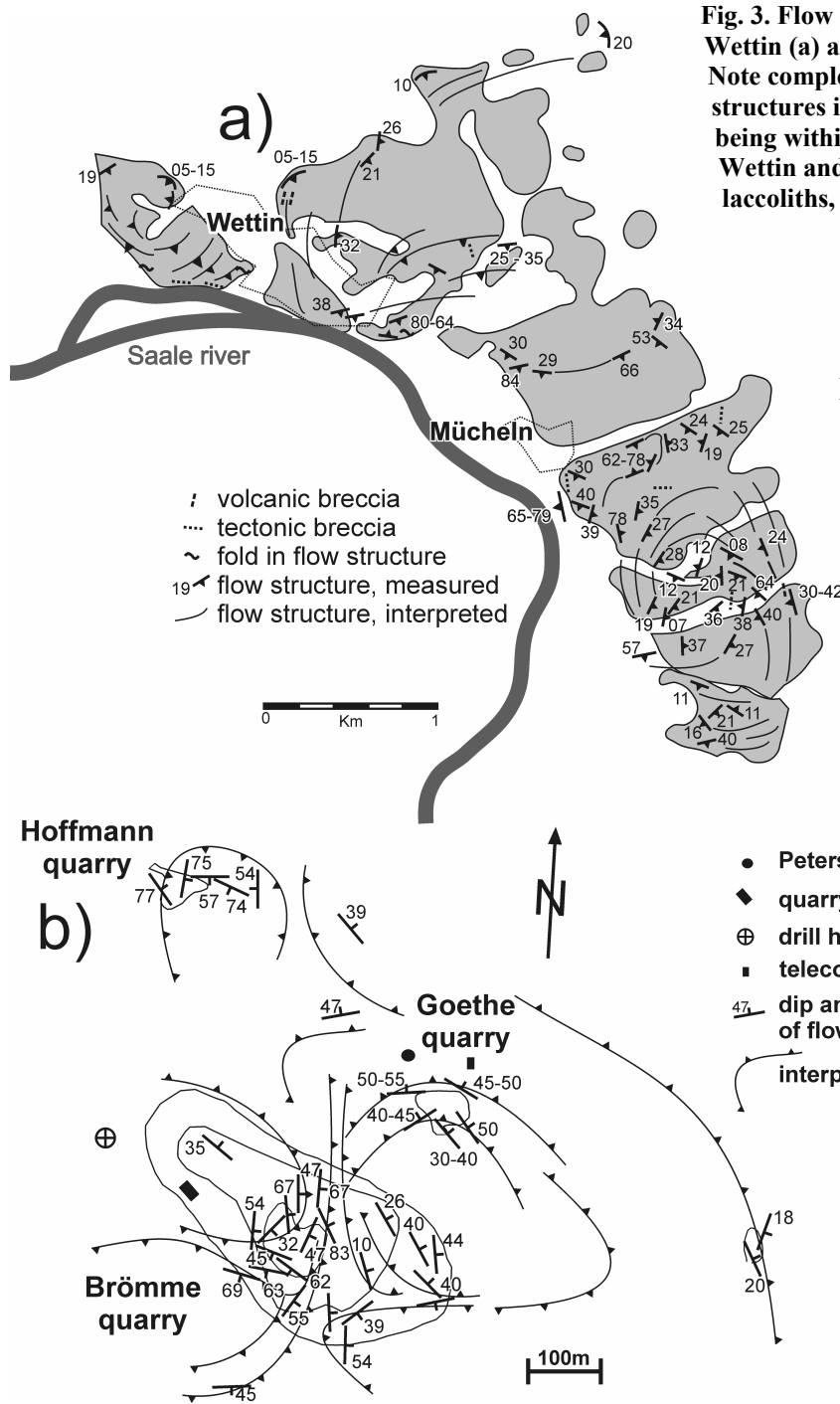


Fig. 3. Flow structures in the small crystal Wettin (a) and Petersberg (b) laccoliths. Note complex bowl and cupola shaped structures indicating the erosional level being within lower (S Wettin) or upper (N Wettin and Petersberg) regions of the laccoliths, respectively.

In order to tackle the striking apparent homogeneity of the laccoliths and understand their evolution, crystal size distributions (CSD) and spatial distribution patterns (SDP) of the phenocrysts quartz,

plagioclase and K-feldspar were determined from image analysis data of 120 samples of the HVC laccoliths. Detailed quantitative textural analysis can greatly aid the

understanding of igneous rocks. This study increases the pool of available quantitative textural data towards coarse crystal populations. Additional emphasis is put on the contact zones of the laccoliths mainly in drill cores. Melt inclusion data indicate high volatile contents early in the crystallization history and complement the intrusive models of the laccoliths.

In the following sections, the laccoliths of the HVC shall be introduced with a subcrop map followed by qualitative observations on a macro-, outcrop, sample and thin section scale. Presentation of quantitative petrographic data makes up the bulk of the results. The presentation of data is completed with model calculations for crystallization, filling and cooling of the laccoliths.

Laccoliths of the HVC

The map (Fig. 2) was inspired by Schwab (1965), newly available drill cores, arrangement of host rocks, quantitative petrographic data and comparison with other laccolith complexes. Data from hundreds of shallow level drillings carried out for construction purpose and quarry exploration have been worked into the subcrop map. Each traditional unit of the HVC shall now be treated separately.

Wettin Laccolith

The westernmost small crystal Wettin laccolith is comprised of three distinct units: the small Schweitzerling in the NW corner (EXN-1), the northern and the southern part of the main Wettin unit (boundary approx. at EXN-7). The shape of the flow structures (Fig. 3) strongly suggests such a configuration: cupola shaped structures suggest a roof region of a small laccolithic body in the Schweitzerling area (Nickel et al. 1967; Fink & Anderson 2000). The boundary zone between the northern and southern parts exhibits more irregularly shaped flow foliation than the interior of each part. Furthermore, breccias and breccia filled cracks appear in this area. In the northern part, flow foliation is centred around a feeder or roof region of an intrusion; in the southern part, flow foliations suggest a feeder region (Fig. 3). The boundaries of the parts of the Wettin laccolith are not as thoroughly substantiated by quantitative petrographic data (see section on quantitative petrography below) as the other HVC laccoliths', because drill core samples do not exist as abundantly.

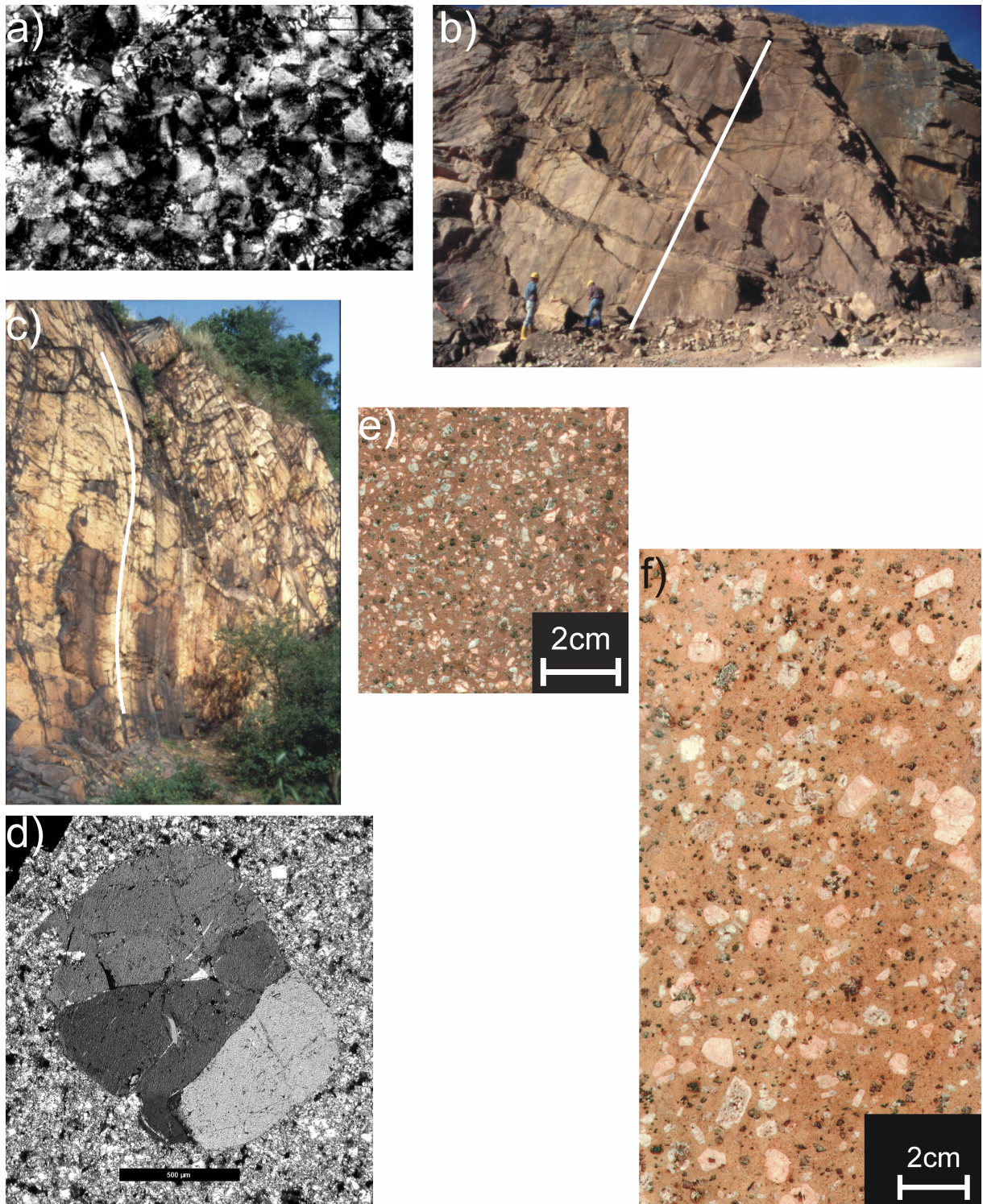


Fig. 4. a) Spherulites in the groundmass point out carapace facies (Petersberg laccolith near the Petersberg summit, see Fig. 2 and 3b). b, c) Outcrop photos of flow structures in the Petersberg laccolith (quarries Brömme and Hoffmann, Fig. 3b). d) Broken, rotated and annealed quartz phenocrysts from the Petersberg laccolith. e, f) Example textures of a small crystal (Petersberg laccolith) and large crystal rhyolite (Löbejün laccolith).

Löbejün Laccolith

This laccolith has been divided into two units – a northern and a southern one – as suggested by geophysical (Lange 2000) and quantitative petrographic (see below) investigations. In the northern part, occurrence of pockets of host rock trapped between large crystal rhyolite

suggests a pattern of magma batches in analogy to similar cryptodome/laccolith intrusions in the Saar-Nahe basin (Haneke 1987; Breitzkreuz & Mock in press). Therefore, boundaries between such batches have been sketched in and the NW margin of the laccolith has been shaped according to this model (Fig. 2). This will be further elaborated below.

The western margin of the Wettin and the SW margin of the Löbejün laccolith as well as the lower Rotliegend sediments in the NW of the Wettin laccolith are cut off by the Halle fault (Schwab 1965; Knoth et al. 1998). Therefore, the true extent of the laccoliths might be larger than shown in the map.

Petersberg Laccolith

Batch-wise intrusion has been recognised for this laccolith using quantitative petrography (Mock et al. 2003). Batch boundaries are postulated in analogy to the Löbejün laccolith. They are substantiated by quantitative petrography (see below), by outcrop pattern and geophysical evidence (Lange 2000). The complex architecture of flow foliation structures measured around the Petersberg itself (Fig. 3) also provides evidence in favour of this scenario.

Landsberg and Schwerz Laccoliths

The Landsberg laccolith compensates a lack of surface outcrop with larger abundance and availability of drill core samples. The intrusive mechanism is similar to the other laccoliths (see Quantitative Petrography below), but the divisions on the map are more speculative due to poor outcrop conditions and occurrence of different varieties of rhyolite in the area of Landsberg. Magma belonging to the Landsberg rhyolites dyked into the older Schwerz laccolith and the eastern part of the Petersberg laccolith (Fig. 2).

The Schwerz laccolith has long been recognized as a complex, composite intrusion (Schulz 1936; Löffler 1979; Krauß 1999). The relations of different rock types are too detailed for the scale of this map. They have been examined in an active quarry in the area (Krauß 1999).

Dimensions of the laccoliths

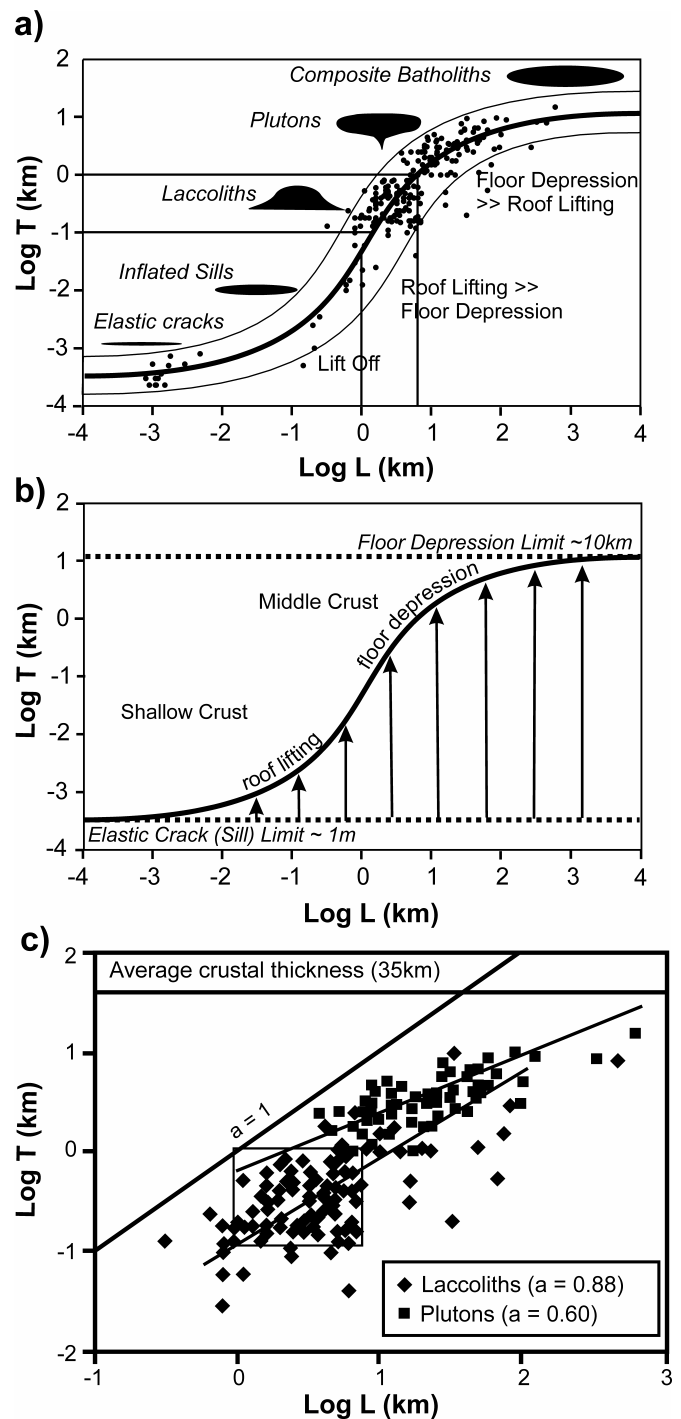
Intrusions seem to obey power law relationships on a large variety of scales (micro-cracks and large batholiths Cruden & McCaffrey 2002; McCaffrey & Cruden 2002). Dimensional data of the Halle laccoliths falls well within the limits of the S-shaped curve in a logarithmic diagram of intrusion width vs. thickness (Fig. 5). Thicknesses of the laccoliths were estimated from drillings (Löbejün laccolith >700 m, Petersberg ~500 m, Landsberg >500 m, Wettin ~300 m). These thicknesses are also used for the model calculations below. The smaller units proposed

in this study allow a horizontal dimension between about 1 and 10 km. Large units imply a deep level of intrusion (Corry 1988; Cruden 1998). Since the laccoliths have been demonstrated to have intruded at a very shallow level (see above), the extent of individual laccoliths must not be too large in order to fit the power law model (Fig. 5).

Fig. 5. a) Compilation of tabular intrusion thickness, T , and width, L , data. Solid curve and shaded area indicate a visually fitted S-curve to the data, and its limits, respectively. Representative intrusion styles are shown adjacent to the relevant parts of the data. Limits for Halle laccoliths are shown in vertical and horizontal lines. Data points from Cruden and McCaffrey (2002). b) Proposed interpretation of the S-curve, in terms of lower and upper growth limits, dominant emplacement mechanism and depth. Arrows indicate vertical growth trajectories along a possible, end-member growth curve with a slope $a = \text{infinity}$. c) Detail of the data set for laccoliths and plutons with average crustal thickness shown as limit for intrusions. Power law curves for laccoliths and plutons are indicated from Petford et al. (2000). Box indicates limits for the Halle laccoliths.

Laccolith margin geometries and textures

Contacts of the intrusions are generally very sharp. Breccias at several locations on up to a m-scale indicate brittle deformation during emplacement (Fig. 6). Especially in drill cores WisBaw 1452/80 (Fig. 7) and Brachwitz 2/62 (Fig. 8), clasts within the breccias exhibit a jigsaw fit texture. They might be interpreted as peperitic margins or more generally as autobreccias of the intruding rhyolite incorporating unconsolidated volcanogenic host rock sediment. In Brachwitz 2/62, the breccias are assumed to form an envelope around the finger-like apophysae of the Wettin laccolith (Fig. 8). The coherent rhyolite appears in carapace



facies with spherulitic groundmass and perlitic cracks (Fig. 8). A possible finger-like intrusive mechanism is also proposed for the Landsberg laccolith in the eastern part of the HVC (Fig. 9). Similar intrusive mechanisms have been shown for laccolith complexes (Dockstader et al. 1973; Corry 1988; Manickam & Homsy 1994). The concept of finger or batch-wise intrusion will be further elaborated below (see Discussion). Few drilled upper contacts in the Landsberg and Löbejün laccoliths indicate a degree of ductile shearing in the magma on a cm-scale (Fig. 6). But coherent rhyolite prevails beyond the very thin contact zones. Quantitative petrographic properties of the textures do not change significantly towards contacts (see below), but statistically valid investigations regarding size and spatial distributions of phenocrysts on the scale of the thin contact zones are not possible. However, an interesting trend in the textures can be observed in scaling analysis of CSD data (see section on quantitative petrography).

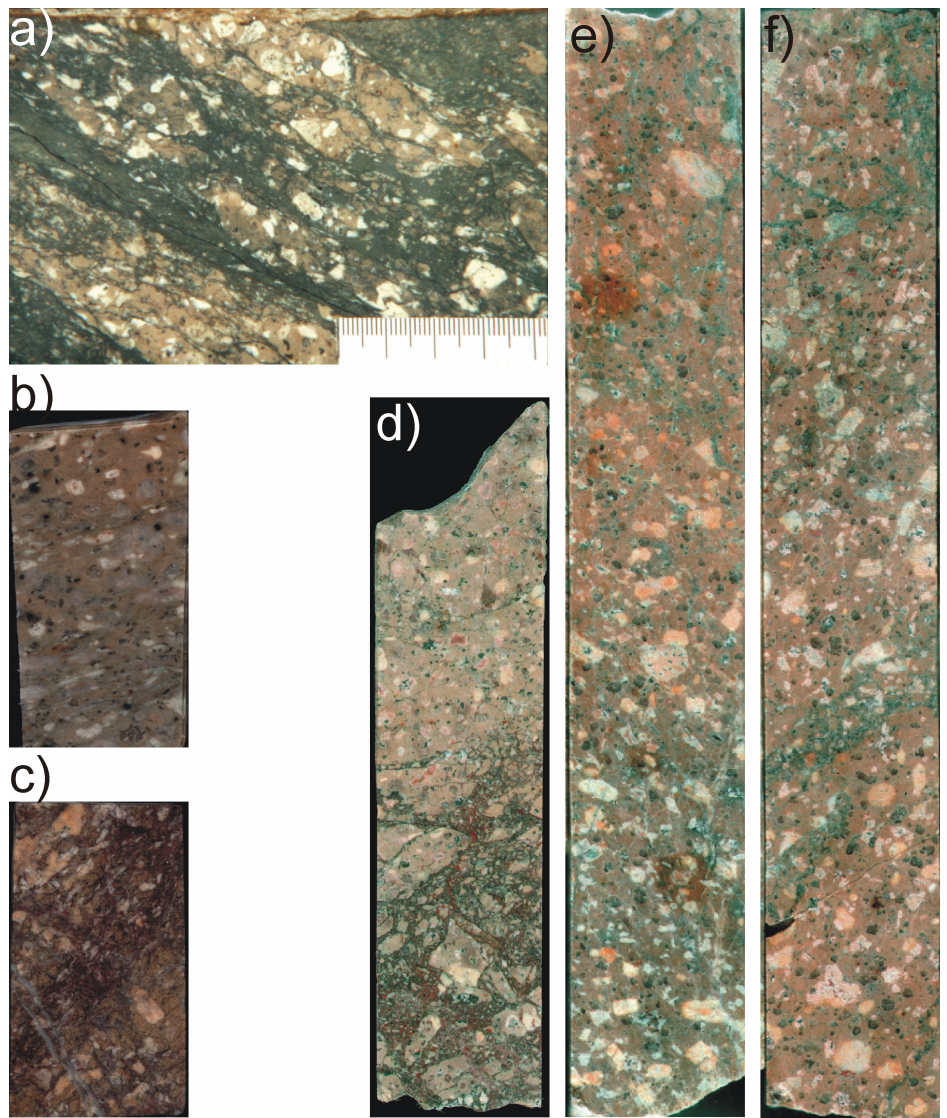


Fig. 6. Samples of contact zones of the laccoliths. a) Sheared contact of Löbejün laccolith. b) Sheared contact from Landsberg laccolith (drill core WisBaw 1391/80). c) Brecciated contact from Landsberg laccolith (drill core WisBaw 1391/80). d) Jigsaw-fit breccia from Landsberg laccolith (drill core WisBaw 1452/80). e, f) Slightly brecciated rhyolite samples from Landsberg laccolith (drill core WisBaw 1452/80).

Flow foliation

Flow foliation develops by differential movement of phenocrysts and silicate liquid during magmatic flow. Phenocrysts only rotate readily at low crystal contents. High crystallinities cause crystals to interact with each other, thus preventing rotation and record of strain in the flowing magma (Smith 2002). Irregular crystal abundance domains are relatively common in basalt and it is not yet clear whether these textures form by clustering of crystals during flow, disruption of texture during flow or disruption of texture during degassing. In one example from basalts in the Lamington Volcanics of Australia, irregular domains have been modified by shearing on crystal-poor domains between crystal-rich clusters (Smith 1998). In another example, phenocrysts in radial dykes of a Miocene volcano at Lyttelton, New Zealand, exhibit an oblique pattern in relation to flow direction. Lineations and foliations, thus formed, are complex and do not indicate flow direction simply by preferred orientations (Shelley 1985). In Shelley's example from New Zealand, secondary shears crenulate layers of feldspar laths, while feldspars continue to grow after flow has ceased. These examples show the importance of rotation and aggregation of crystals for the recognition of flow foliation structures. Even in highly viscous rhyolitic magmas, the redistribution of crystals during magmatic flow is an important mechanism for the evolution of rock textures (Mock et al. 2003).

Flow foliation and flow structures are recognised in the small crystal rhyolites by aligned vesicles, zones of increased phenocryst abundance and preferred orientations and a preferred cleavage along these zones (Schwab 1970; Breitzkreuz et al. 1998). Tectonic joints and cleavage often superimpose flow foliation. The large crystal rhyolites do not exhibit such flow structures and essentially no vesicles. Vesiculation in the small crystal rhyolite is not pervasive. It is probably due to late stage degassing of an already slightly degassed magma (see Discussion).

Good outcrop conditions around the Petersberg (Fig. 2) allow detailed measurement of a complex bowl and cupola shaped flow foliation (Fig. 3). The Wettin laccolith also exhibits complex flow structures indicating possible feeder channels (Fig. 3). In comparison to flow structures found in rhyolitic lavas and intrusions elsewhere (Nickel et al. 1967; Fink 1987; Smith 2002), these observations strongly indicate an intrusive origin of the Halle rhyolites.

Quantitative petrography and small scale textures

To link rock textures to processes of rock formation both have to be quantified. Textures can be quantified with methods of image analysis on images of thin sections or rock slabs. The most basic datum is abundance of a phase for bulk rock samples on one hand side and size of

individual particles (area, long and short axes) on the other. Particle size has been used so far in crystal size distribution (CSD) analysis for a variety of igneous rocks with a focus on microlite populations in mafic rocks (e.g. Cashman & Marsh 1988; Hammer et al. 1999; Castro et al. 2003). Additional relevant information on the evolution of rocks comes from analysis of spatial arrangement of grains (spatial distribution pattern, SDP, Jerram et al. 1996; Jerram et al. 2003). The orientation of grains, the shapes (aspect ratios), the curvature of the outlines etc. can also be analysed quantitatively from data obtained by image analysis. In this section, methods and data of detailed petrographic investigations of the HVC laccoliths (modal abundances, CSDs, SDPs and orientation of the phenocrysts) are presented.

Drill core and outcrop sample location

Because of exceptional stratigraphic control and availability of samples, all laccoliths were sampled in detail with a representative number of outcrop samples (Fig. 2, Tab. 1). Eight drill cores were sampled in varying detail for quantitative petrographic analysis (Tab. 1). The rhyolite in drill core WisBaw 1452/80 is often highly brecciated and has probably been sunk near the margin of the Landsberg laccolith (Fig. 7). In drill cores WisBaw 1391/80, 1392/80 and 1408/80, brecciation is not as pervasive as in 1452. The Wettin laccolith in drill core Brachwitz 2/62 (Kunert 1995) displays a similar intrusive pattern as the Landsberg laccolith (see above). Two samples of large crystal rhyolite were retrieved from the lower part of this core. The Schlettau drill cores 2 and 5 only yielded three samples for quantitative petrography (samples HA-7 and HA-8, Tab. 1). Drill core Petersberg 9/60 (Kampe & Remy 1960), samples 90499 to 92860 (Fig. 2), has been intensively studied and its textural properties interpreted by Mock et al. (2003). Drill cores are available at the core depository of the geological survey of Sachsen-Anhalt, Köthener Str. 34, 06118 Halle, Germany.

Sample preparation

The rhyolite is often strongly affected by alteration, namely chloritization and partly albitization and hematization. Quartz crystals are unaltered and appear black, greyish or clear depending on the remaining portion of crystal left after cutting and their background matrix. They are often broken, the fragments show varying extinction angles and have, thus, been slightly rotated and annealed (Fig. 4). K-feldspar crystals retain a pinkish-red colour with abundant clear parts. Plagioclase crystals appear greenish grey with abundant black inclusions. Twinning is abundant among feldspars, zoning is not.

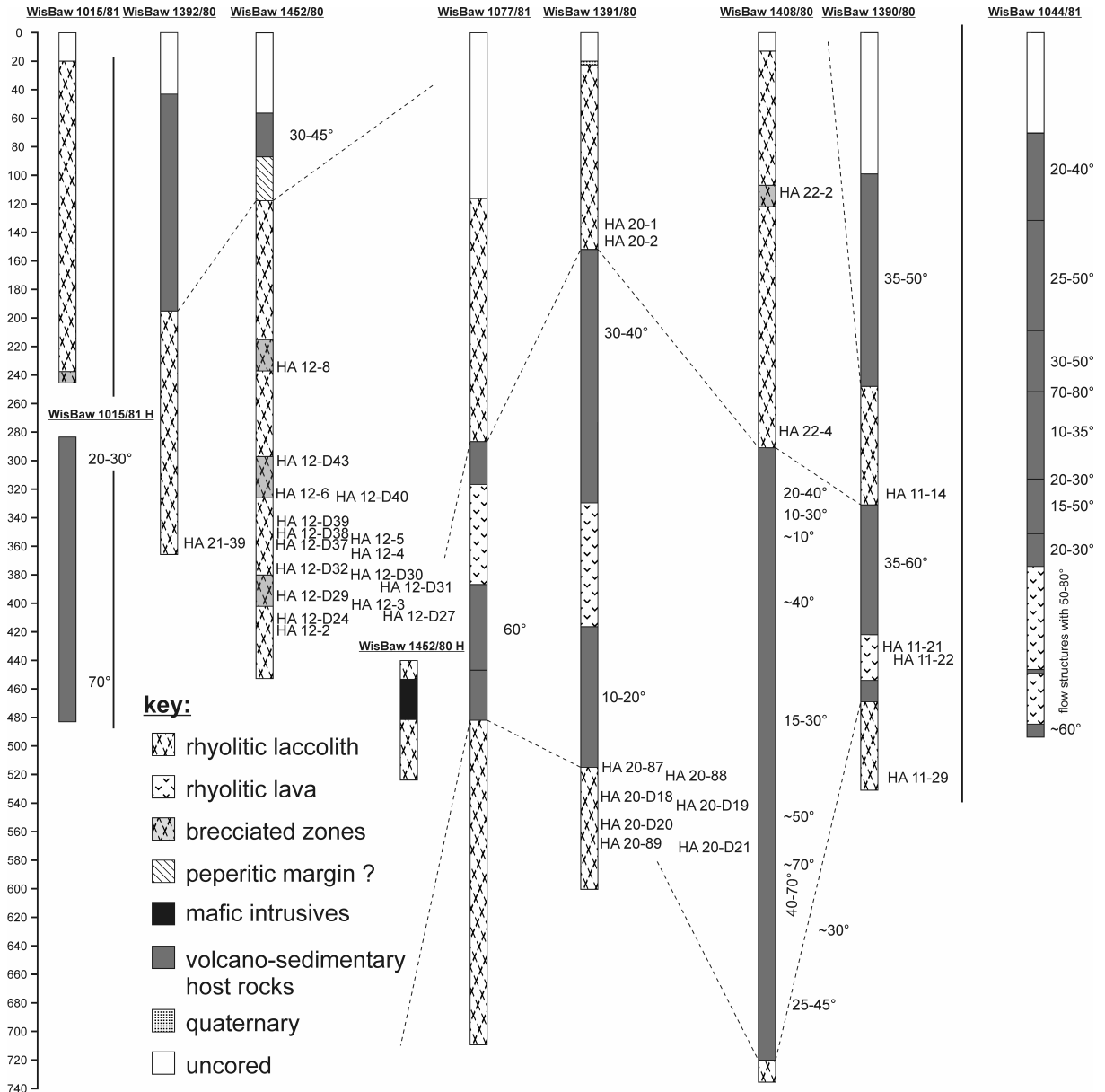


Fig. 7. Logs of drill cores WisBaw 1015/81, 1077/81, 1044/81, 1390/80 (HA-11), 1391/80 (HA-20), 1408/80 (HA-22), 1452/80 (HA-12) showing sample positions and lithologies present. Dip angles of host rocks measured in drill cores and possible correlations are indicated. Cores in the centre are located along a line (see Fig. 2, Tab. 1). Depth scale in m.

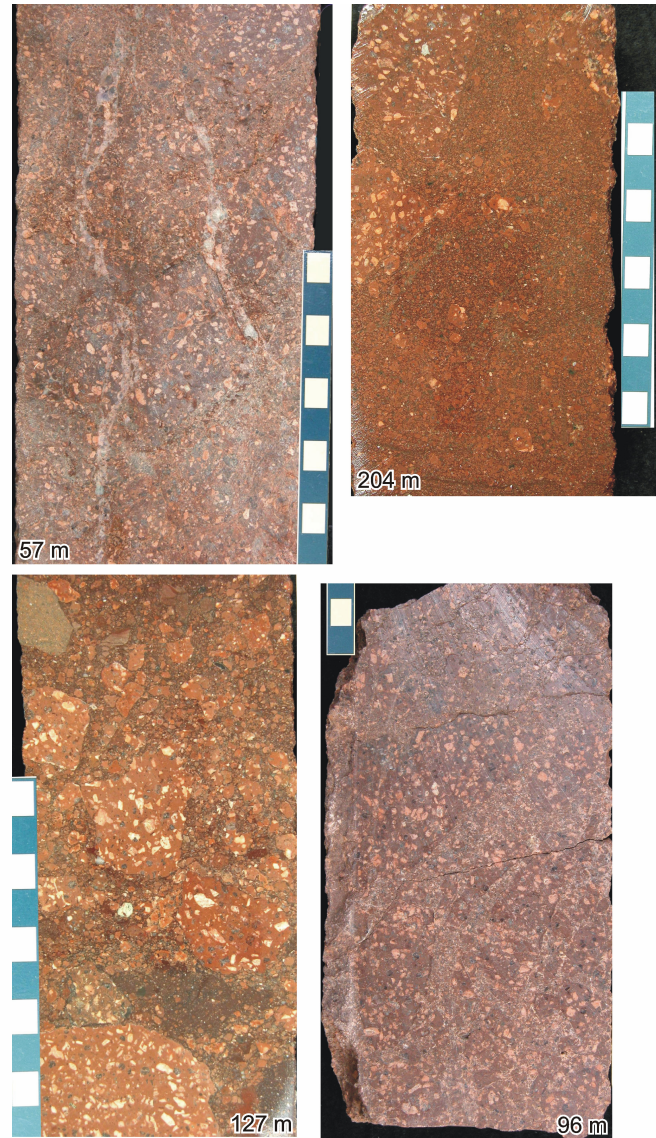
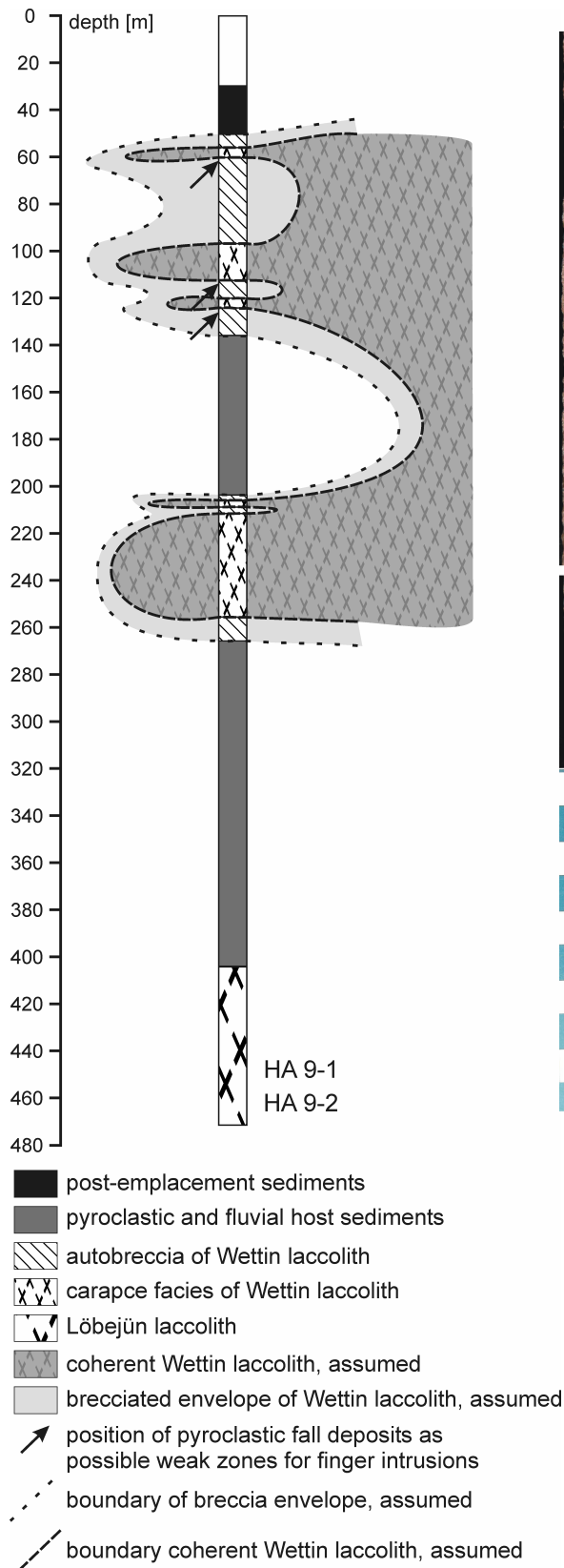


Fig. 8. Simplified log of drill core Brachwitz 2/62. Small crystal Wettin rhyolite and large crystal Löbejün rhyolite are present. Outline of Wettin rhyolite is indicated as interpreted from distribution of peperitic (?) or brecciated marginal facies of some finger-like apophysae from the main laccolith. Sample textures show varying degrees of disintegration of Wettin rhyolite from different depths. Scale bars with 1 cm squares

Tab. 1. All samples used in this study. DAT: data acquisition technique; T: phenocrysts were drawn on transparencies, then scanned and analysed automatically; 2: digital images of sample slabs were manually classified in the computer, then analysed automatically; CCM: digital images of sample slabs were manually classified and analysed in the computer in one go; DC: drill core sample; NOP: number of phenocrysts (K-feldspar|plagioclase|quartz); CL: characteristic length (K-feldspar|plagioclase|quartz)

No.	Sample name	Sample location	DAT	Rem.	NOP			CL			Kf %	Pl %	Qz %	GM %
1	HA-11-14	WisBaw1390/80	T	DC	127	44	148	2.040	1.280	0.591	10.762	2.121	5.065	82.051
2	HA-11-21	WisBaw1390/80	T	DC	160	86	173	2.310	1.452	0.513	11.670	3.521	4.697	80.112
3	HA-11-22	WisBaw1390/80	T	DC	87	54	107	1.675	1.084	0.627	6.344	1.521	3.596	88.539
4	HA-11-29	WisBaw1390/80	T	DC	130	97	95	1.743	1.745	0.603	10.623	7.114	4.101	78.162
5	HA-12-8	WisBaw1452/80	CCM	DC	79	339	214	2.904	1.606	0.972	9.474	11.131	6.934	72.461
6	HA-12-D43	WisBaw1452/80	CCM	DC	197	434	384	1.524	1.731	1.484	11.200	9.144	8.222	71.433
7	HA-12-D40	WisBaw1452/80	CCM	DC	118	384	363	1.740	1.345	1.134	10.047	10.322	8.369	71.262
8	HA-12-6	WisBaw1452/80	CCM	DC	112	599	487	1.696	1.237	0.849	9.694	11.798	8.625	69.883
9	HA-12-D39	WisBaw1452/80	CCM	DC	141	881	664	2.888	1.093	0.721	5.310	7.923	6.202	80.565
10	HA-12-D38-A	WisBaw1452/80	CCM	DC	162	350	297	1.100	1.379	0.820	11.764	10.877	6.942	70.418
11	HA-12-D38-B	WisBaw1452/80	CCM	DC	138	350	364	2.432	1.394	0.797	9.567	6.071	7.429	76.933
12	HA-12-5	WisBaw1452/80	CCM	DC	253	630	504	1.656	0.891	0.691	8.907	7.735	5.578	77.780
13	HA-12-D37	WisBaw1452/80	CCM	DC	143	588	433	2.925	1.198	0.852	13.493	10.676	7.555	68.276
14	HA-12-4	WisBaw1452/80	CCM	DC	132	547	403	2.801	1.802	1.001	9.956	10.735	7.435	71.874
15	HA-12-D32	WisBaw1452/80	CCM	DC	306	635	724	2.486	1.762	1.279	12.225	9.545	8.015	70.215
16	HA-12-D31-A-X	WisBaw1452/80	CCM	DC	160	816	422	3.540	1.186	1.228	12.886	10.670	7.341	69.103
17	HA-12-D31-B-D-C	WisBaw1452/80	CCM	DC	126	865	447	3.689	1.430	0.876	11.767	11.633	6.612	69.988
18	HA-12-D31-F-G	WisBaw1452/80	CCM	DC	158	873	497	2.874	1.132	1.029	9.015	12.279	7.302	71.404
19	HA-12-D30	WisBaw1452/80	CCM	DC	128	399	324	2.241	1.222	1.078	11.044	10.858	7.798	70.301
20	HA-12-D29	WisBaw1452/80	CCM	DC	242	1083	615	1.835	0.872	0.928	12.681	10.023	8.472	68.823
21	HA-12-D27-A	WisBaw1452/80	CCM	DC	191	897	479	2.182	0.911	1.350	11.916	10.376	7.971	69.737
22	HA-12-D27-B	WisBaw1452/80	CCM	DC	193	920	528	2.196	1.254	0.760	12.545	10.994	9.015	67.446
23	HA-12-D24	WisBaw1452/80	CCM	DC	137	389	395	1.676	1.098	1.449	9.953	9.460	9.957	70.631
24	HA-20-1	WisBaw1391/80	2	DC	73	341	249	3.576	1.673	1.030	11.727	11.207	6.343	70.723
25	HA-20-D18	WisBaw1391/80	CCM	DC	114	502	462	2.967	1.467	0.785	12.675	10.838	6.895	69.592
26	HA-20-D19	WisBaw1391/80	CCM	DC	107	437	431	2.407	1.475	0.669	11.533	11.762	7.293	69.413
27	HA-20-D20	WisBaw1391/80	CCM	DC	405	1827	923	3.231	1.972	0.830	10.430	11.917	5.865	71.787
28	HA-20-D20-02	WisBaw1391/80	CCM	DC	551	2177	1129	2.439	1.639	1.131	11.625	10.996	7.299	70.080
29	HA-20-89	WisBaw1391/80	CCM	DC	131	655	464	3.384	2.086	0.945	9.703	11.221	6.784	72.292
30	HA-20-D21	WisBaw1391/80	CCM	DC	204	693	611	2.401	1.256	0.805	12.972	11.733	6.769	68.527
31	HA-21-39	WisBaw1392/80	2	DC	123	358	366	3.407	1.771	0.925	12.320	10.000	6.139	71.541
32	HA-22-2	WisBaw1408/80	2	DC	76	254	217	2.933	1.941	0.864	9.259	11.053	7.051	72.637
33	HA-22-4	WisBaw1408/80	2	DC	330	859	454	1.596	1.627	0.905	7.453	10.850	4.710	76.988
34	HA-27-8-97-3A	Spitzberg	T		275	686	1548	3.642	1.759	0.828	13.086	5.905	2.462	78.547
35	HA-27-8-97-3B	Spitzberg	T		294	812	1105	3.484	1.935	0.960	12.496	6.452	3.294	77.757
36	HA-27-8-97-5	Stbr. Quetz	T		383	863	617	1.295	1.090	0.590	8.186	8.419	4.013	79.381
37	HA-6A	Spitzberg	T		139	488	318	3.970	1.513	0.990	11.494	8.002	4.699	75.804
38	HA-6B	Spitzberg	T		69	257	323	4.618	2.288	1.033	13.929	9.260	6.574	70.236
39	HA-18-9	Löbejün-Haltberg	T		208	809	1272	3.209	1.996	0.762	12.226	3.858	5.952	77.964
40	HA-18-10-A	Löbejün-Kautzenberg	T		240	636	537	3.111	1.926	1.034	13.064	11.950	6.267	68.720

Geometry and textures of Halle laccoliths

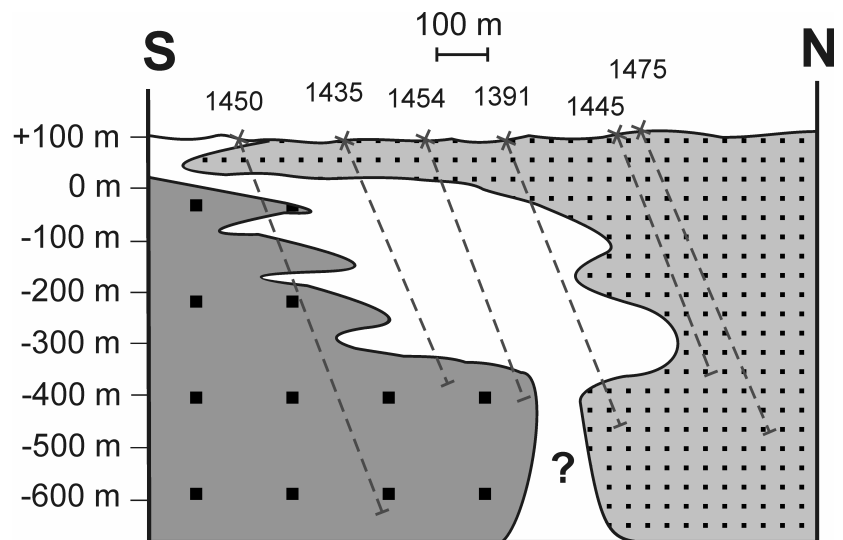
No.	Sample name	Sample location	DAT	Rem.	NOP			CL			Kf %	Pl %	Qz %	GM %
41	HA-18-10B	Löbejün-Kautzenberg	T		328	1440	1597	3.306	2.208	0.914	13.933	8.578	5.242	72.247
42	HA-18-11a	Stbr. Löbejün	T		731	2352	2317	3.306	1.652	0.753	14.866	9.382	7.425	68.327
43	HA-18-11b	Stbr. Löbejün	T		785	2113	2034	3.065	1.764	0.921	7.215	8.270	4.250	80.266
44	HA-18-11c	Stbr. Löbejün	T		911	2536	2325	2.797	1.536	0.767	9.764	9.296	5.028	75.912
45	HA-18-11D	Stbr. Löbejün	T		381	493	1488	3.570	1.854	0.959	9.353	7.608	4.579	78.459
46	HA-18-12	Krosigk	T		224	616	794	3.263	1.560	0.814	9.193	5.373	5.941	79.492
47	HA-18-5	Lerchenhügel	T		287	295	758	3.783	1.613	0.904	9.595	3.927	3.829	82.650
48	HA-18-15	Trebitz	T		135	368	456	3.944	1.899	1.217	10.394	8.553	6.286	74.767
49	HA-18-2B	Neutz-Lettewitz	T		201	530	576	2.803	1.890	0.772	8.292	7.740	4.262	79.706
50	HA-18-2A	Neutz-Lettewitz	T		249	856	871	3.111	1.658	0.657	8.579	9.506	5.311	76.604
51	HA-18-14	Löbejün-Haltberg	T		155	329	499	2.984	1.572	1.455	13.545	10.198	7.320	68.937
52	HA-19-20	BAB143-17	2		356	1481	915	3.628	1.798	0.966	12.906	10.061	6.910	70.123
53	HA-18-13	Krosigk-Teufelsgrund	T		160	553	1057	3.161	1.640	0.996	12.275	9.729	6.957	71.039
54	HA-19-B2	Lerchenhügel	2	DC	138	515	490	3.669	1.842	0.843	10.384	5.126	3.324	81.167
55	HA-19-15	BAB143-16	2	DC	324	718	607	4.000	1.851	1.081	11.784	9.476	7.049	71.692
56	HA-19-B1	Lerchenhügel	2	DC	159	627	594	2.968	1.867	0.739	11.636	8.902	7.197	72.266
57	HA-7-2	Schlettau5	T	DC	247	371	499	3.876	1.940	0.919	9.422	7.622	6.531	76.425
58	HA-18-7	Löbejün-W	T		93	304	515	3.213	1.626	0.832	8.073	7.748	3.025	81.154
59	HA-18-7A	Löbejün-W	T		126	522	855	3.196	2.245	0.868	10.094	8.932	6.782	74.192
60	HA-18-8A	Löbejün-NW	T		362	1159	1619	3.517	1.910	0.928	9.867	9.458	8.666	72.009
61	HA-19-B3	Lerchenhügel	2	DC	108	452	444	3.493	2.142	0.838	13.385	5.549	3.954	77.113
62	HA-7-4	Schlettau5	T	DC	166	708	376	3.296	1.513	1.075	10.602	7.629	7.610	74.159
63	HA-18-4	Brachwitz-E	T		177	767	975	3.460	1.970	0.806	7.980	8.101	6.026	77.893
64	HA-18-6	Löbejün-Gottgau	T		155	500	671	3.123	1.628	0.942	11.019	8.408	6.482	74.091
65	HA-9-2	Brachwitz	T	DC	116	319	380	3.505	1.461	0.769	11.759	5.906	5.446	76.889
66	HA-9-1	Brachwitz	T	DC	116	199	354	3.590	2.186	0.947	11.126	8.522	6.398	73.954
67	HA-2-9a	Petersberg	T		799	1192	1109	1.294	0.983	0.703	6.061	9.034	3.755	81.150
68	HA-2-8a	Petersberg	T		2021	1234	1190	1.207	1.148	0.575	9.757	6.209	3.840	80.194
69	HA-27-8-97-7	Stbr Hoffmann	T		1990	1758	1289	1.357	1.550	0.643	7.662	6.622	3.206	82.510
70	HA-2-4	Petersberg	T		524	866	385	1.513	1.175	0.827	8.720	10.699	3.435	77.146
71	HA-27-8-97-6	Abatasinenberg	T		295	857	836	1.413	1.231	0.593	4.075	8.430	4.500	82.995
72	HA-17-02-02-A	Brachstedt/Niemberg: Burgstetten	CCM		1733	2846	1055	0.725	0.760	0.385	9.298	10.103	6.370	74.229
73	HA-17-02-02-B	Brachstedt/Niemberg: Burgstetten	CCM		1299	1186	1239	0.538	0.691	0.486	9.816	8.096	9.128	72.960
74	90499a	Petersberg9	T	DC	1554	998	1085	1.067	1.191	0.692	4.723	3.572	3.600	88.105
75	90499b	Petersberg9	T	DC	1045	838	989	1.034	1.063	0.699	4.928	6.170	4.097	84.805
76	90499c	Petersberg9	T	DC	1198	897	812	0.969	0.923	0.684	4.341	4.117	3.143	88.399
77	HA-27-9-96-7	Stadtpark	T		262	473	245	1.173	1.063	0.629	5.604	9.436	3.152	81.808
78	HA-8-2	Schlettau2	T	DC	239	1200	544	1.692	1.064	0.649	3.527	6.288	1.890	88.295
79	91671a	Petersberg9	T	DC	1331	641	1340	1.121	1.048	0.634	5.275	5.284	2.431	87.009
80	91671b	Petersberg9	T	DC	810	550	853	1.361	1.053	0.652	7.096	6.454	3.628	82.822
81	91843a	Petersberg9	T	DC	634	545	563	1.288	1.040	0.543	7.279	6.236	3.705	82.780
82	91843b	Petersberg9	T	DC	684	664	605	1.180	0.798	0.564	8.218	5.418	3.414	82.949
83	91843c	Petersberg9	T	DC	391	340	495	1.195	0.968	0.500	9.872	7.504	4.870	77.754
84	92235a	Petersberg9	T	DC	532	481	780	1.118	0.832	0.604	5.782	5.803	3.619	84.796
85	92235b	Petersberg9	T	DC	764	599	858	0.974	1.050	0.537	5.520	6.545	3.312	84.623
86	92508a	Petersberg9	T	DC	1057	1191	1064	1.285	1.105	0.580	6.000	4.598	2.163	87.239
87	92508b	Petersberg9	T	DC	737	876	631	1.447	1.208	0.576	11.361	6.659	4.214	77.766
88	92508c	Petersberg9	T	DC	1264	856	806	1.285	1.043	0.719	5.025	4.330	3.280	87.364
89	92860a	Petersberg9	T	DC	713	626	563	1.180	1.104	0.673	8.934	7.261	4.413	79.391
90	92860b	Petersberg9	T	DC	651	621	714	1.047	1.166	0.568	7.364	8.656	3.418	80.562

Geometry and textures of Halle laccoliths

No.	Sample name	Sample location	DAT	Rem.	NOP			CL			Kf %	Pl %	Qz %	GM %
91	92860c	Petersberg9	T	DC	890	728	683	1.113	0.989	0.673	8.837	9.139	5.068	76.956
92	GKgang	Stbr Schwerz	T		279	524	577	3.603	1.954	0.965	12.834	8.225	5.754	73.187
93	Gkgross-1-a	Stbr Schwerz	T		135	314	226	2.758	1.532	0.654	11.330	8.463	4.463	75.745
94	Gkgross-2-a	Stbr Schwerz	T		120	279	201	3.559	1.457	0.729	13.671	8.500	4.430	73.398
95	HA-5-3	Stbr.Schwerz	T		516	412	343	1.569	1.603	0.956	8.537	6.871	4.560	80.032
96	HA-5-5	Stbr. Schwerz	T		640	314	182	1.250	2.002	0.693	8.113	7.420	1.680	82.787
97	GKbraun-1-a	Stbr Schwerz	T		310	393	435	2.063	1.375	0.731	9.174	7.274	4.887	78.665
98	Gkbraun-2-a	Stbr Schwerz	T		160	175	278	2.073	1.912	0.867	10.134	7.302	5.410	77.154
99	GKbraun3-a	Stbr Schwerz	T		81	100	133	2.426	1.734	0.763	10.300	7.400	4.854	77.446
100	Gkschwarz-1-a	Stbr Schwerz	T		251	495	242	1.266	1.355	0.608	6.699	9.461	3.689	80.152
101	EXN-1-1A	Schweizerling	T		873	835	555	1.149	1.271	0.565	4.371	3.683	2.571	89.374
102	EXN-3-1A	Wettin-Liebecke	T		392	280	165	1.251	1.289	0.609	8.676	6.288	2.685	82.351
103	EXN-3-2A	Wettin-Liebecke	T		296	198	133	1.570	1.482	0.712	8.192	7.189	2.747	81.872
104	EXN-3-3A	Wettin-Liebecke	T		176	123	93	1.445	2.013	0.418	8.896	7.187	3.161	80.756
105	EXN-4-1A	Wettin-Liebecke	T		177	161	115	1.311	1.420	0.775	9.615	9.036	4.537	76.812
106	EXN-4-2A	Wettin-Liebecke	T		178	119	156	1.298	1.506	0.730	7.648	6.474	5.450	80.429
107	EXN-4-3A	Wettin-Liebecke	T		284	194	187	1.150	0.932	0.654	8.089	6.303	4.206	81.402
108	EXN-5-1A	Wettin-Liebecke	T		321	162	230	1.542	1.972	0.607	8.390	5.725	3.833	82.052
109	EXN-5-2A	Wettin-Liebecke	T		296	172	155	1.357	1.691	0.755	7.345	6.927	3.845	81.883
110	EXN-5-3A	Wettin-Liebecke	T		200	156	119	1.559	1.245	0.794	10.428	7.610	3.459	78.503
111	HA-26-8-97-5	Schweizerling	T		1541	1321	2373	1.318	1.325	0.751	10.684	9.498	8.509	71.309
112	HA-26-8-97-5b	Schweizerling	T		465	332	449	1.123	1.299	0.672	10.660	11.464	6.824	71.053
113	HA-26-8-97-2	Döblitz-E	T		377	808	543	1.069	0.843	0.643	4.928	4.406	2.887	87.780
114	EXN-7-1A	Wettin-Mücheln	T		227	153	87	1.480	1.261	0.771	7.750	4.643	1.774	85.833
115	EXN-7-2A	Wettin-Mücheln	T		212	146	131	1.409	1.448	0.637	7.379	5.106	2.706	84.809
116	EXN-7-3A	Wettin-Mücheln	T		110	89	61	1.285	1.265	0.802	7.805	6.181	3.274	82.739
117	HA-16-4-97a	LauchengrundA	T		507	888	572	1.221	1.163	0.685	7.021	5.035	4.885	83.059
118	HA-16-4-97b	LauchengrundB	T		395	587	325	1.172	1.126	0.737	9.343	7.949	5.124	77.584
119	HA-16-4-97c	LauchengrundC	T		449	902	460	1.421	1.082	0.618	8.578	5.449	5.966	80.007
120	HA-26-8-97-3	Lauchengrund-W	T		598	402	348	1.515	1.169	0.688	6.486	3.848	2.027	87.639

Generally, it is possible to retrieve size distribution data in a number of ways (Higgins 2000). Physical separation of mineral grains and subsequent sieving is a classical and most reliable method, but not always feasible for solidified hard rock (Rudashevsky et al. 1995). Some rock types allow automatic image classification, but this method can only utilize colour differences of visible reflected or transparent light (Marschallinger 1997). Multivariate statistics of the images' three or four channels (RGB or CMYK) might yield satisfactory results in some cases. Large sample sizes, alteration, very similar colour properties or complicated structure require manual image classification facilitated by easy to use digitizing tablets and pens and high resolution images even from live imaging systems. Moreover, manual image classification is often more reliable than automatic classification experiments.

Fig. 9. Hypothetical N-S cross section through Landsberg and Petersberg (?) laccoliths with contacts found in six drill cores. Number of drill core indicated. Drill core 1391 sampled in this study. Other logs recorded during drilling. White = host rock sediments; location see Fig. 2.



All samples were cut at least once. Some samples allowed more than one slab to be produced in different orientations (compare Mock et al. 2003). On one set of samples (see Tab. 1), phenocrysts were outlined by hand on transparency. This was then scanned with 180 dpi and digital images were cross checked with the sample slab to ensure representation of individual phenocrysts by singular areas on the image. Images were analysed automatically with image analysis software (KS300 by KONTRON ELEKTRONIK Imaging System). Detection limit for phenocrysts in this approach is given by the size of the pen used to outline crystals (~0.1 mm). Another set of sample slabs was roughly polished and spray varnished, enabling scanning directly on a flatbed scanner with 400 dpi (detection limit 0.06 mm, size of 1 pixel). Digital images, thus retrieved, were manually classified for the three felsic phenocrysts. Scanned images were compared with sample slabs under a stereomicroscope and different phenocrysts marked with coloured overlays on the image using standard image editing software (CorelPhotopaint). Classified images were analysed automatically (see above).

Alternatively, images were classified and analysed in one step using a different version of the image analysis software (KS100). Due to the state of alteration of samples and highly ambiguous colour properties of phases, automatic classification of scanned sample slabs was not possible. Nevertheless, different phases could still be recognised with confidence by mineralogically experienced examiners.

From image analysis, positions, areas, axes and orientations of all felsic phenocrysts were retrieved. The sum of areas of one phenocryst phase divided by the sample area gave that phase's modal abundance (Delesse 1848; Higgins 2002). Long axes of phenocrysts were used in CSD analysis, position data analysed according to SDP method and orientation of phenocrysts' long axes enabled estimation of preferred orientations present. Further details on quantitative petrographic methods can be found in more specific contributions on laccoliths of the HVC (Mock et al. 2003; Mock & Jerram submitted). In the following sections, different methods and data of quantitative petrography are presented in detail.

Phenocryst petrography, feldspar mineral chemistry and melt inclusions

Crystallinity of rhyolites retrieved from image analysis ranges from 10 to 35% phenocrysts (Fig. 10). Samples with small phenocryst sizes show a tendency towards slightly less phenocryst crystallinity than large crystal samples. This tendency is supported by average modal abundances (see means in Fig. 10a). Relative modal abundances are rather homogeneous for all samples with 10 to 40% quartz and about equal amounts of the two feldspars. Some large crystal samples are richer in K-feldspar at the expense of plagioclase by about 10% (Fig. 10b). Larger K-feldspars are less abundant by number, whereas plagioclase and quartz have about equal numbers for small and large crystal varieties (Fig. 10c). Maximum sizes of K-feldspar phenocrysts distinguish the two varieties very well; mean sizes are a less reliable indicator (Fig. 10d, e). In general, phenocrysts do not show a preferred orientation of their long axes.

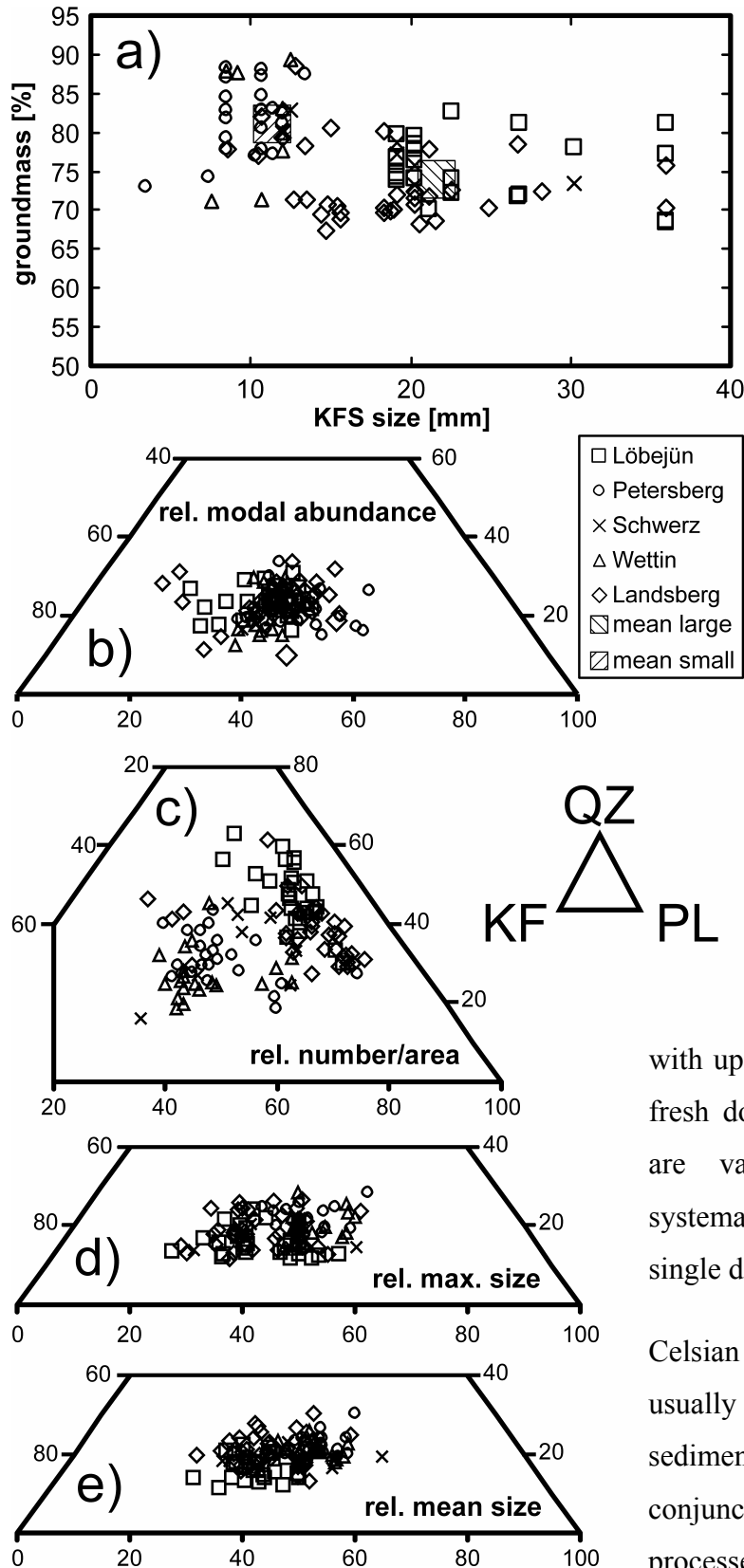


Fig. 10. a) Groundmass percentage vs. maximum size of K-feldspar phenocrysts. b) Relative modal abundance, c) relative number per unit area, d) maximum sizes and e) mean sizes of felsic phenocrysts of 120 porphyritic rhyolite samples.

Phenocryst plagioclase ranges in composition from andesine to oligoclase. Microprobe work shows up to three types of unaltered K-feldspar (Romer et al. 2001): (1) orthoclase with Or 60-70, (2) orthoclase with Or 90-100, and (3) Ba-rich orthoclase with up to 2.8 wt% BaO (Fig. 11). Within fresh domains of K-feldspar, Ba contents are variable, but constant or with systematic oscillatory growth zonation in single domains (Romer et al. 2001).

Celsian and other Ba-rich feldspars are usually restricted in occurrence to sedimentary and metasedimentary rocks in conjunction with exhalative hydrothermal processes and low- to medium-grade metamorphism (Candelas Moro et al.

2001). In the HVC, unusual occurrence of Ba-rich orthoclase – together with enrichment in K, Ba and Rb and lower contents of Na, REE, Y, and Nb in some samples (Romer et al. 2001) – cannot be explained by fractional crystallization alone. These anomalies can be interpreted to

reflect contrasting modal abundance of Th-poor monazite (LREE), xenotime (Y, HREE) and Ba-enriched K-feldspar (K_2O , Rb, Ba). These minerals may represent cumulus phases, material inherited from the source or contaminants from wall rocks. Variability in abundance of relatively immobile elements Nb, Y and REE cannot be explained in terms of post-magmatic alteration as demonstrated by a disturbed Rb/Sr isotopic system, because other severely altered rhyolites do not show the same element pattern. Furthermore, alteration is not displayed at all in Nd-isotopy (Romer et al. 2001).

Many melt inclusions (Fig. 12) show elevated contents of a fluid phase (Tab. 2 and Rainer Thomas, pers. comm.). In contrast, whole rock geochemical data suggest very low fluid contents (Romer et al. 2001). This implies early degassing during magma ascent, an interpretation supported by abundantly observed broken phenocrysts of quartz and subordinately feldspar (Fig. 4).

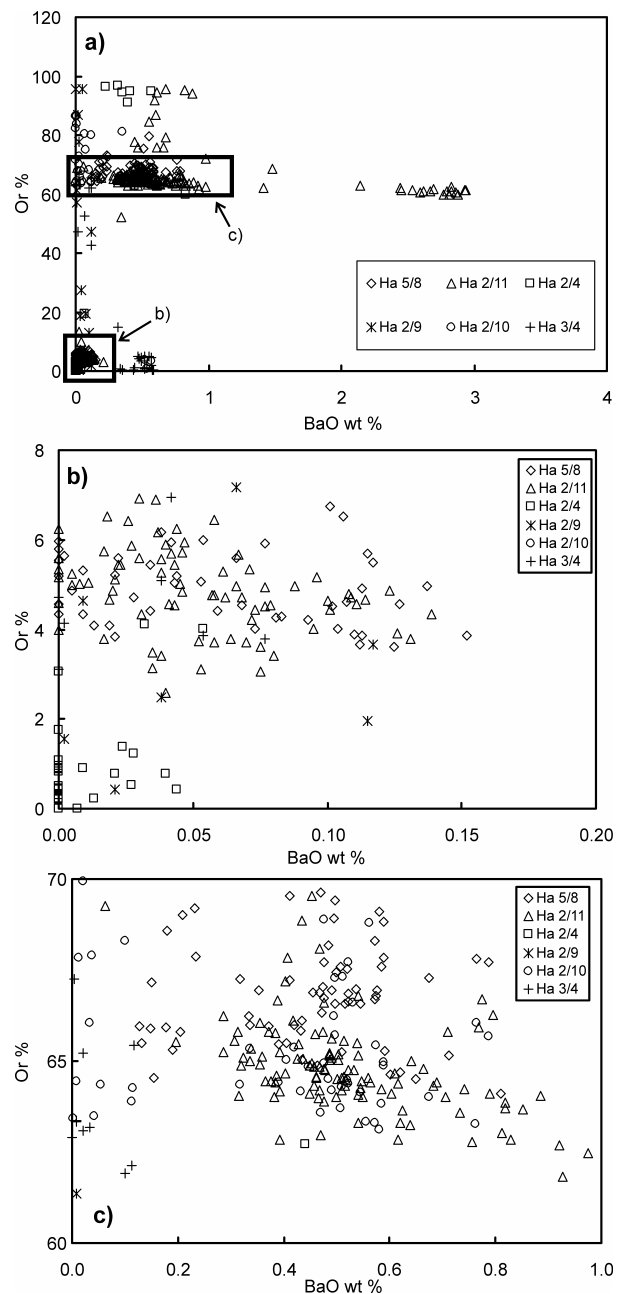


Fig. 11. a) Analyses of Ba content plotted vs. amount of orthoclase from microprobe analyses (CIPW norm). b,c) details of a.

Tab. 2. a) Main element data of 14 melt inclusions from the HVC. b) Water content of melt inclusions from the HVC (Rainer Thomas, pers. comm.).

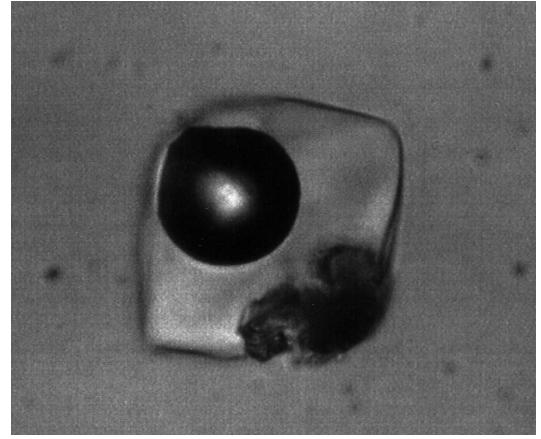
a)	Qtz phenocrysts	Qtz phenocryst	Matrix Qtz
SiO ₂	68.81 ± 0.62	69.02	70.00
TiO ₂	0.08 ± 0.02	0.12	0.08
Al ₂ O ₃	16.06 ± 0.70	16.93	16.29
FeO	0.57 ± 0.22	0.20	1.14
MnO	0.03	0.01	0.06
MgO	0.03	0.01	0.02
CaO	0.65 ± 0.08	0.68	0.30
Na ₂ O	3.30 ± 0.24	3.33	3.18
K ₂ O	6.25 ± 0.23	5.86	6.36
FeO	0.22 ± 0.05	0.20	0.25
Cl	0.04	0.03	0.08
P ₂ O ₅	0.03	0.01	0.09
H ₂ O	2.60 ± 0.44	2.30	1.43
Sum	98.67	98.70	99.28
n	11	1	2

b) sample	laccolith	H ₂ O (wt%)	σ	n	remark
HA2-1	Petersb.	1.14	0.14	8	
HA2-1	Petersb.	6.24		1	dark inclusion
HA6	Landsb.	0.82	0.13	6	
HA6	Landsb.	2.33	0.15	11	large inclusions
HA6	Landsb.	3.62	0.4	5	120µm
HA7-4	Landsb.	2.1	0.28	15	
HA27-9-96-7-a	Petersb.	0.83	0.1	7	alpha-quartz
HA27-9-96-7-b	Petersb.	1.54	0.13	11	
HA27-9-96-7-c	Petersb.	2.3	0.37	6	
HA16-4-97	Wettin	1.2	0.15	12	pyroxene
HA5-5	Schwerz	1.18	0.33	13	
HA5-10	Schwerz	1.01	0.12	13	
HA5-11	Schwerz	1.09	0.12	10	
HA5-10-95-29	Schwerz	0.58	0.02	12	alpha-quartz

Crystal size distribution (CSD)

In general

Textures of igneous rocks are a result of often complex P-T-X-evolutions (Marsh 1998; Zieg & Marsh 2002). Phenocrysts frequently provide insight into even the early stages of the magmatic system they form in (Knesel et al. 1999). Complex magmatic histories predominate in the rock record (e.g. Hawkesworth et al. 2000), but simple crystallization histories are also found (e.g. Higgins 1996b, a).

Fig. 12. Melt inclusion in a quartz phenocryst.

CSD analysis is a well established tool in quantitative petrography (Marsh 1998; Higgins 2000; Zieg & Marsh 2002) surviving a recent discussion about its statistical viability (Pan 2001; Marsh & Higgins 2002; Pan 2002a, b; Schaeben et al. 2002). It has been applied to various geological problems in recent times (Burkhard 2002; Eberl et al. 2002; Higgins 2002; Bindeman 2003; Castro et al. 2003; Higgins & Roberge 2003; Jerram et al. 2003; Turner et al. 2003). CSD studies so far tried to reveal conditions of crystallization within rising, cooling or erupting magma batches. While succeeding to determine growth rates, nucleation rates, cooling times and textural coarsening (Cashman 1992; Wilhelm & Wörner 1996; Higgins 1998; Hammer et al. 1999), CSDs have not been utilized to reveal internal structure within large, very homogeneous intrusive bodies of magma.

Other examples of CSD studies include:

- concave down lognormal CSDs of quartz and zircon phenocrysts from pumice clasts in voluminous ash flow tuffs resulting from surface-controlled, size dependent growth by layer nucleation in silicic magmas at low supersaturation and fingerprinting different magma batches (layers) in products of the same eruption (Bindeman 2003),
- strongly curved, concave up plagioclase CSDs observed in andesitic eruptive products of Soufrière Hills volcano, Montserrat formed by repeated cycles of linear undercooling (nucleation and growth) and temperature buffered textural coarsening (Higgins & Roberge 2003),
- kinked and curved CSDs resulting from mixing of distinct crystal populations, sharp variations in growth and/or nucleation rate, or from crystal settling (Higgins 1996b),

Complex CSDs may arise as an artefact of shape variability in the natural population. In most CSD studies, crystal growth rates are assumed constant which is generally not known *a priori* (Castro et al. 2003). Variable growth and nucleation rates might lead to irregularities in crystal shapes and the spatial arrangement of crystals might be disturbed by magma flow. These variations might not be detectable in CSD analysis alone (Mock & Jerram submitted). Straight CSDs might be a result of complex variations of growth and nucleation rates as well as of a simple crystallization history. Crystals grow either size-dependently (proportionately) and size-independently (disproportionately). In proportionate growth, the relative size difference among crystals remains constant, in disproportionate growth, it is absolute distance (Kile & Eberl 2003). Proportionate growth produces log-normal CSDs frequently found in natural systems. Conventional models for CSD often assume disproportionate growth models not confirmed in experiments. Thus, interpretation of CSDs (non-linear or straight) to reveal certain petrological processes has to be done with care.

CSDs are represented as graphs of population density N (natural logarithm of the amount of crystals per size bin per sample volume as mm^{-4}) vs. size L (mm) giving usually downward to the right sloping curves. CSD slope and occurrence of irregularities and departures from straight lines provide unique parameters of samples from the same magmatic system.

In the Halle Laccoliths

Here, CSDs (and SDPs presented in the next section) are used to differentiate large laccoliths and constrain a crystallization time scale, setting an evolutionary time frame for the laccolith complex together with other model calculations (presented at the end of this chapter). Additional quantitative petrographic studies have been carried out on samples from the Petersberg laccolith (Mock et al. 2003; Mock & Jerram submitted).

CSDs are all straight (Fig. 13). Their regression coefficients are all above 0.9 (only linear parts of the CSDs used for regressions, Castro et al. 2003). However, they tend to decline towards small size ends. This can be attributed either to textural coarsening (Higgins 1999b), or it is an artefact of data acquisition, i.e. small sections of crystals are less easily identified and, therefore, less abundant. CSDs from the Löbejün laccolith seem to be very uniform, although samples from northern and southern parts are plotted in one CSD-plot. Within the Landsberg laccolith, CSDs vary to a greater extent. The small crystal laccoliths of Wettin and Petersberg display uniform CSDs again (Fig. 13).

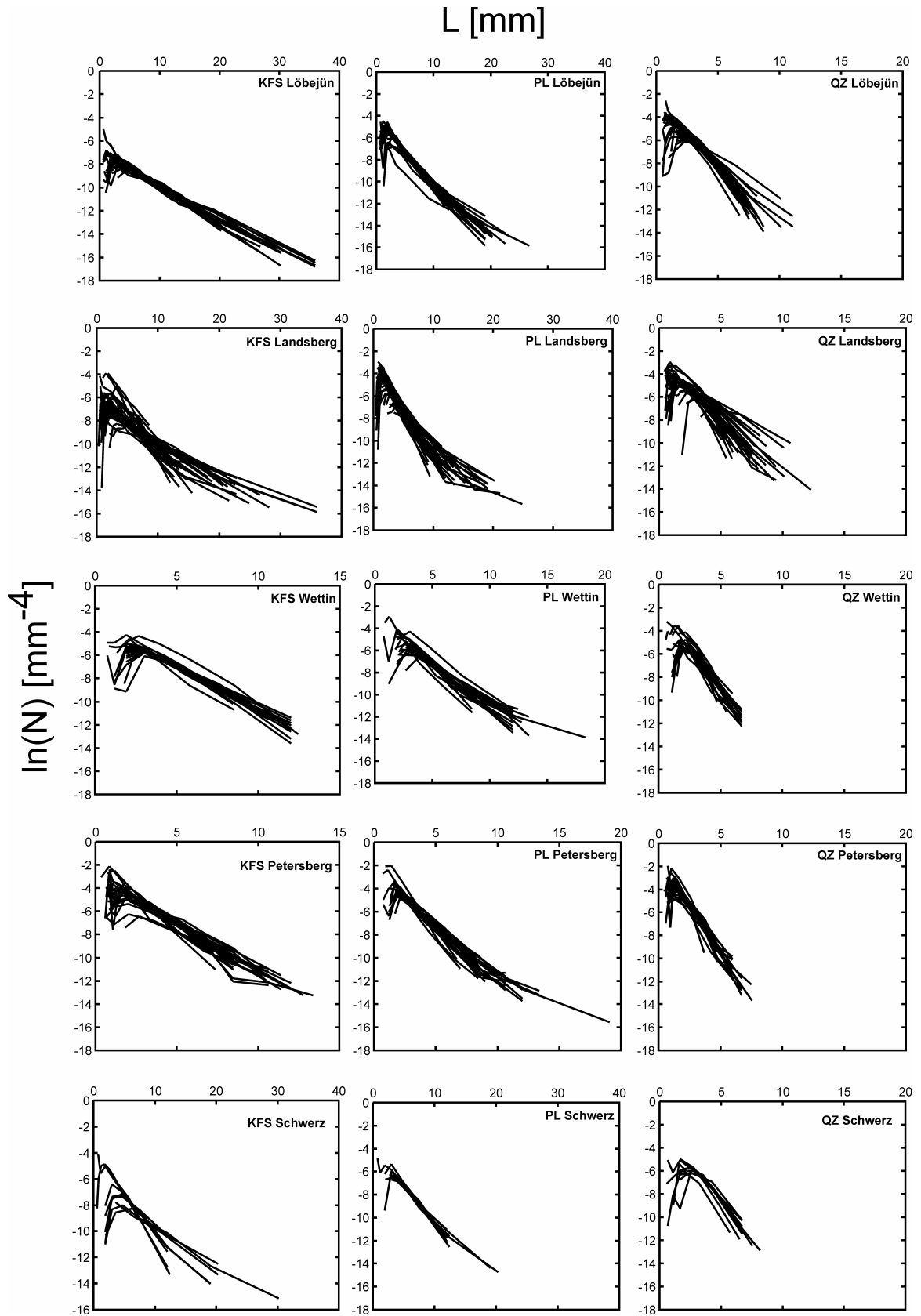


Fig. 13. Crystal size distributions of all samples of this study. All laccoliths show remarkably straight and simple CSDs for the size range within the error of the correction method (see Higgins, 2000). Textural coarsening might be indicated by small size parts of CSD-plots.

CSD slope is known as characteristic length (a product of growth rate and growth time) and can be plotted against modal abundance to indicate textural coarsening (Fig. 14). Furthermore, the product of these parameters is plotted vs. sample elevation (Fig. 15) displaying variability within a laccolith (see Discussion and Higgins 1999a, 2000, 2002). Textural coarsening trends can only be seen for K-feldspars in the Landsberg and Löbejün laccoliths and the more complex Schwerz laccolith (Fig. 14). This pattern might indicate textural coarsening within one magma batch or reflect complex intrusive patterns exhibited in drill cores and outcrops (Figs. 2, 3, 7, 8, 9).

In scaling analysis of CSDs as suggested by Zieg and Marsh (2002, see above), mean lengths of crystals and a total number normalized to modal abundance should correlate in a linear array with slope 1 (Fig. 16). Correlation coefficients in this plot are reasonably close to one, but some K-feldspar data points deviate. They stem from drill cores in the margin of the Landsberg laccolith (WisBaw 1452/80 and 1392/80) with intensely brecciated zones. The relevance of this observation will be discussed below.

Spatial distribution pattern (SDP)

SDP analysis quantifies the spatial arrangement of a rock's constituents with R-values (Kretz 1969; Jerram et al. 1996; Jerram & Cheadle 2000). It, thereby, distinguishes touching from non-touching frameworks (Jerram et al. 2003) and has already been applied to samples from the Petersberg laccolith demonstrating batch-wise intrusion (Mock et al. 2003). Coordinates of phenocryst centres were used to calculate R-values using an MSWindows based program developed by M. Higgins (pers. comm.) with the equations given in Jerram et al. (1996). The R-value is based on nearest neighbour distances (NND) of actual grain centres and the mean NND expected for a random distribution of spheres of same population size and density. An R-value was calculated for a whole slab using grain centre data of all phenocrysts and, separately, for each phenocryst phase.

Fig. 14. Characteristic length (slope) of the CSD vs. modal abundance of each phenocryst phase. Textural coarsening is revealed by positive correlation trends (Higgins, 1999; 2000; 2002).

R-values are plotted vs. groundmass proportion (Fig. 17). Small crystal samples plot very close to the line for a random distribution of spheres (RSDL, Finney 1970; Jerram et al. 1996) and have a tendency to more ordered patterns above that line. Large crystal samples, on the other hand, plot almost exclusively below RSDL and suggest more clustered phenocryst populations. They also reach the line discriminating touching from non-touching frameworks (Fig. 17), but do not fall well into the touching framework field as the literature examples do (Jerram et al. 1996; Jerram et al. 2003).

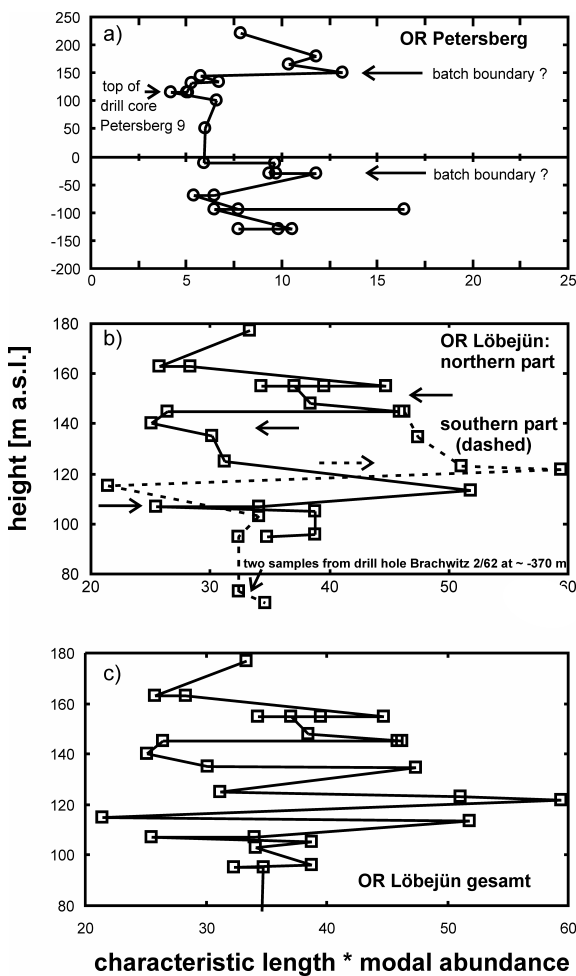
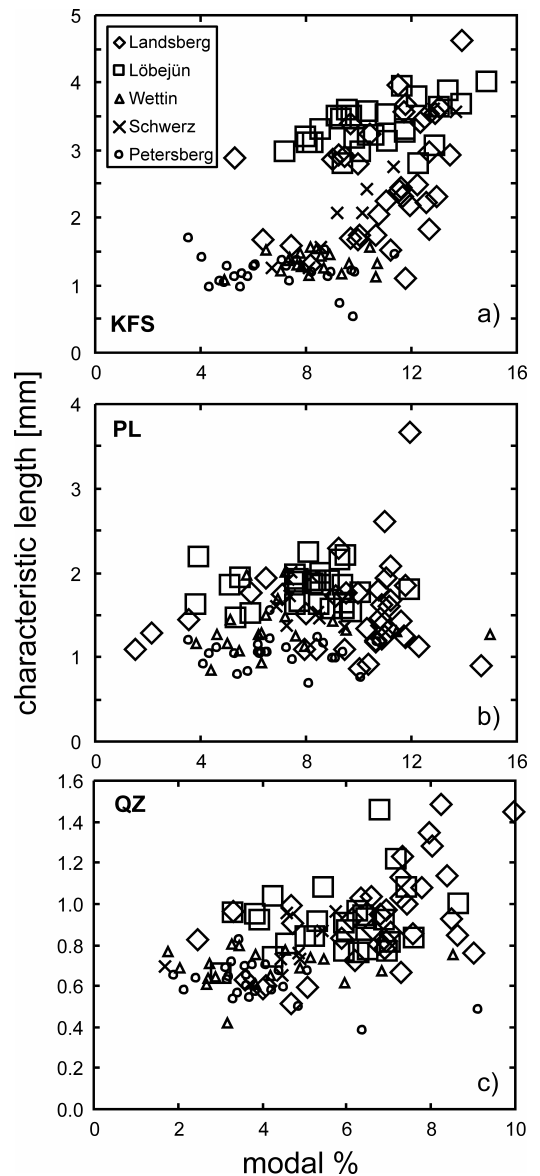


Fig. 15. Characteristic length (slope of CSD) times modal abundance vs. topographic elevation of sample site for a) Petersberg laccolith, b) northern and southern parts of Löbejün laccolith and c) undifferentiated Löbejün laccolith samples. Differentiating northern and southern part of the intrusion reveals characteristic patterns in this plot attributed to intrusion of distinct magmatic pulses.

Differences between R-values of whole samples and R-values of single phenocryst phases show a reasonably good correlation of the feldspars suggesting similar SDPs (Fig. 18). Quartz correlates better with plagioclase than with K-feldspar. These observations underline the differences between phenocryst phases apparent from CSD analysis.

Variability of SDPs in a diagram of sample elevation vs. R-value (Fig. 19) suggests internal structures, possibly boundaries between magma batches (Mock et al. 2003). Northern and southern part of the Löbejün laccolith are also clearly distinguished (Fig. 19e).

Model calculations for cooling, filling and crystallization

Order of magnitude calculations have been carried out using dimensional and petrographic data presented here to establish timescales of laccolith formation. Timescales given by radiometric dating (see Geological setting above and Breitzkreuz & Kennedy 1999) straddle several million years. Three different scales can be estimated from the following considerations:

Timescale of cooling and solidification (Tab. 3)

A general estimate for solidification times of igneous bodies (Turcotte & Schubert 2002) is given by:

$$t_s = \frac{b^2}{4\kappa\lambda_2^2} \quad (04)$$

with b: half thickness of the intrusion, κ : thermal diffusivity, and λ : a coefficient determined using error function and parameters of latent heat of crystallization, heat capacity and temperature difference between magma and country rock as in:

$$\frac{L\sqrt{\pi}}{c_p(T_m - T_0)} = \frac{e^{-\lambda_2^2}}{\lambda_2(1 + \operatorname{erf}\lambda_2)} \quad (05)$$

where L (latent heat of crystallization) is varied from 100 to 1000 kJkg⁻¹, c_p : heat capacity (Tab. 3), and T: temperature of melt (index m) and country rock (index 0).

Tab. 3. Results of calculations of solidification times for the Halle laccoliths.

thermal conductivity k (kgms ⁻³ K ⁻¹)	2.4	3.8
thermal diffusivity kappa (m ² s ⁻¹)	1.23E-06	1.15E-06
temperature difference (K)	800	
Pi	3.14159	
latent heat (Jkg ⁻¹)	100000	1000000
lambda range	1	0.3
half thickness (m)	100	500
solidification time (a)	64	763
	1607	19068

Thermal diffusivity κ is calculated as

$$\kappa = \frac{k}{\rho c_p} \quad (06)$$

with k: thermal conductivity (2.4...3.8 for granites, Turcotte & Schubert 2002), ρ : density, Tab. 4).

Tab. 4. Properties of mineral phases in the Halle laccoliths taken from Philpotts, 1990.

	molecular weights (kgmol ⁻¹)	Densities (kgm ⁻³)	abundance Halle
Anorthite	0,27821	2760	4
Albite	0,262224	2620	26
Quartz	0,060085	2650	30
K-feldspar	0,278337	2600	34
Annite	0,51189	3300	3
Phlogopite	0,417286	2700	3
weighted average Halle	0,219842	2650,6	100

Heat capacities are a function of temperature and are calculated according to (Philpotts 1990):

$$c_p = a + bT - \frac{c}{T^2} \quad (07)$$

where T is temperature and a,b,c are coefficients (Tab. 5). These order of magnitude calculations suggest relatively rapid cooling times for the HVC laccoliths on the order of several tens of thousands of years.

Tab. 5. Heat capacities for minerals of the Halle laccoliths. Albite is differentiated into two regions of temperature. Weighted averages are calculated according to average abundances found in this study.

	a	b $\times 10^3$	c $\times 10^{-5}$	c_p : 1100K	c_p : 750K	c_p : 450K	c_p : 300K
An	264.89	61.9	64.6	327.64	299.83	260.84	211.68
ab(473-1200K)	342.59	14.87	209.84	341.60	316.44	245.66	113.90
qz	46.94	34.31	11.3	83.75	70.66	56.80	44.68
kfs	320.57	18.04	125.29	330.06	311.83	266.82	186.77
annite	445.3	124.56	80.79	575.64	524.36	461.46	392.90
phlogopite	420.95	120.42	89.96	545.98	495.27	430.71	357.12
weight. av. Halle				272.92	252.08	208.83	137.49
ab(298-473K)	258.15	58.16	62.8	316.94	290.61	253.31	205.82
weight. av. Halle				266.50	245.36	210.82	161.39
c_p per weight				1241.42	1146.62	958.95	734.10

Timescale of emplacement (Tab. 6)

An estimate for magma velocity in a dyke according to Petford et al. (1994) is:

$$v_a = \frac{g\Delta\rho\omega^2}{12\mu_m} \quad (08)$$

with g : acceleration due to gravity, $\Delta\rho$: density contrast with country rock (buoyancy), ω : dyke width, and μ_m : melt viscosity. Numerical values of these parameters have been estimated for the Halle laccoliths and results of this model show relatively rapid emplacement by mechanical means alone. Furthermore, the timescale determined from this model is roughly similar to the timescale of cooling.

Tab. 6. Estimates of filling times for some characteristic HVC laccoliths.

acc. due to gravity (ms^{-2})	10		
density contrast (kgm^{-3})	200	150	100
number of feeder dikes	1	2	5
dike width (m)	20	10	5
melt viscosity (Pas)	1.00E+08		
dike length (m)	100		
flow velocity (ms^{-1})	6.67E-04	1.25E-04	2.08E-05
cross sectional area (m^2)	2000	1000	500
magma filling rate (m^3s^{-1})	1.33	0.25	0.05
volume of laccolith (m^3)	4.00E+10	2.00E+10	1.00E+10
filling time (a)	951.29	2536.78	6088.28

Timescale of crystallization

Results of CSD analysis provide a measure for growth rate and growth time for a crystal population. With the assumption of appropriate growth rates, a minimum time for crystal growth can be calculated. Accordingly, with an additional means of age determination, growth rates can be computed. Known growth rates from magmatic systems with a range of compositions mainly come from experiments (Swanson 1977; Cashman 1993) or numerical analysis (Lasaga 1982; Spohn et al. 1988). Rates are in the range of 3×10^{-6} cm/s (~3 mm/d) to 1×10^{-10} cm/s (~1 mm/a) according to experimental results from silicic systems, whereas growth rates for plagioclase in basaltic magmas are usually taken to be lower (1×10^{-11} cm/s, Swanson 1977; Cashman 1993). Rates also depend on amount of undercooling (higher with larger undercooling) and volatile content (lower with an H₂O-rich vapour phase).

With these rates and the above CSD slopes, HVC laccoliths' crystal populations might have formed on a timescale between 10 days (taken higher values for growth rates combined with steepest CSD slopes) and a couple of 1000 years (lowest growth rates with shallowest slopes) assuming linear crystal growth rates. Straight and simple CSDs do not suggest a complicated growth history, but detailed three-dimensional reconstruction of phenocrysts revealed complex shapes not expected for crystals with a simple growth history (Mock & Jerram submitted).

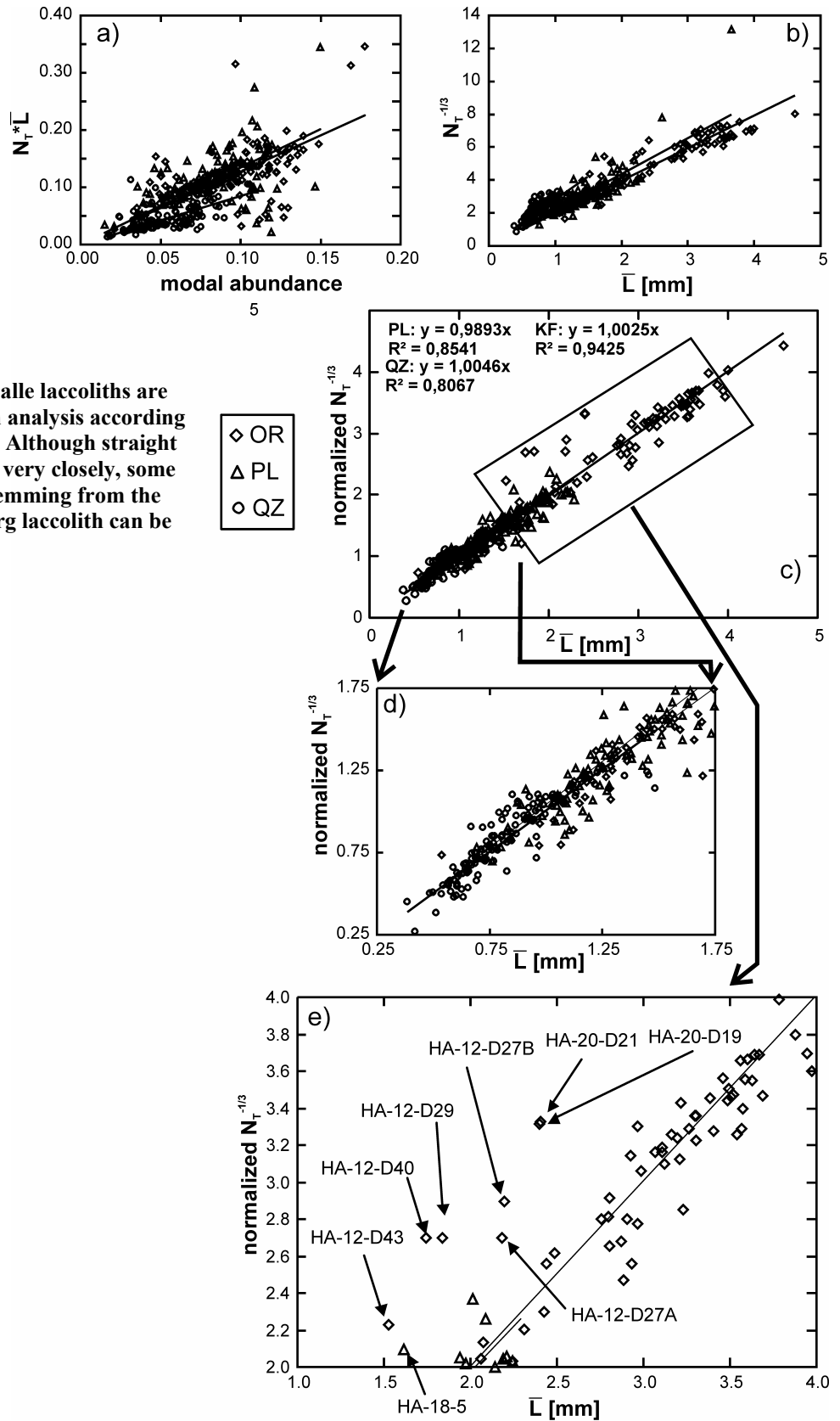


Fig. 16. Samples from Halle laccoliths are subject to normalization analysis according to Zieg & Marsh (2002). Although straight line requirement is kept very closely, some deviations of samples stemming from the margins of the Landsberg laccolith can be detected.

Discussion

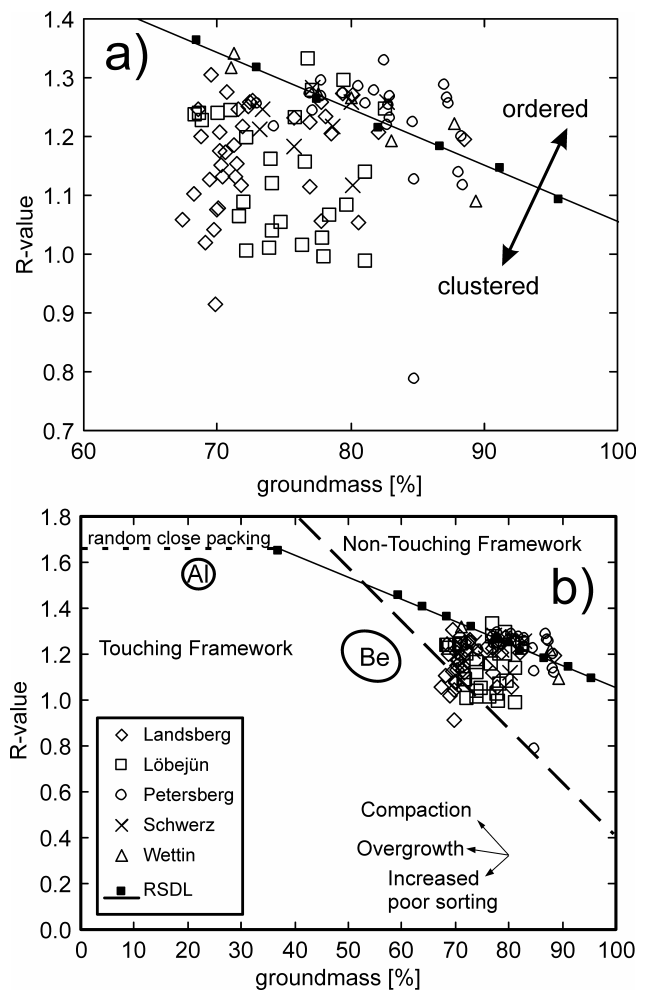
In the light of these observations, first, the long standing discussion about the emplacement mechanism of the porphyritic rhyolites shall be elaborated on. Considerations about the origin of different textural varieties follow. Detailed structures and petrographic data are then evaluated and interpreted. Finally, general aspects of magma ascent and emplacement shall be discussed.

Lava flow or laccolith?

The most important feature distinguishing lava flows from intrusions is the abundance of peperitic margins or marginal breccias only at the bottom of the former but at the top and bottom of the latter (McPhie et al. 1993). Unfortunately, the HVC laccoliths expose very few upper contacts. There are in-situ breccias in a possibly peperitic facies (Figs. 7, 8, 9). Some marginal samples also show sheared contacts indicative of ductile deformation during intrusion. Arrangement of breccias and coherent facies in drill cores (Figs. 7, 8, 9) strongly suggests intrusion of fingers extending from the main laccolith body. Large thicknesses and wide spatial extent of most of the small crystal rhyolite units are a strong indicator of an intrusive emplacement albeit a very shallow one.

Many features present in the HVC laccoliths are also found in silicic lavas: spherulites, glassy groundmass, flow banding. Additionally, felsic lavas have a distinct lithology varying between coarsely vesicular pumice, finely vesicular pumice and dense obsidian (e.g. Fink 1987; Smith & Houston 1994; Fink & Anderson 2000). These varieties have different rheologies, because viscosity of felsic magma increases with increasing vesicularity at low shear rates (e.g. Castro & Cashman 1999; Spera 2000). Analysis of structures developing in extruding felsic magmas might yield strain rates and flow directions (Smith 2002 and references therein). But highly complex features exhibited by subaerial SiO₂-rich lava flows cannot be found in the Halle rhyolites. Available data on structures of flow foliations (Fig. 3) indicate intrusion due to predominant occurrence of cupola shapes (see Nickel et al. 1967; Fink 1987). Relatively large phenocryst sizes and high crystallinity compared to most obsidian flows also advocate intrusion. The largest rhyolitic lava bodies, on the other hand, are in the range of 30-60 km³, a similar scale as the Halle rhyolites (Christiansen & Hildreth 1989).

Fig. 17. Spatial distribution pattern of all felsic phenocrysts in the Halle Laccolith Complex. a) Large crystal samples (Landsberg, Löbejün, partly Schwerz) are more clustered than small crystal ones (Petersberg, Wettin, partly Schwerz). b) Global view of R-value vs. groundmass diagram to show relation of Halle samples to published SDPs. Al: Alexo komatiite; Be: Belingwe komatiite; textural trends and division between touching and non-touching frameworks are also indicated (see Jerram et al., 2003 and Jerram et al., 1996); RSDL: random sphere distribution line.



Different crystal populations and levels of emplacement

The Halle rhyolites being laccoliths, two possibilities for the origin of different phenocryst populations and levels of emplacement remain: either, differences originate in the source region, phenocryst populations stem from different magma sources and developed early in the magmatic system, or, phenocryst populations differentiate in late stages of the intrusive process or even after emplacement.

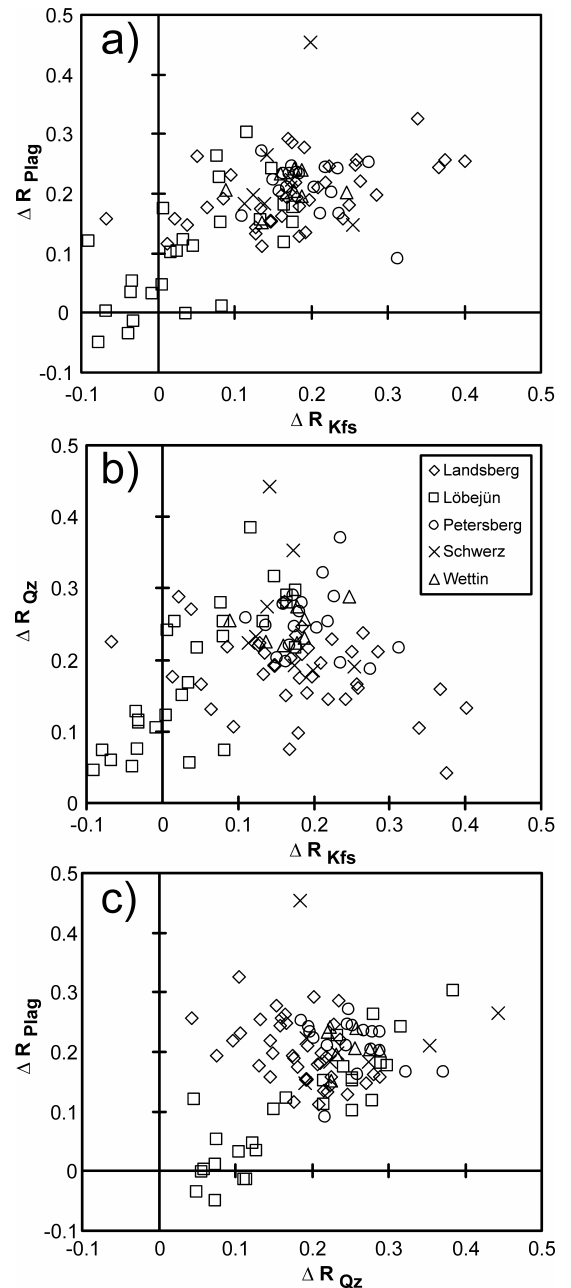
Conditions of crystallization

Geochemistry (Romer et al. 2001) and tectonic considerations (Breitkreuz & Mock in press) suggest a large, homogeneous upper crustal magma chamber feeding all intrusions of the laccolith complex. Therefore, the two varieties cannot stem from different reservoirs and differences can only develop during magma ascent from this high level storage region.

Larger phenocrysts require longer residence times. Only sizes of K-feldspar phenocryst differentiate varieties of the Halle rhyolites significantly (Fig. 10). If post-emplacement growth can be excluded, ascent and intrusion times must be longer for large crystal rhyolites, at the same time, providing favourable growth conditions for K-feldspar (the main

distinguishing phase). Indeed, large crystal laccoliths are larger on average requiring longer filling times and producing more latent heat of crystallization to buffer crystal growth. A possible scenario might be as follows: In the upper crustal magma chamber (Fig. 20), quartz crystallizes probably exclusively, maybe with incipient crystallization of K-feldspar. Upon tapping of the chamber, pressure is released considerably and quartz ceases to crystallize, whereas first K-feldspar and then additional plagioclase form. With decreasing pressure, cotectic lines move accordingly (Johannes & Holtz 1996). Duration of the last step (simultaneous growth of two feldspars) determines differences between the two size varieties of the Halle rhyolites (Fig. 21).

Fig. 18. Correlation plots of difference between single phase R-values and R-value for all felsic phenocrysts. a) plagioclase and K-feldspar; b) quartz and K-feldspar; c) plagioclase and quartz. Plagioclase and K-feldspar correlate best indicating a similar SDP for the two feldspars. Worst correlation exists between quartz and K-feldspar; plagioclase and quartz show intermediate correlation. Some R-values of feldspars are higher than R-values for all phenocrysts (negative Δ -values).



Magma viscosities

Magma viscosities increase with increasing solid fraction. Simple models of dependency of viscosity on CSD and crystal shape distributions are available (Spera 2000). For a given solid fraction (in this case $\sim 20\%$), magma viscosity is about 1-2 times as large as melt viscosity (relative viscosity). Crystallinity contrasts of the two varieties are less than 0.1 or 10% (Fig. 10a). Therefore, the large crystal rhyolite magma is slightly more viscous than the small crystal one

(Spera 2000) and, thus, its ascent velocity is lower (eq. 08). As mentioned above, longer ascent times must be responsible for different crystal populations. The viscosity effect might, therefore, give a positive feedback to the development of these differences.

Magma densities

Magmas with significantly different densities ($>10 \text{ kg/m}^3$) will emplace at different crustal levels (Corry 1988). Magma densities of the Halle rhyolites are calculated with average modal abundances determined (Tab. 1) and densities of K-feldspar (2550 kg/m^3), plagioclase (2620 kg/m^3), quartz (2650 kg/m^3), volatile free rhyolitic liquid at 1GPa with (2520 kg/m^3) and without (2540 kg/m^3) 1% H_2O and at 0.1 MPa with (2320 kg/m^3) and without (2360 kg/m^3) 1% H_2O (Deer et al. 1992; Spera 2000). Density contrasts increase with decreasing pressure. From source region to level of emplacement, the magma loses – according to this simple model – around 150 kg/m^3 in density. Average large crystal rhyolite magmas are $\sim 17\text{-}20 \text{ kg/m}^3$ denser near the level of emplacement than small crystal ones. Different units span a density range of $\sim 25 \text{ kg/m}^3$ (Fig. 22). Therefore, large and small crystal rhyolite magmas intrude into different levels. Under the assumption of a linear relationship between host rock density (sedimentary basin fill) and depth, levels of emplacement would differ by $\sim 1\%$. Furthermore, assuming a very shallow emplacement of the laccoliths ($<1000 \text{ m}$), absolute differences of these levels would be in the order of 10s of metres. Therefore, it is highly questionable whether different stratigraphic positions of the laccoliths might be resolved at all.

Details of crystal populations: magma batches and marginal effects

After emplacement of the laccoliths, quantitative petrographic observations shall be discussed. In intrusions, crystal sizes decrease from interior to margin and crystal number increases. This might also hold true for boundary zones between two magma batches of a larger intrusion. Characteristic lengths and modal abundances plotted vs. sample position reveal these relations, even if samples are not as stratigraphically constrained as in drill cores. Tectonically changed orientation of an intrusion is not as relevant as in studies of structural geology, since in topographic sections, different positions in a laccolith are sampled and CSD and SDP studies are independent of sample orientation. Nevertheless, significant post-intrusion tilting of the HVC laccoliths is excluded since underlying strata display flat bedding and regional tectonics do not indicate strong deformation (Schwab 1977).

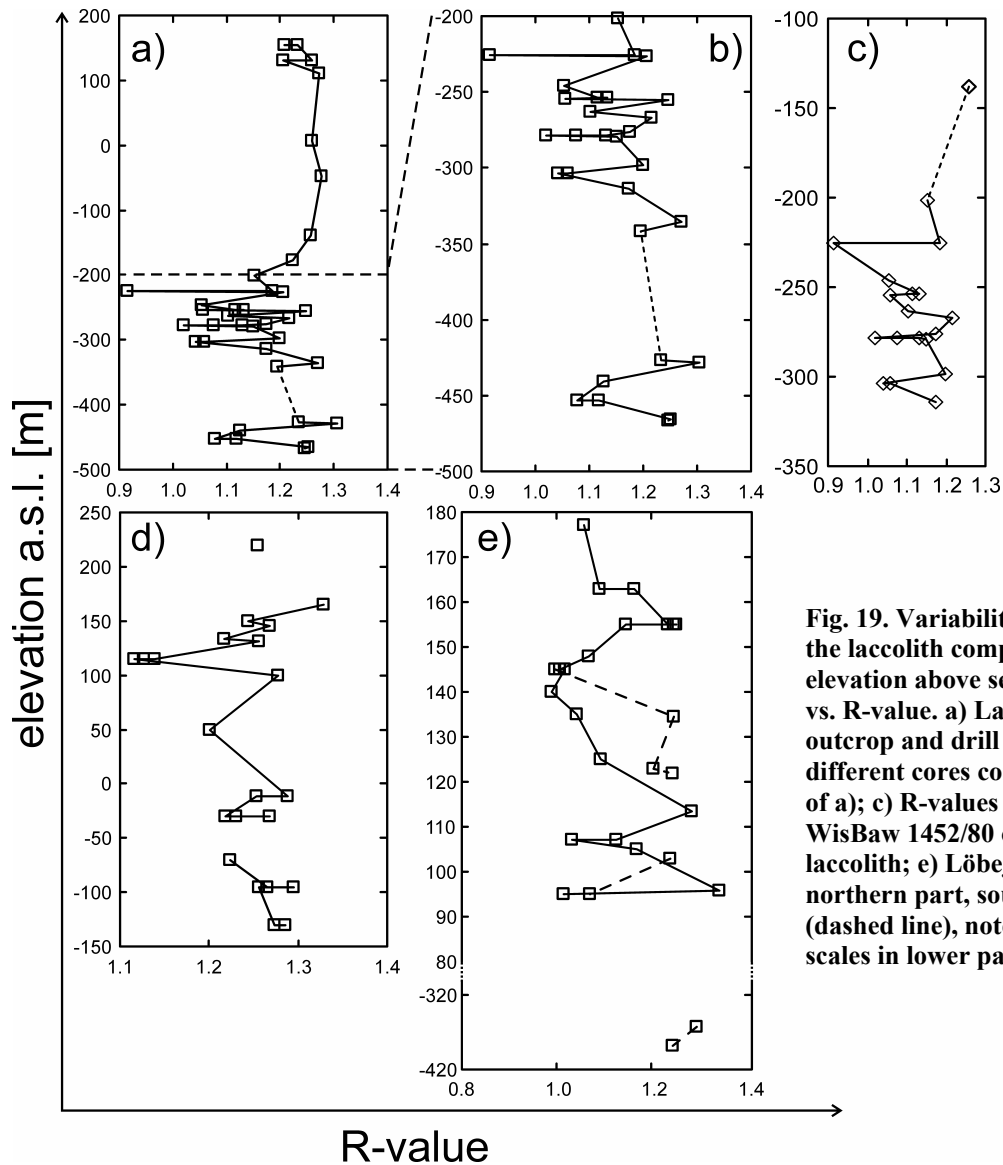


Fig. 19. Variability of R-values in the laccolith complexes. Sample elevation above sea level is plotted vs. R-value. a) Landsberg laccolith, outcrop and drill core samples from different cores combined; b) detail of a); c) R-values from drill core WisBaw 1452/80 only; d) Petersberg laccolith; e) Löbejün laccolith, northern part, southern part (dashed line), note different depth scales in lower part.

Several magmatic pulses are suggested for each part of the Löbejün laccolith, if samples are examined according to their position (Fig. 15), whereas, plotting all Löbejün samples together, no clear picture is revealed (Fig. 15c). Similar batch-wise intrusion is proposed for the Landsberg laccolith (Figs. 15, 19). Additionally, marginal facies is detected in normalized CSD parameters (Fig. 16). Increased marginal nucleation leads to a higher number of crystals, while mean size due to large inherited crystals remains similar compared to the rest of the intrusion, especially, without significant flow sorting. SDP plots (Fig. 19) also suggest intrusion by subsequent magma batches. R-value can reveal changes in spatial arrangement of grains. Jerram et al. (1996) showed increasing R-values coupled with decreasing groundmass proportion due to compaction, overgrowth leading to a less pronounced decrease in

groundmass proportion with a slight increase in R-value and grain size sorting causing larger R-values and higher groundmass proportions.

Clearly, phenocryst populations of the Halle laccoliths are not subject to major compaction processes because of high magma viscosities. Neither do they form touching frameworks (Mock & Jerram submitted). Spread on R-value vs. groundmass plots (Fig. 17) might be interpreted by sorting processes within the intruding magma. Some samples show low R-values corresponding to poorly sorted crystal populations unaffected by magmatic flow in discrete shear bands. More sorted samples stem from zones more affected by magmatic flow and situated between two magma batches (see Mock et al. 2003). Several boundaries between intrusive batches can be proposed (Figs. 2, 19). SDP data agree well with distribution of characteristic lengths (Fig. 15) and interpretation of flow structures. In the upper part of the Petersberg laccolith (Fig. 3), complex flow structures indicate interference of several batches. Potentially, this laccolith is only one intrusion of an even larger complex (Fig. 2). Similarly, the Wettin laccolith shows a bowl and cupola arrangement of flow structures converging at batch boundaries. Generally, flow structures are less complex here than in the Petersberg laccolith (see also Exner 1998; Mock et al. 1999). Elsewhere, many laccolith complexes also show complex zonation and intrusion patterns (e.g. Rocchi et al. 2002).

time frame for the whole laccolith complex from radiometric dating:

21 Ma for all laccoliths (including standard deviations)

15 Ma without oldest precursor (Schwerz)

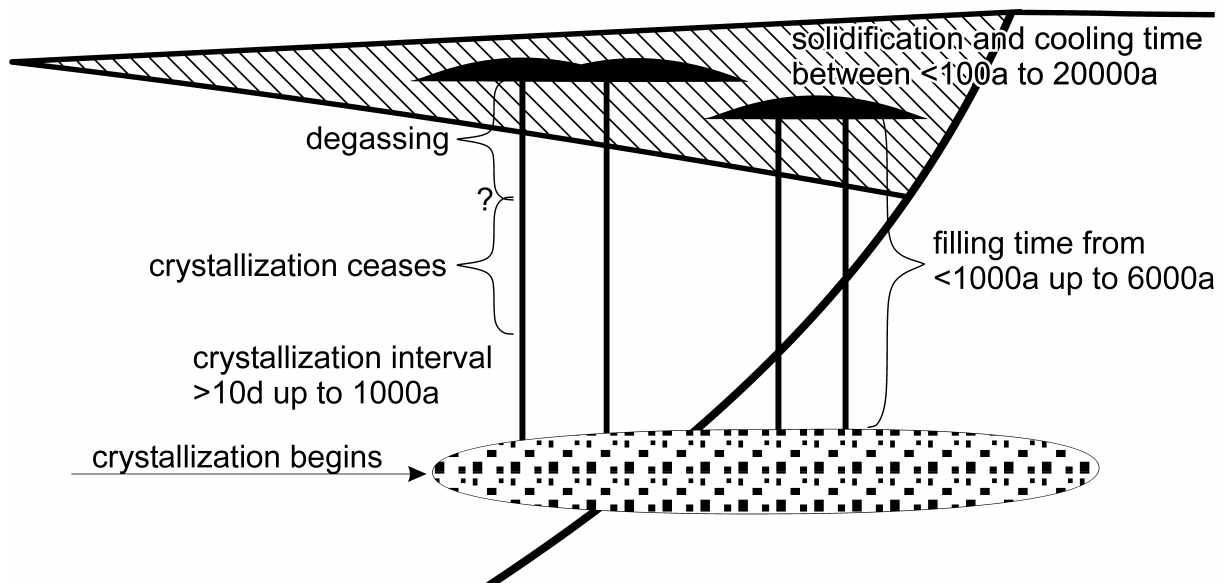


Fig. 20. Sketch of the upper part of the magmatic plumbing system of the Halle laccoliths. Timescales investigated and discussed in this study are indicated. See text for further discussion.

Ascent, emplacement, crystal growth: a volatile perspective

A position of the upper crustal magma chamber – reservoir for the HVC laccoliths (Breitkreuz & Mock in press) – is constrained by basement xenoliths (gneisses, amphibolite) below the basement/Rotliegend boundary. Granitic xenoliths might be remnants of solidified parts of the magma chamber. Phenocryst crystallization starts in the magma reservoir or even deeper in the magmatic plumbing system ceasing at some stage during ascent as suggested by constraints given by the magma's degassing history (Fig. 20).

In order not to erupt explosively, silicic magma needs to degas sufficiently during ascent (Eichelberger et al. 1986). Fragmented quartz phenocrysts strongly indicate early, rapid but non-explosive degassing (Fig. 4). Volatiles were able to escape into unconsolidated basin sediments. Because of high viscosity and sluggish magmatic flow, fragments of crystals were not separated and partly annealed as shown by different extinction angles of respective fragments (Fig. 4). Elevated volatile contents of the early magma in melt inclusion data (Fig. 12, Tab. 2) strongly support early degassing, because they are not found in the rhyolitic laccoliths today (Romer et al. 2001). Thus, shallow emplacement is advocated, because pathways for volatiles away from the magma are to be the more efficient the shallower degassing takes place. Confinement of volatiles in the magma until a very late stage of ascent would lead either to fragmentation of the magma and its explosive eruption or to eruption of the magma as a lava dome or flow. Thus, the magma must have been degassed prior to emplacement.

Ascent, emplacement and crystallization are relatively rapid processes as suggested by model calculations limiting time available for degassing. Moreover, degassing must take place after considerable crystal growth because of the size of broken phenocrysts and post-degassing or post-emplacement phenocryst growth would lead to more annealing and overgrowth than observed. The exact limit where crystallization ceases and degassing begins is not well constrained (Fig. 20).

Solidification and filling model calculations give a slightly wider time frame for laccolith formation than crystallization. Therefore, formation of phenocryst populations is not limited by laccolith formation. Radiometric dates, at last, render the intrusion of each laccolith or laccolith complex (the units discussed above) a mere ephemeral episode in the active time of intrusive magmatism in the HVC (Fig. 20).

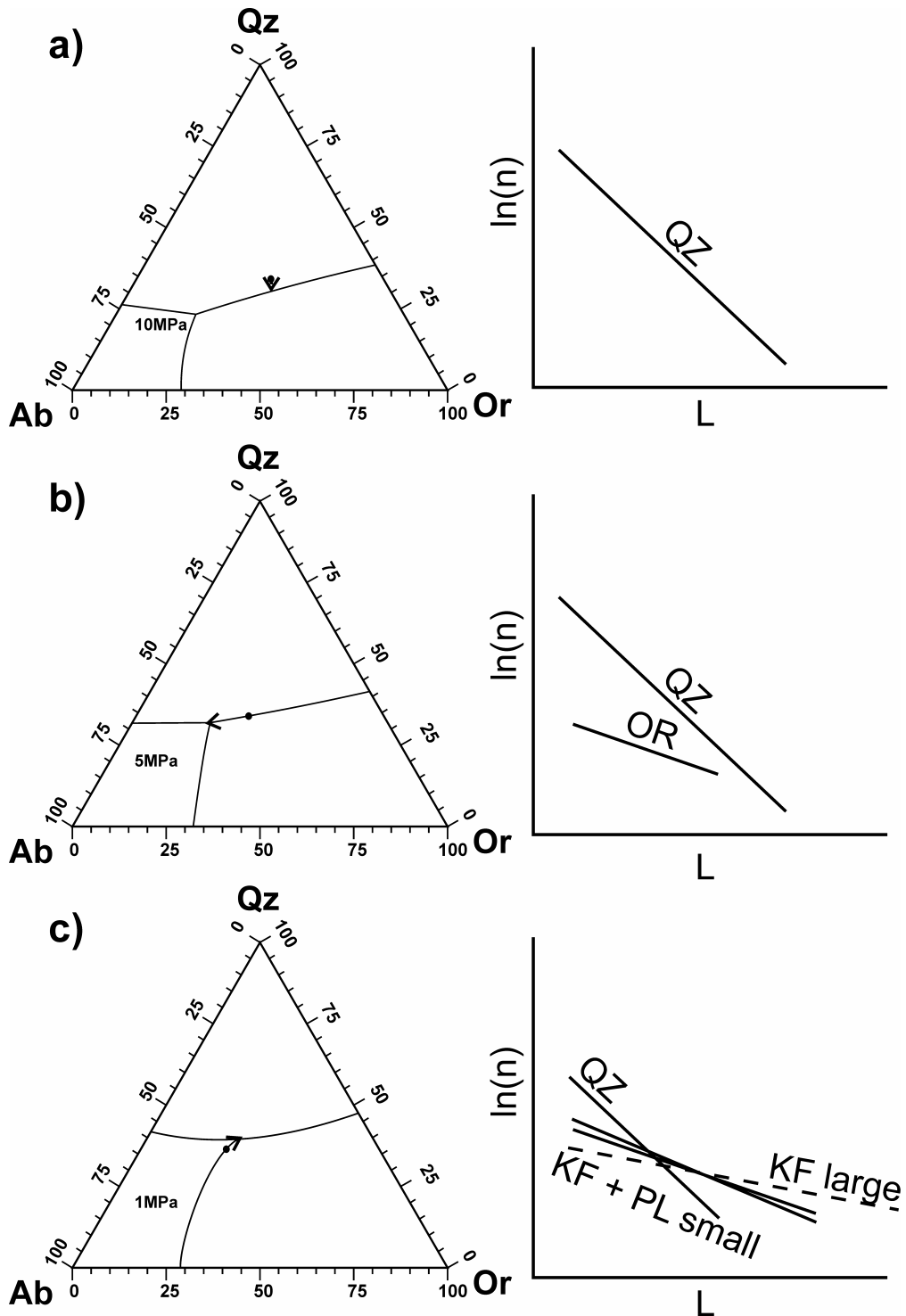
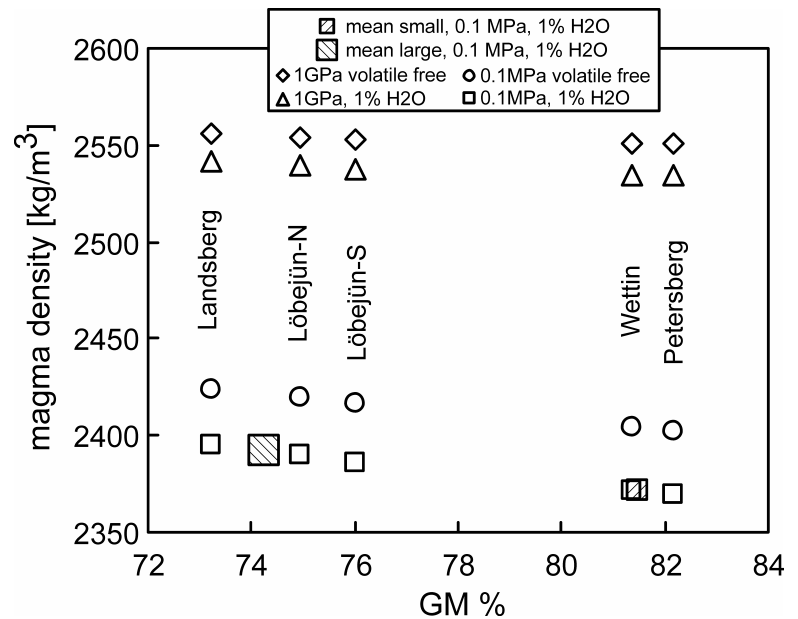


Fig. 21. a) Beginning of crystallization. For a normative composition of the Halle laccoliths (Romer et al. 2001), only quartz crystallizes initially in the upper crustal magma chamber, producing a simple CSD (right). b) After tapping of the magma chamber, quartz and alkali feldspar phase nucleate and grow simultaneously until after a short amount of ascent, quartz ultimately ceases to crystallize and begins resorption. Cotectic line between quartz and alkali feldspar moves away from the liquid composition due to ongoing rapid pressure release. Thus, only orthoclase crystallizes for a while. c) After yet further ascent (pressure release), the liquid composition meets the cotectic line separating the two feldspar phases. These can now crystallize simultaneously. It is the duration of this stage that discriminates the two textural varieties of rhyolitic laccoliths in the HVC. Cotectic lines according to Johannes & Holtz (1996).

Fig. 22. Magma density vs. groundmass proportion of the Halle laccoliths. Magma densities are calculated from mean modal abundances of felsic phenocrysts in each unit (two main crystal size varieties) and densities of phenocryst phases (from Deer et al. 1992). Density of rhyolitic melt from Spera (2000). Density contrast between magmas at shallow and deep levels is between 100 and 150 kg/m³, between 17 and 20 kg/m³ for means of two size varieties and span around 25 kg/m³ for the different units. Density contrasts are more pronounced at shallower levels.



Conclusions

Reviews of existing literature, new qualitative petrographic observations on different scales and detailed quantitative petrographic data of phenocryst populations in rhyolitic laccoliths of the Permocarbiniferous Halle Volcanic Complex were presented, interpreted and complemented by published and unpublished geochemical data with the following conclusions:

- Contact aureoles of laccoliths are negligible. The contacts of laccoliths are sharp and contact zones thin. Jigsaw-fit breccias dominate. Peperitic (?) and sheared contacts are found. Small crystal units exhibit complex flow foliation structures (bowl and cupola shapes), but lack similarity with lithologies found in rhyolite lavas confirming the intrusive character of the laccoliths. Margins of laccoliths suggest a batch-wise or finger-like intrusion.
- CSDs of felsic phenocrysts are very straight suggesting a simple crystallization history, only contradicted by complex shapes. Characteristic lengths range from 3.42 to 36 mm. Straight CSDs might potentially be the result of complex variations of growth and nucleation rates.
- Phenocrysts are generally randomly distributed with a trend towards clustered arrangements for large crystal rhyolites. Some samples reach the field for touching frameworks (characteristic K-feldspar phenocryst sizes >20 mm), but this result

cannot be supported by qualitative observation. R-values range from 1.34 to 0.78. Phenocryst crystallinities range from 10 to 30% with some rare exceptions being more crystalline.

- Textural rhyolite varieties are distinguished according to size of K-feldspar phenocrysts and phenocryst crystallinity. Varieties developed relatively late in magmatic evolution between tapping of an upper crustal magma chamber and emplacement at very shallow levels. Due to different crystallinities, the two main varieties as well as individual units had a density contrast of up to ~1% causing different emplacement levels of 10s of metres. Viscosity contrasts and CSDs might cause a positive feedback effect on the evolution of these differences.
- CSD and SDP analysis of phenocryst textures revealed internal structures within the laccoliths. Structures are interpreted as boundaries between distinct magma batches forming the intrusions and a marginal facies not immediately obvious from the coherent samples. These structures have not been recognized previously.
- Timescales of formation of the laccoliths range from several million years (radiometric dating) to between 100 and 10,000 a (cooling and filling of the volume of rhyolitic magma) down to between 10 days and 1000 a for phenocryst populations to crystallize (CSD data).

Acknowledgements

Intensive cooperation with M. Schwab is thankfully acknowledged. Discussions with W. Knoth, I. Rappsilber, J. Luge and the late R. Kunert and H. K. Löffler contributed to our understanding of the HVC. The staff at the Landesamt für Geologie und Bergwesen, Sachsen-Anhalt in Halle are thanked for access and sampling permits of the drill cores, M. Magnus and his staff for sample preparation and help with the image analysis. Rainer Thomas (GFZ) is thanked for measurements of melt inclusions. T. Lohr, J. Neff, S. Henkel, U. Wnorowska and other student assistants help with the determination of the quantitative petrographic data. Their help is thankfully acknowledged. This study profited from fruitful discussion with D. Jerram and S. Egenhoff. A number of German Research Council (DFG) grants provided support since 1995.

References

- Anthes, G. & Reischmann, T. (2001): Timing of granitoid magmatism in the eastern mid-German crystalline rise. - *J. Geodyn.*, **31**: 119-143.
- Arthaud, F. & Matte, P. (1977): Late Paleozoic strike-slip faulting in southern Europe and Northern Africa: results of right-lateral shear zone between the Appalachians and the Urals. - *Geol. Soc. Am. Bull.*, **88**: 1305-1320.
- Awdankiewicz, M. (1998): Volcanism in a late Variscan intramontane trough: Carboniferous and Permian volcanic centres of the Intra-Sudetic Basin, SW Poland. - *Geologia sudetica*, **32(1)**: 13-47.
- Bates, R. L. & Jackson, J. A. (1987): *Glossary of Geology*. 788 S. Alexandria, Virginia (American Geological Institute).
- Beyschlag, F. & Fritsch, K. (1899): Das jüngere Steinkohlengebirge in der Provinz Sachsen und den angrenzenden Gebieten. - *Abh. Preus. Geol. LA*, **10**.
- Billings, M. P. (1974): *Structural Geology*. 606 S. Englewood Cliffs (Prentice-Hall Inc.).
- Bindeman, I. N. (2003): Crystal sizes in evolving silicic magma chambers. - *Geology*, **31(4)**: 367-370.
- Brecht, G. (1999): Authigene Phyllosilikate in permokarbonen SiO₂-reichen Vulkaniten Ostdeutschlands. - *Berliner geowissenschaftliche Abhandlungen*, **A201**: 1-181.
- Breitkreuz, C., Exner, M. & Schwab, M. (1998): Quantitative Erfassung des Platznahme- und Kristallisationsgefüges rhyolithischer Lakkolithe am Beispiel des oberkarbonen Wettiner Porphyrs bei Halle/S. - *Terra Nostra*, **98/2**: 34-36.
- Breitkreuz, C. & Kennedy, A. (1999): Magmatic flare-up at the Carboniferous/ Permian boundary in the NE German Basin revealed by SHRIMP zircon ages. - *Tectonophysics*, **302(3-4)**: 307-326.
- Breitkreuz, C. & Mock, A. (in press): Are laccolith complexes characteristic of transtensional basin systems? - Examples from Permocarboniferous Central Europe. - *In*: Breitkreuz, C. &

- Petford, N. (eds.) Physical geology of high-level magmatic systems. London (Geological Society London) Special Publications,
- Büchner, C. & Kunert, R. (1997): Pyroklastische Äquivalente der intrusiven Halleschen Rhyolithe. - *Mitt. Geol. Sachsen-Anhalt*, **3**: 37-57.
- Burkhard, D. J. M. (2002): Kinetics of crystallization: example of micro-crystallization in basalt lava. - *Contrib. Mineral. Petrol.*, **142**: 724-737.
- Candelas Moro, M., Cembranos, M. K. & Fernandez, A. (2001): Celsian, (Ba,K)-feldspar and cymrite from sedex barite deposits of Zamora, Spain. - *Can. Mineral.*, **39(4)**: 1039-1051.
- Cashman, K. V. (1992): Groundmass crystallization of Mount St. Helens dacite 1980-1986: a tool for interpreting shallow magmatic processes. - *Contrib. Mineral. Petrol.*, **109**: 431-449.
- Cashman, K. V. (1993): Relationship between plagioclase crystallization and cooling rate in basaltic melts. - *Contrib. Mineral. Petrol.*, **113(1)**: 126-142.
- Cashman, K. V. & Marsh, B. D. (1988): Crystal Size Distribution (CSD) in rocks and the kinetics and dynamics of crystallization II: Makaopuhi lava lake. - *Contrib. Mineral. Petrol.*, **99**: 292-305.
- Castro, J. M. & Cashman, K. V. (1999): Constraints on rheology of obsidian lavas based on mesoscopic folds. - *J. Struct. Geol.*, **21**: 807-819.
- Castro, J. M., Cashman, K. V. & Manga, M. (2003): A technique for measuring 3D crystal-size distributions of prismatic microlites in obsidian. - *Amer. Mineral.*, **88(8-9)**: 1230-1240.
- Christiansen, R. L. & Hildreth, W. (1989): Voluminous rhyolitic lavas of broad extent on the Yellowstone Plateau. IAVCEI General Assembly, Santa Fe, USA, 52.
- Corry, C. E. (1988): Laccoliths; Mechanics of emplacement and growth. - Geological Society of America Special Paper, **220**, 110 S. Boulder, Colorado (Geological Society of America).
- Cruden, A. R. (1998): On the emplacement of tabular granites. - *J. Geol. Soc. London*, **155**: 853-862.

- Cruden, A. R. & McCaffrey, K. J. W. (2002): Different scaling laws for sills, laccoliths and plutons: Mechanical thresholds on roof lifting and floor depression. First International Workshop: Physical Geology of Subvolcanic Systems - Laccoliths, Sills, and Dykes (LASI), Freiberg, Technische Universität Bergakademie Freiberg, Institut für Geologie, 15-17.
- Deer, W. A., Howie, R. A. & Zussman, J. (1992): The Rock Forming Minerals. 696 S. Harlow (Longman).
- Delesse, M. A. (1848): Procédé mécanique pour déterminer la composition des roches. - Annales des Mines, **13**: 379-388.
- Dixon, J. M. & Simpson, D. G. (1987): Centrifuge modelling of laccolith intrusion. - J. Struct. Geol., **9(1)**: 87-103.
- Dockstader, D. R., Muller, O. H., Pollard, D. D. & Cosgrove, J. W. (1973): Fluid Instability as a Mechanism for the Formation of "Fingers" on a Sill Periphery. - EOS, Trans. Amer. Geophys. Union, **54(4)**: 461.
- Eberl, D., Kile, D. E. & Drits, V. A. (2002): On geological interpretations of crystal size distributions: Constant vs. proportionate growth. - Amer. Mineral., **87(8-9)**: 1235-1241.
- Eichelberger, J. C., Carrigan, C. R., Westrich, H. R. & Price, R. H. (1986): Non-explosive silicic volcanism. - Nature, **323**: 598-602.
- Eigenfeld, F. & Schwab, M. (1974): Zur geotektonischen Stellung des permosilesischen subsequenten Vulkanismus in Mitteleuropa. - Zeitschrift für Geologische Wissenschaften, **2(2)**: 115-137.
- Exner, M. (1998): Kartierung des Verbreitungsgebietes des Wettiner Rhyolithes und seines näheren Umfeldes. Diplomkartierung, Martin-Luther-Universität Halle.
- Fink, J. H. (1987): The Emplacement of Silicic Domes and Lava Flows. - Spec. Pap. Geol. Soc. Amer., **212**: 103-111.

- Fink, J. H. & Anderson, S. W. (2000): Lava domes and coulees. - *In*: Sigurdsson, H., Houghton, B. F., McNutt, S. R., Rymer, H., Stix, J. & Ballard, R. (eds.) Encyclopedia of volcanoes. San Diego (Academic Press) 307-319.
- Finney, J. L. (1970): The geometry of random packing. - Proceedings of the Royal Society of London, Series A, **319**: 479-493.
- Gädeke, R. (1960): Beiträge zur Petrographie der porphyrischen Gesteine in Mitteldeutschland. - Wissenschaftliche Zeitschrift der Martin-Luther-Universität Halle-Wittenberg, **9**: 115-128.
- Geißler, M. (2002): Sedimentäre und vulkanische Lithofaziestypen eines permokarbonen Beckensystems im NE von Halle/S. - Ein typisches Beispiel für die Halle Formation? Sediment 2002, Darmstadt, DGG, 70.
- German-Stratigraphic-Commission (2002). Stratigraphic Table of Germany, Deutsche Stratigraphische Kommission.
- Haase, E. (1938): Die hallischen Porphyre. - Jahrbuch des Halleschen Verbandes, N. F., **16**: 77-116.
- Haase, E. (1943): Die Porphyrite von Löbejün. - Nova Acta Leopoldina, **12(85)**: 281-336.
- Hafermalz, H.-J., Knoth, W. & Löffler, H.-K. (1980): Granit als Xenolith im feinkristallinen Porphyr vom Petersberg nördlich Halle. - Zeitschrift für Geologische Wissenschaften, **8(11)**: 1449-1459.
- Hammer, J. E., Cashman, K. V., Hoblitt, R. P. & Newman, S. (1999): Degassing and microlite crystallization during pre-climactic events of the 1991 eruption of Mt. Pinatubo, Philippines. - Bull. Volcanol., **60(5)**: 355-380.
- Haneke, J. (1987): Der Donnersberg. - Pollichia-Buch, **10**, 147 S. Bad Dürkheim (Pfalzmuseum für Naturkunde).

- Hawkesworth, C. J., Blake, S., Evans, P., Hughes, R., MacDonald, R., Thomas, L. E., Turner, S. P. & Zellmer, G. (2000): Time scales of crystal fractionation in magma chambers; integrating physical, isotopic and geochemical perspectives. - *J. Petrol.*, **41(7)**: 991-1006.
- Henk, A. (1997): Gravitational orogenic collapse vs plate-boundary stresses: a numerical modelling approach to the Permo-Carboniferous evolution of Central Europe. - *Geol. Rundschau*, **86(1)**: 39-55.
- Higgins, M. D. (1996a): Crystal size distributions and other quantitative textural measurements in lavas and tuff from Egmont Volcano (Mt. Taranaki), New Zealand. - *Bull. Volcanol.*, **58**: 194-204.
- Higgins, M. D. (1996b): Magma dynamics beneath Kameni Volcano, Thera, Greece, as revealed by crystal size and shape measurements. - *J. Volcan. Geotherm. Res.*, **70(1-2)**: 37-48.
- Higgins, M. D. (1998): Origin of anorthosite by textural coarsening: quantitative measurements of a natural sequence of textural development. - *J. Petrol.*, **39**: 1307-1323.
- Higgins, M. D. (1999a): Origin of megacrysts in granitoids by textural coarsening: A crystal size distribution (CSD) study of microcline in the Cathedral Peak Granodiorite, Sierra Nevada, California. - *In*: Castro, A., Fernández, C. & Vigneresse, J. L. (eds.) *Understanding granites: Integrating new and classical techniques*. London (The Geological Society of London) Special Publications, 207-219.
- Higgins, M. D. (1999b): The Role of Textural Coarsening (Ostwald Ripening) in the Solidification of the Kiglapait Intrusion: A Crystal Size Distribution (CSD) Approach. EUG 10, Strasbourg, Cambridge Publications, 684.
- Higgins, M. D. (2000): Measurement of crystal size distributions. - *Amer. Mineral.*, **85(9)**: 1105-1116.
- Higgins, M. D. (2002): Closure in crystal size distribution (CSD), verification of CSD calculations and the significance of CSD fans. - *Amer. Mineral.*, **87**: 160-164.

- Higgins, M. D. & Roberge, J. (2003): Crystal Size Distribution of Plagioclase and Amphibole from Soufrière Hills Volcano, Montserrat: Evidence for Dynamic Crystallization-Textural Coarsening Cycles. - *J. Petrol.*, **44(8)**: 1401-1411.
- Jacobs, J. & Breitzkreuz, C. (2003): Zircon and apatite fission-track thermochronology of Late Carboniferous volcanic rocks of the NE German Basin. - *Int J Earth Sciences*, **92(2)**: 165-172.
- Jerram, D. A., Cheadle, M. C. & Philpotts, A. R. (2003): Quantifying the Building Blocks of Igneous Rocks: Are Clustered Crystal Frameworks the Foundation? - *J. Petrol.*, **44(11)**: 2033-2051.
- Jerram, D. A. & Cheadle, M. J. (2000): On the cluster analysis of grains and crystals in rocks. - *Amer. Mineral.*, **85**: 47-67.
- Jerram, D. A., Cheadle, M. J., Hunter, R. H. & Elliott, M. T. (1996): The spatial distribution of grains and crystals in rocks. - *Contrib. Mineral. Petrol.*, **125**: 60-74.
- Johannes, W. & Holtz, F. (1996): Petrogenesis and experimental petrology of granitic rocks. - *Minerals and Rocks*, 335 S. Berlin (Springer).
- Kampe, A., Luge, J. & Schwab, M. (1965): Die Lagerungsverhältnisse in der nördlichen Umrandung des Löbejüner Porphyrs bei Halle (Saale). - *Geologie*, **14**: 26-46.
- Kampe, A. & Remy, W. (1960): Mitteilungen zur Stratigraphie im Raume des Petersberges bei Halle. - *Montanwissenschaftliche Berichte - Deutsche Akademie der Wissenschaften*, Berlin, **2**: 364-374.
- Kelch, H. (1963): Mineralogisch-petrographische Untersuchungen am Rhyolith Typ Hohnsdorf nördlich Halle/S. - *Geologie*, **12(4)**: 401-438.
- Kerr, A. D. & Pollard, D. D. (1998): Toward more realistic formulations for the analysis of laccoliths. - *J. Struct. Geol.*, **20(12)**: 1783-1793.
- Kile, D. E. & Eberl, D. D. (2003): On the origin of size-dependent and size-independent crystal growth: Influence of advection and diffusion. - *Amer. Mineral.*, **88(10)**: 1514-1521.

- Klaus, D. (1964): Neue endogene Kontakte aus dem Westteil des Halleschen Porphyrkomplexes. - Berichte der Geologischen Gesellschaft der DDR, **9(2)**: 259-267.
- Knesel, K. M., Davidson, J. P. & Duffield, W. A. (1999): Evolution of silicic magma through assimilation and subsequent recharge; evidence from Sr isotopes in sanidine phenocrysts, Taylor Creek Rhyolite, NM. - J. Petrol., **40(5)**: 773-786.
- Knoth, W., Kriebel, U., Radzinski, K.-H. & Thomae, M. (1998): Die geologischen Verhältnisse von Halle und Umgebung. - Hall. Jb. Geowiss. B(**Beiheft 4**): 7-34.
- Koch, R. A. (1966): Die kombinierte Paläovulkananalyse des Petersberger Quarzporphyrmassivs nördlich Halle/S. - Geophys. Geol. Z. Leipzig, **9**: 67-88.
- Koch, R. A. (1967a): Kontakterscheinungen zwischen Petersberger Quarzporphyr und seinem Nebengestein. - Gesell. Geol. Wiss. Ber. B, **12(4)**: 417-427.
- Koch, R. A. (1967b): Zur Petrographie und Mineralogie des Petersberger Quarzporphyrs. - Gesell. Geol. Wiss. Ber. B, **12(3)**: 267-278.
- Koch, R. A. (1979): Zum Problem der Genese der schwarz-, grau- und grügefärbten Quarzprophyre im Halleschen Eruptionsgebiet. - Hall. Jb. Geowiss., **4**: 29-44.
- Koch, R. A. (1981): Die Großxenolithe im großkristallinen Quarzporphyr des Galgenberges von Halle (Saale). - Hall. Jb. Geowiss., **6**: 105-106.
- Koch, R. A. & Fischer, K. (1961): Die Bedeutung eines Gneiseinschlusses im großkristallinen Quarzporphyr von Löbejün. - Geologie, **10(1)**: 81-89.
- Krauß, G. (1999): Die Geologie im Raum Schwerz-Quetzdölsdorf (bei Halle/Saale). Diplomkartierung, Martin-Luther-Universität Halle.
- Kretz, R. (1969): On the spatial distribution of crystals in rocks. - Lithos, **2(1)**: 39-65.
- Kunert, R. (1978): Zur Platznahme rhyolithischer Laven. - Zeitschrift für Geologische Wissenschaften, **6(9)**: 1145-1160.
- Kunert, R. (1995): Die Lithostratigraphie der Rotliegend-Schichten in der nördlichen Saalesenke bei Halle. - Mitt. Geol. Sachsen-Anhalt, **1**: 69-84.

- Lange, D. (2000): Geophysikalisch-geologische Untersuchung und dreidimensionale Modellierung des Halleschen Porphyrkomplexes. MSc (Diplom), FU Berlin.
- Lasaga, A. C. (1982): Toward a master equation in crystal growth. - *Am. J. Sci.*, **282(10)**: 1264-1288.
- Laspeyres, H. (1864): Beitrag zur Kenntnis der Porphyre und petrographische Beschreibung der quarzführenden Porphyre in der Umgegend von Halle an der Saale. - *Z. dt. geol. Ges.*, **16**: 367-460.
- Laspeyres, H. (1875): Geognostische Darstellung des Steinkohlegebirges in der Gegend nördlich von Halle an der Saale. - *Abhandlungen der Preußischen Geologischen Landesanstalt* S. Berlin (Preußische Geologische Landesanstalt).
- Löffler, H. K. (1979): Die Petrographie der Porphyr/Porphyr-Kontakte, die Altersfolge der Porphyre am Windmühlenberg südwestlich von Schwerz und die Porphyre des Quetzer Berges. - *Hall. Jb. Geowiss.*, **4**: 55-68.
- Löffler, H. K. (1983): Die Grundmassen der sauren Eruptivgesteine des Halleschen Paläovulkanit-Komplexes und die Ursache ihrer Verschiedenheit. - *Hall. Jb. Geowiss.*, **8**: 31-42.
- Löffler, H.-K. (1986): Genetische und vulkanologische Betrachtungen an Hand petrographischer Studien an Mineralen der sauren Ergußgesteine des Halleschen Paläovulkanit-Komplexes. - *Hall. Jb. Geowiss.*, **11**: 95-104.
- Löffler, H. K. & Seydewitz, H. J. (1983): Petrographie und Petrochemie der sauren Vulkanite und Subvulkanite im östlichen Teil des Halleschen Paläovulkanit-Komplexes. - *Zeitschrift für Geologische Wissenschaften*, **11**: 579-602.
- Lorenz, V. & Haneke, J. (in press): Relationship between diatremes, dykes, sills, laccoliths, intrusive-extrusive domes, lava flows, and tephra deposits with unconsolidated water-saturated sediments in the Late Variscan intermontane Saar-Nahe-Basin, SW Germany. - *In*:

- Breitkreuz, C. & Petford, N. (eds.) Physical geology of high-level magmatic systems. London (Geological Society of London) Special Publications,
- Lorenz, V. & Nicholls, I. A. (1984): Plate and intraplate processes of Hercynian Europe during the Late Paleozoic. - *Tectonophysics*, **107**: 25-56.
- Manickam, O. & Homsy, G. M. (1994): Simulation of viscous fingering in miscible displacements with nonmonotonic viscosity profiles. - *Phys. Fluids*, **6(1)**: 95-107.
- Marschallinger, R. (1997): Automatic mineral classification in the macroscopic scale. - *Comput. Geosci.*, **23(1)**: 119-126.
- Marsh, B. D. (1998): On the interpretation of crystal size distributions in magmatic systems. - *J. Petrol.*, **39(4)**: 553-599.
- Marsh, B. D. & Higgins, M. D. (2002): Inherited Correlation in Crystal Size Distribution - Comment. - *Geology*, **30(3)**: 284-285.
- McCaffrey, K. J. W. & Cruden, A. R. (2002): Dimensional Data and Growth Models for Intrusions. First International Workshop: Physical Geology of Subvolcanic Systems - Laccoliths, Sills, and Dykes (LASI), Freiberg, Technische Universität Bergakademie Freiberg, Institut für Geologie, 37-39.
- McCaffrey, K. J. W. & Petford, N. (1997): Are granitic intrusions scale invariant? - *J. Geol. Soc. London*, **154(Part 1)**: 1-4.
- McPhie, J. (1993): The Tennant Creek porphyry revisited: A synsedimentary sill with peperite margins, Early Proterozoic, Northern Territory. - *Austral. J. E.S.*, **40**: 545-558.
- McPhie, J., Doyle, M. G. & Allen, R. L. (1993): *Volcanic Textures*. 198 S. Hobart, Tasmania (CODES Key Centre, University of Tasmania).
- Minakami, T., Ishikawa, T. & Yagi, K. (1951): The 1944 eruption of Volcano Usu in Hokkaido, Japan. - *Volcanological Bulletin*, **11**: 5-157.

- Mock, A., Exner, M., Lange, D., Breitzkreuz, C., Schwab, M. & Ehling, B.-C. (1999):
Räumliche Erfassung des Fließgefüges der kleinporphyrischen Lakkolithe im Halle-Vulkanit-
Komplex. - Mitt. Geol. Sachsen-Anhalt, **5**: 169-175.
- Mock, A. & Jerram, D. A. (submitted): Crystal size distributions in three dimensions: insights
from the 3D reconstruction of a highly porphyritic rock texture. - Earth Planet. Sci. Lett.
- Mock, A., Jerram, D. A. & Breitzkreuz, C. (2003): Using quantitative textural analysis to
understand the emplacement of shallow level rhyolitic laccoliths - a case study from the Halle
volcanic complex, Germany. - J. Petrol., **44(5)**: 833-849.
- Morgan, S. S., Law, R. D. & Nyman, M. W. (1998): Laccolith-like emplacement model for
the Papoose Flat Pluton based on porphyroblast-matrix analysis. - Geol. Soc. Am. Bull.,
110(1): 96-110.
- Neumann, E.-R., Olsen, K. H., Baldrige, W. S. & Sundvoll, B. (1992): The Oslo Rift: a
review. - Tectonophysics, **208**: 1-18.
- Nickel, E., Kock, H. & Nungässer, W. (1967): Modellversuche zur Fließregelung in
Graniten. - Schweiz. Mineral. Petrgraph. Mitt., **47**: 399-497.
- Oncken, O. (1997): Transformation of a magmatic arc and an orogenic root during oblique
collision and its consequences for the evolution of the European Variscides (Mid-German
Crystalline Rise). - Geol. Rundschau, **86(1)**: 2-20.
- Pan, Y. (2001): Inherited correlation in crystal size distribution. - Geology, **29(3)**: 227-230.
- Pan, Y. (2002a): Inherited Correlation in Crystal Size Distribution - Reply. - Geology, **30(3)**:
283-284.
- Pan, Y. (2002b): Inherited Correlation in Crystal Size Distribution - Reply. - Geology, **30(3)**:
285-286.
- Petford, N., Cruden, A. R., McCaffrey, K. J. W. & Vigneresse, J. L. (2000): Granite magma
formation, transport and emplacement in the Earth's crust. - Nature, **408(6813)**: 669-673.

- Petford, N., Lister, J. R. & Kerr, R. C. (1994): The ascent of felsic magmas in dykes. - *Lithos*, **32(1-2)**: 161-168.
- Philpotts, A. R. (1990): *Principles of Igneous and Metamorphic Petrology*. 498 S. Upper Saddle River, N.J. (Prentice Hall).
- Plögert, I., Tomaschewski, M., Geißler, M., Breitzkreuz, C., Ehling, B.-C. & Hartkopf-Froeder, C. (2001): Sedimentation und Vulkanismus in einem subtropischen terrestrischen Beckensystem: Oberkarbonische Abfolgen in Bohrungen östlich von Halle/S. *Sediment* 2001, Jena, DGG, 77.
- Rocchi, S., Westerman, D. S., Dini, A., Innocenti, F. & Tonarini, S. (2002): Two-stage growth of laccoliths at Elba Island, Italy. - *Geology*, **30(11)**: 983-986.
- Röllig, G. & Schirmer, B. (1978): Zum Stoffbestand der subsequenten variszischen Vulkanite im Südteil der DDR. - *Zeitschrift für Geologische Wissenschaften*, **6(9)**: 1101-1118.
- Roman Berdiel, T., Gapais, D. & Brun, J. P. (1995): Analogue models of laccolith formation. - *J. Struct. Geol.*, **17(9)**: 1337-1346.
- Romer, R., Förster, H.-J. & Breitzkreuz, C. (2001): Intracontinental extensional magmatism with a subduction fingerprint: the late Carboniferous Halle Volcanic Complex (Germany). - *Contrib. Mineral. Petrol.*, **141(1)**: 201-221.
- Rudashevsky, N. S., Burakov, B. E., Lupal, S. D., Thalhammer, A. R. & Saini-Eidukat, B. (1995): Liberation of accessory minerals from various rock types by electric-pulse disintegration- method and application. - *Transactions of the Institution of Mining and Metallurgy*, **104**: C25-29.
- Rüffer, T., Brecht, G. & Breitzkreuz, C. (1998): Seesedimente im Bereich des Halleschen Lakkolith-Komplexes: ein permisches Gilbert-Delta. *Sediment '98*, Erlangen, Institut für Geologie der Friedrich-Alexander-Universität Erlangen-Nürnberg, 84.
- Schaeben, H., Boogaart, G. v. d., Mock, A. & Breitzkreuz, C. (2002): Inherited Correlation in Crystal Size Distribution - Comment. - *Geology*, **30(3)**: 282-283.

- Schneider, J. W. (1996): Biostratigraphie des kontinentalen Oberkarbon und Perm im Thüringer Wald, SW-Saale-Senke - Stand und Probleme. - Beitr. Geol. Thür., **3**: 121-151.
- Schneider, J. W., Rössler, R. & Gaitzsch, B. (1994): Time lines of the Late Variscan volcanism - a holostratigraphic synthesis. - Zbl. Geol. Paläont., **5/6**: 477-490.
- Schneider, J. W., Schretzenmayr, S. & Gaitzsch, B. (1998): Excursion Guide Rotliegend Reservoirs at the Margin of the Southern Permian Basin. - Leipzig. Geowiss., **7**: 15-44.
- Schulz, J. (1936): Beiträge zur Kenntnis des Rotliegenden und Karbon bei Halle und Wettin. - Jb. Hall. Verb. Erf., **14**: 153-184.
- Schwab, M. (1962): Über die Inkohlung der Steinkohlen im Nördlichen Saaletrog bei Halle. - Geologie, **11(8)**: 917-942.
- Schwab, M. (1965): Tektonische Untersuchungen im Permokarbon nördlich von Halle/Saale. - Freiberg. Forschungsh., **C139**: 1-109.
- Schwab, M. (1970): Die Beziehungen der subsequenten Vulkanite des Permosiles zum variszischen Orogen, dargestellt unter besonderer Berücksichtigung des Halleschen Vulkanitkomplexes. - Geologie, **19**: 249-280.
- Schwab, M. (1977): Zur paläotektonischen Entwicklung des Halleschen Permosilesgebietes (Nordöstlicher Saaletrog). - Hall. Jb. Geowiss., **1**: 69-84.
- Shelley, D. (1985): Determining paleo-flow directions from groundmass fabrics in the Lyttelton radial dykes, New Zealand. - J. Volcan. Geotherm. Res., **25**: 69-79.
- Siegert, C. (1967a): Die zeitliche und räumliche Entwicklung des intermediären Vulkanismus im Halleschen Permokarbonkomplex. - Geologie, **16**: 889-900.
- Siegert, C. (1967b): Zur Petrochemie der Vulkanite des Halleschen Permokarbonkomplexes. - Geologie, **16**: 1122-1135.
- Smith, J. V. (1998): Interpretation of domainal groundmass textures in basalt lavas of the southern Lamington Volcanics, eastern Australia. - J. Geophys. Res., **103(B11)**: 27383-27391.

- Smith, J. V. (2002): Structural analysis of flow-related textures in lavas. - *Earth-Science Reviews*, **57**: 279-297.
- Smith, J. V. & Houston, E. C. (1994): Folds produced by gravity spreading of a banded rhyolite lava flow. - *J. Volcan. Geotherm. Res.*, **63**: 89-94.
- Spera, F. J. (2000): Physical properties of magma. - *In*: Sigurdsson, H., Houghton, B. F., McNutt, S. R., Rymer, H. & Stix, J. (eds.) *Encyclopedia of Volcanoes*. New York (Academic Press) 171-190.
- Spohn, T., Hort, M. & Fischer, H. (1988): Numerical simulation of the crystallization of multicomponent melts in thin dikes or sills - 1. The liquidus phase. - *J. Geophys. Res.*, **93(B5)**: 4880-4894.
- Steiner, W. (1960): Zur Geologie des Halleschen Vulkanitkomplexes. - *Geologie*, **9**: 492-512.
- Stollhofen, H. (1998): Facies architecture variations and seismogenic structures in the Carboniferous-Permian Saar-Nahe Basin (SW Germany): evidence for extension-related transfer fault activity. - *Sedimentary Geology*, **119(1-2)**: 47-83.
- Stollhofen, H. & Stanistreet, I. G. (1994): Interaction between bimodal volcanism, fluvial sedimentation and basin development in the Permo-Carboniferous Saar-Nahe Basin (south-west Germany). - *Basin Res.*, **6**: 245-267.
- Störr, M. (1983): Die Kaolinlagerstätten der Deutschen Demokratischen Republik. - *Schriftenr. geol. Wiss.*, **18**: 1-226.
- Sundvoll, B., Neumann, E. R., Larsen, B. T. & Tuen, E. (1990): Age relations among Oslo Rift magmatic rocks; implications for tectonic and magmatic modelling. - *Tectonophysics*, **178(1)**: 67-87.
- Swanson, S. E. (1977): Relation of nucleation and crystal-growth rate to the development of granitic textures. - *Amer. Mineral.*, **62**: 966-978.

- Tait, J. A., Bachtadse, V., Franke, W. & Soffel, H. C. (1997): Geodynamic evolution of the European Variscan fold belt: palaeomagnetic and geological constraints. - *Geol. Rundschau*, **86(3)**: 585-598.
- Turcotte, D. L. & Schubert, G. (2002): *Geodynamics*. 456 S. Cambridge (Cambridge University Press).
- Turner, S. P., George, R., Jerram, D. A., Carpenter, N. & Hawkesworth, C. J. (2003): Case studies of plagioclase growth and residence times in island arc lavas from Tonga and the Lesser Antilles, and a model to reconcile discordant age information. - *Earth Planet. Sci. Lett.*, **214**: 279-294.
- Upton, B. G. J. (1994): Regional setting of Carboniferous volcanism in the Midland Valley of Scotland. - *Transactions of the Royal Society of Edinburgh: Earth Sciences*, **84(3-4)**: 209-212.
- Veltheim, F. W. W. v. (1940): *Geognostische Betrachtung der alten Sandsteinformation am Harz und in den nördlich und östlich davon belegenen Landstrichen (Manuskript 1821-1829)*. - *Jb. Hall. Verb. NF*, **18**: 15-292.
- Wilhelm, S. & Wörner, G. (1996): Crystal size distribution in Jurassic Ferrar flows and sills (Victoria Land, Antarctica); evidence for processes of cooling, nucleation, and crystallisation. - *Contrib. Mineral. Petrol.*, **125(1)**: 1-15.
- Zenzri, H. & Keer, L. M. (2001): Mechanical analyses of the emplacement of laccoliths and lopoliths. - *J. Geophys. Res.*, **106(B7)**: 13781-13792.
- Zieg, M. J. & Marsh, B. D. (2002): Crystal size distribution and scaling laws in the quantification of igneous textures. - *J. Petrol.*, **43(1)**: 85-101.

Part II

For copyright reasons, part two of this dissertation does not appear in this online version. It is an article published in Journal of Petrology by Oxford University Press:

Mock, A., Jerram, D. A. & Breitzkreuz, C. (2003): Using quantitative textural analysis to understand the emplacement of shallow level rhyolitic laccoliths - a case study from the Halle volcanic complex, Germany. – Journal of Petrology, **44(5)**: 833-849.

It can be ordered or purchased under the following addresses:

Journals Subscription Department
Oxford University Press
Great Clarendon Street
Oxford, OX2 6DP, UK
Tel: +44 (0)1865 353907
Fax: +44 (0)1865 353485

<http://petrology.oupjournals.org/>

Part III

Crystal size distributions in three dimensions: insights from the 3D reconstruction of a highly porphyritic rock texture

Alexander Mock and Dougal A. Jerram

submitted to Earth and Planetary Science Letters

Table of contents

Abstract.....	2
Introduction	2
Quantifying textures of igneous rocks.....	2
Geological overview of sample locality	4
Procedure of 3D reconstruction.....	5
The 3D model of felsic phenocrysts.....	9
True 3D crystal lengths and shapes.....	9
Modelling results with equant shapes.....	11
Testing reproducibility of CSD at different sample volumes.....	12
Comparing 3D and 2D CSDs	13
Discussion.....	15
Variability within the sample cube.....	15
2D-3D-correction	16
Crystal growth and crystal shapes	18
Touching frameworks and magma rheology	21
Conclusions and outlook	21
Acknowledgements	22
References	23

Abstract

Crystal populations in volcanic and plutonic rocks preserve a vital record of the magmatic system they have developed from, for example information about crystal sizes, size distributions and shapes yield important information about the growth history and residence time in magmatic/volcanic systems. In this contribution, serial sectioning has been employed to a sample of porphyritic rhyolite from a Permocarboneous laccolith to reconstruct the felsic phenocrysts in three dimensions in order to determine their true shapes, sizes and three dimensional size distributions. Models 1) of all three phases (quartz, plagioclase and K-feldspar) with 217 crystals, and 2) a larger model containing 1599 K-feldspar crystals were reconstructed in three dimensions. The model with all three phases shows that crystals do not form a touching framework in three dimensions and that individual crystals are growing freely in the melt prior to quenching of the texture. Crystal shapes are complicated, with aspect ratios varying from 1.7:1.5:1 to 8.7:1.9:1, and often do not resemble crystallographic shapes expected for phenocrysts growing relatively unhindered from a silicate liquid indicating complex growth histories. In contrast, the three dimensional size distributions are very simple and straight. They are compared with size distributions obtained and stereologically corrected from individual sections. Three dimensional size distributions agree well with stereologically corrected data from a larger sample, but considerable scatter is produced for two dimensional data from sections used for three dimensional reconstruction. Tests on the large three dimensional model show that CSDs can be robustly reproduced with a sampling size of greater than ~ 200 crystals. The method of three dimensional reconstruction is applied here to a geological material unsuitable for previously demonstrated three dimensional reconstruction methods. The methodology presented here, though still relatively time consuming, should become more and more routinely applicable.

Introduction

Quantifying textures of igneous rocks

Igneous rocks are often characterised by one or more crystal phases which have grown under certain crystallising conditions. In relatively quickly cooled volcanic and shallow intrusions, resultant textures of these phases may be rapidly frozen in. In other examples, igneous textures result from slow cooling and crystallising conditions in deeper plutonic rocks. A

major key to understanding the formation of igneous rocks is to link these textures to processes known or assumed to be active during their genesis. For this purpose, arrangement of constituents of rocks (i.e. the spatial arrangement of the mineral grains), three dimensional (3D) size distribution of crystals present and the nature of constituents (geochemistry and mineralogy) must be quantified [for an overview see among others 1, 2-11].

Topics such as mixing of magmas with different crystal populations [12], effusion rates and magma system volumes [13] and magma chamber processes [14] are but a few examples of application of quantitative textural investigation to resolve questions about the origin of igneous rocks. Nevertheless, quantification of inherently 3D igneous textures has been inhibited by general limitation to two dimensional (2D) sections through a rock. 2D sections are sufficient to determine bulk abundances of phases with precision [15, 16], but especially in size distribution studies, correction for 2D-3D effects is necessary [17]. It has been limited in earlier studies to a purely dimensional means [raise to the power of 1.5, e.g. 18]. Stereology has brought major improvements to these correction methods [e.g. 17, 19, 20, 21]. However, true 3D arrangement of complexly shaped natural particles in any opaque solid remains obscure with corrections being approximate. Methods do exist to make a rock's interior immediately available for observation in 3D. These include computed x-ray tomography (CT) [22-24] and confocal microscopy [25, 26] as non-destructive techniques, or serial sectioning/erosion as a destructive method [27-30]. But these methods are limited: CT and confocal techniques to rather small sample sizes and, in the case of tomography, to limited contrast in density between constituents and groundmass in many igneous rocks. Serial sectioning or erosion is more versatile, albeit very time consuming if the material to be analysed is not suitable for automatic image classification and analysis, and limited by grain size.

In recent years, the employment of the method of crystal size distribution (CSD) analysis to igneous petrology has brought major insight into magmatic processes [18, 31-33]. In this technique, 3D size distribution of crystals in rocks is calculated by measuring 2D size distributions in cross-section and employing stereological techniques to convert 2D observations into true 3D [17]. Such crystal size data can then be used to determine magma residence times, crystallization history and mixing events between different crystal populations [34-36]. A direct method for measuring 3D crystal size distributions (CSDs) in thick thin-sections has been proposed by Castro et al. [26]. This method is restricted to the determination of microlites smaller than the common thickness of thin sections (~30 μm) and

samples with low crystallinity, because it employs optical serial sectioning by focussing in intervals of 1 μm through a thick section and determines positions of intersections of crystals in individual section planes. Nevertheless, that study has shown that CSDs determined from intersection distributions with stereological methods [17, 19, 37] compare reasonably well with true 3D data for the central part of CSDs. Clearly, more good examples of true 3D crystal populations are desirable to help refine methods of 3D reconstruction and to test existing conversion techniques from 2D to 3D.

In this study, the phenocryst population of one sample, a highly porphyritic subvolcanic rhyolite from the Permocarbiniferous Halle Volcanic Complex (HVC), is investigated. True 3D texture of phenocrysts is reconstructed digitally using a combination of serial grinding, imaging and virtual 3D software. The aim is to determine shape, size and spatial arrangement of the felsic phenocrysts present (quartz, plagioclase and K-feldspar) in 3D, to compare those results with previously determined 2D textural data [38], and to investigate methods of 3D textural analysis more thoroughly. Discussion is aimed at use of such 3D textural analysis techniques and pros and pitfalls of 2D versus 3D CSD measurements.

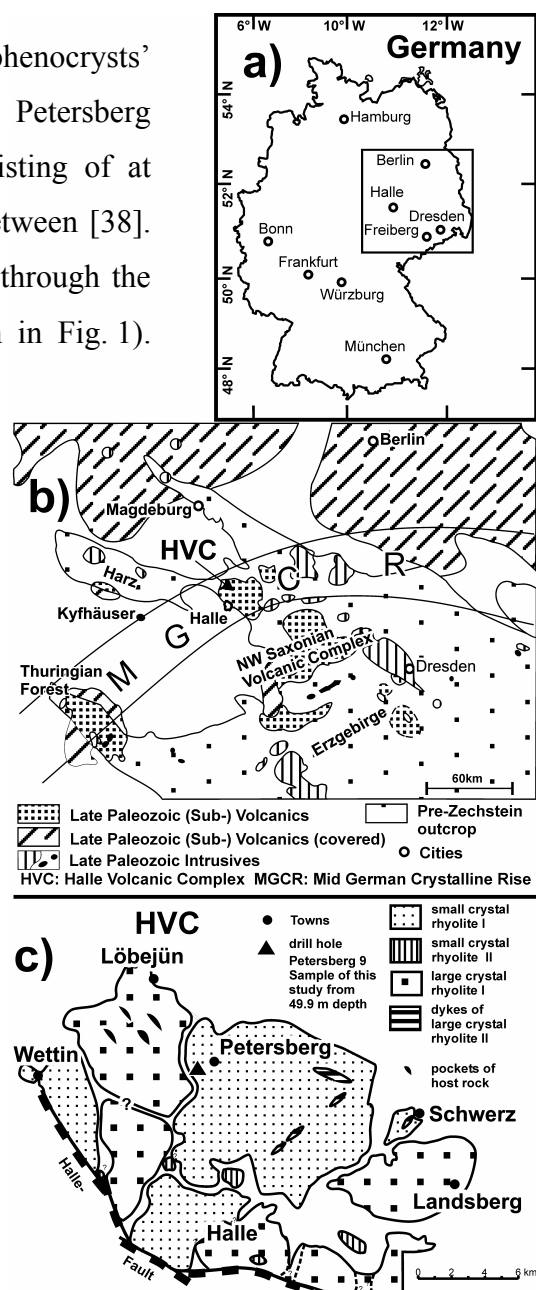
Geological overview of sample locality

The HVC is situated in the Saale Basin in Eastern Germany – one of several late Palaeozoic transtensional volcano-sedimentary basins in the area of the decaying Variscan orogen [39, 40]. Magmatism here culminated in the \pm contemporaneous emplacement of voluminous porphyritic rhyolitic laccoliths of about 200 km^3 altogether (Landsberg, Löbejün, Petersberg, Wettin, Schwerz units, Fig. 1). Of these laccolith units, Löbejün and Landsberg units have large feldspar phenocrysts up to ~ 30 mm long axis; the Landsberg unit also contains a variant with smaller phenocrysts. Wettin and Petersberg units both have smaller feldspar phenocrysts (~ 5 -10 mm) with the Wettin unit containing small schlieren-like domains with larger phenocrysts. The Schwerz unit is slightly older and textures are more varied than those of the other units.

Country rock below the lower contacts consists of a succession of grey silt- and mudstones with several fine sandstone beds and coal seams (Wettin subformation) and a fluvio-limnic succession of reddish-grey conglomerates, siltstones, clays, and sandstones with abundant volcanoclastics [Halle formation 41, 42]. These sedimentary rocks crop out as a thin tilted band between Petersberg and Löbejün laccoliths (Fig. 1). The Petersberg laccolith is the largest of the HVC laccoliths with an estimated volume of ~ 60 km^3 . It formed 294 ± 3 Ma ago

[U-Pb SHRIMP dating by 43]. A detailed account of phenocrysts' spatial relationships and size distributions in the Petersberg laccolith revealed an emplacement mechanism consisting of at least two magma batches without major cooling in between [38]. For this study, a sample from drill core Petersberg 9 through the small crystal Petersberg laccolith was used (position in Fig. 1). The drill core was recovered during coal exploration drilling in the 1960s which intersected the margin of the Petersberg laccolith (Fig. 1).

Fig. 1. Sample location and general geology of the study area.



Procedure of 3D reconstruction

Macroscopically clearly visible and identifiable phenocrysts, moderate state of alteration and easy availability of samples from natural outcrops, quarries and drill cores make this rhyolite especially suitable for the present study. The sample used here was recovered from a depth of 49.9 m in the drill core. From the sample, a rectangular slab of $\sim 7.5 \times 8 \times 4 \text{ cm}^3$ was cut (Fig. 2). One of the slab's surfaces was scanned with a conventional flat-bed scanner at 400 dpi giving a pixel size of 0.0635 mm^2 . This also set the lower size limit of a phenocryst section to be recognized on the scanned image. K-feldspar (KF), plagioclase (PL) and quartz (QZ) phenocrysts were identified on the sample and the scan and marked with unambiguous false colours on the digital image using a drawing tablet. The slab's surface was then ground

down for a fixed time. The machine used for grinding was an LP-40 by Logitech Ltd., Glasgow. It was set to a pressure of 3.5 kg/sample and a speed of 70 rounds/min. The grinding powder was SiC with a grain size of 600 and water as dispersion agent.

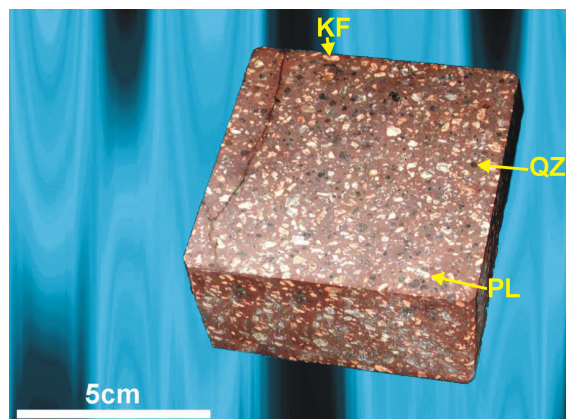


Fig. 2. Sample cube before serial erosion.

300-1000 μm of sample were ground away at each step. In that way, 11 false colour images of phenocrysts in the sample were retrieved (Tab. 1). From the images, crystal size distributions were calculated for phenocrysts with the procedure described in [38] using the method of Higgins [17] and KS300 software (KONTRON ELEKTRONIK Imaging System) for image analysis of manually classified images.

False colour images were geo-referenced with ENVI software (Research Systems, Inc., Boulder, Colorado, USA). Control points were chosen as sample slab corners visible on scanned, false colour images and marked by one single pixel each. Coordinates for the sample image were chosen arbitrarily from a rectangular reference grid (e.g. Universal Transversal Mercator) and scaled to sample size, so that each pixel on the digital image had a virtual size of 1 m^2 . Each section of a phenocryst was turned into a geo-referenced polygon. Files containing the polygons were then incorporated into GOCAD 3D modelling software (<http://gocad.ensg.inpl-nancy.fr/>). Each sample section was given appropriate Z-values (see Tab. 1). Sections representing one phenocryst in different layers were identified and connected into a 3D closed surface by the algorithm digital smooth interpolation [DSI, compare 44] implemented in GOCAD. Singular polygons clearly representing phenocrysts smaller than the section spacing were turned into two dimensional surfaces which were then doubled and set off in a negative and positive Z-direction with a value less than section spacing at that position in order to create a 3D closed surface. Thus, singular sections are all represented by prisms in the 3D model. This latter process is required in order to estimate volume and size of smaller crystals. Due to their small size, errors associated with this estimate are small and systematic.

Some phenocrysts have been fractured, fragments slightly rotated and partly annealed during ascent and emplacement of the magma (Fig. 3l). However, fragments have not been moved considerably away from each other in the flowing magma and – in 3D-reconstruction – it has been possible to link these fragments to form one closed surface representing the original crystal. In this fashion, 3D models of 1) a small volume including all three phases for testing the spatial relationships between the phases and 2) of 1599 KF phenocrysts was generated in order to extract 3D size distribution information.

Tab. 1. top: Properties of serial sections. Textural parameters for KF. Textural parameters of PL (bottom left) and QZ (bottom right) for serial sections. CL = characteristic length.

No.	Area (mm ²)	Spacing (mm)	Z-value (m)	CL (mm)	intercept	L _{max} (mm)	Modal %	No. of XX sections
1	5879	0.4	0.000	0.797	0.459	8.45	4.780	1251
2	5860	0.4	6.299	0.941	0.180	8.45	7.756	816
3	5898	0.4	12.599	0.956	0.250	10.64	6.088	979
4	5854	0.6	22.048	0.856	0.278	8.45	6.470	892
5	5849	0.5	29.922	0.807	0.410	8.45	4.563	1118
6	5871	1.0	45.670	0.799	0.356	8.45	5.355	1001
7	5942	0.4	51.970	0.784	0.346	6.71	4.564	990
8	5898	0.3	56.694	0.775	0.357	6.71	5.193	990
9	5913	0.3	61.419	0.766	0.389	6.71	8.287	1047
10	5932	0.3	66.143	0.788	0.356	6.71	4.510	1046
11	6067	0.3	70.868	0.758	0.356	7.58	7.117	956

No.	CL (mm)	intercept	L _{max} (mm)	Modal %	No. of XX	No.	CL (mm)	intercept	L _{max} (mm)	Modal %	No. of XX
1	0.753	0.609	8.45	3.274	1642	1	0.568	0.414	4.74	4.740	716
2	0.865	0.254	8.45	4.521	1107	2	0.743	0.125	4.74	5.377	411
3	0.805	0.388	8.45	3.986	1230	3	0.699	0.158	4.74	5.481	498
4	0.827	0.260	6.71	4.946	887	4	0.750	0.107	4.74	5.350	427
5	0.764	0.470	8.45	4.075	1171	5	0.700	0.179	4.74	6.171	511
6	0.856	0.334	8.45	4.408	1156	6	0.711	0.157	4.74	5.573	499
7	0.812	0.338	8.45	3.739	1168	7	0.760	0.124	4.74	5.303	462
8	0.790	0.355	8.45	3.566	1127	8	0.768	0.107	4.74	5.452	479
9	0.805	0.247	8.45	6.986	1045	9	0.675	0.193	4.74	5.242	513
10	0.790	0.371	8.45	3.894	1173	10	0.708	0.155	4.74	5.547	518
11	0.760	0.396	7.58	6.665	1130	11	0.673	0.168	5.70	4.559	494

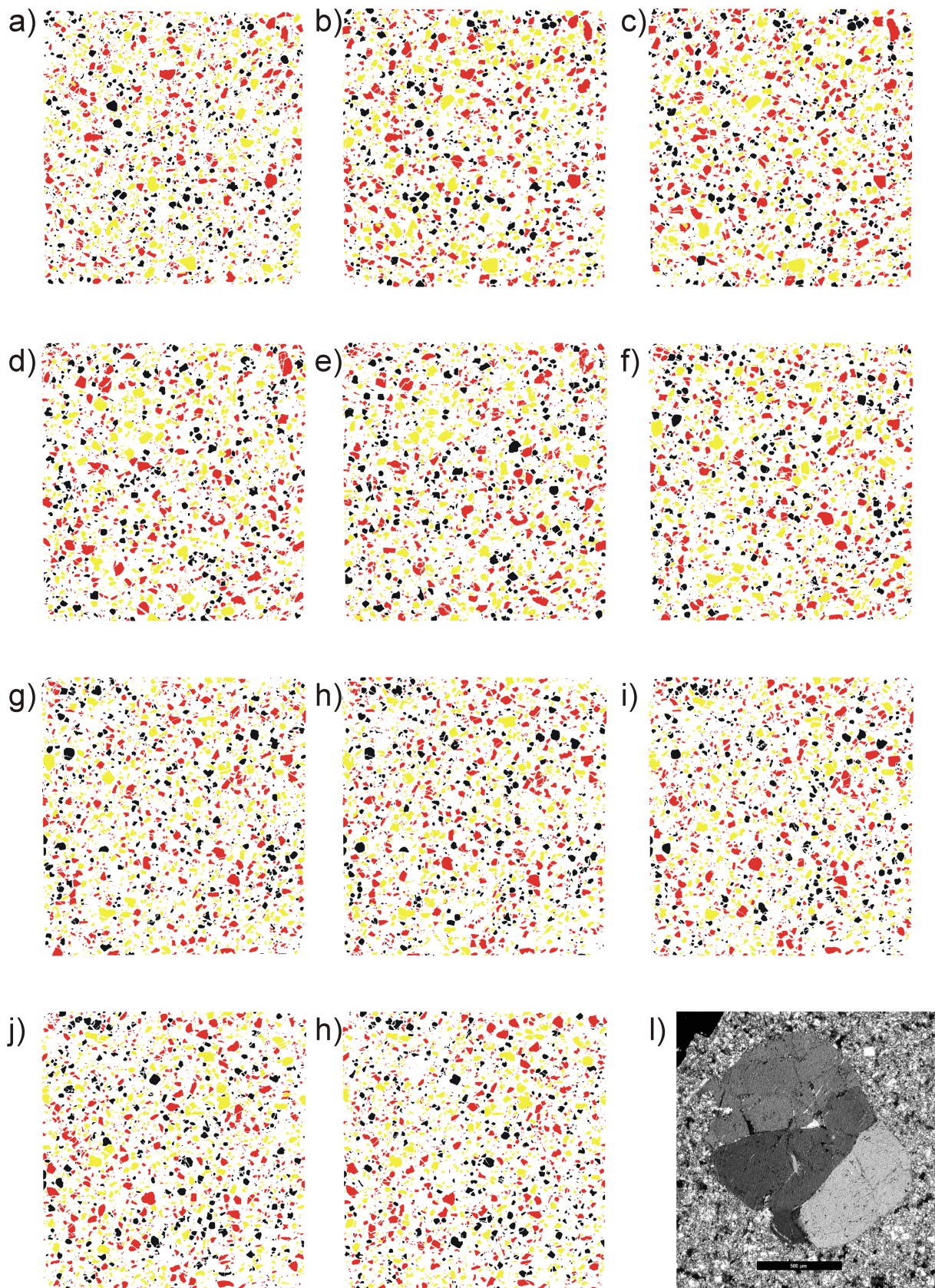


Fig. 3. a-k) Classified images of 11 sample sections. Red: K-feldspar, yellow: plagioclase, black: quartz. l) Example of a broken and subsequently annealed quartz phenocryst from thin section.

The 3D model of felsic phenocrysts

In this section, we will examine results from 3D reconstruction of a population of 1599 KF crystals, in terms of their size distribution, shape and spatial characteristics.

True 3D crystal lengths and shapes

Crystal shapes in the 3D model are defined by triangulated surfaces (*.ts-files in GOCAD), where each crystal is defined by a series of coordinates for nodes at the corner of each triangle making up the surface of the crystal (Fig. 4). To calculate a true 3D long axis of each crystal, a program was written to extract the xyz-coordinates defining each crystal from the *.ts-files, and then to calculate the longest distance between these points defining this as long axis (length) of the crystal. From this data, a true 3D CSD can be plotted and compared to stereologically corrected CSDs from 2D data. Fig. 8 shows the true 3D CSD plot for the 1599 KF phenocrysts of the 3D model. The CSD is characterised by one simple straight slope with a gradient of -0.924 corresponding to a characteristic length of 1.082 mm with a regression coefficient of 0.9976 (only unfilled data points used for regression analysis).

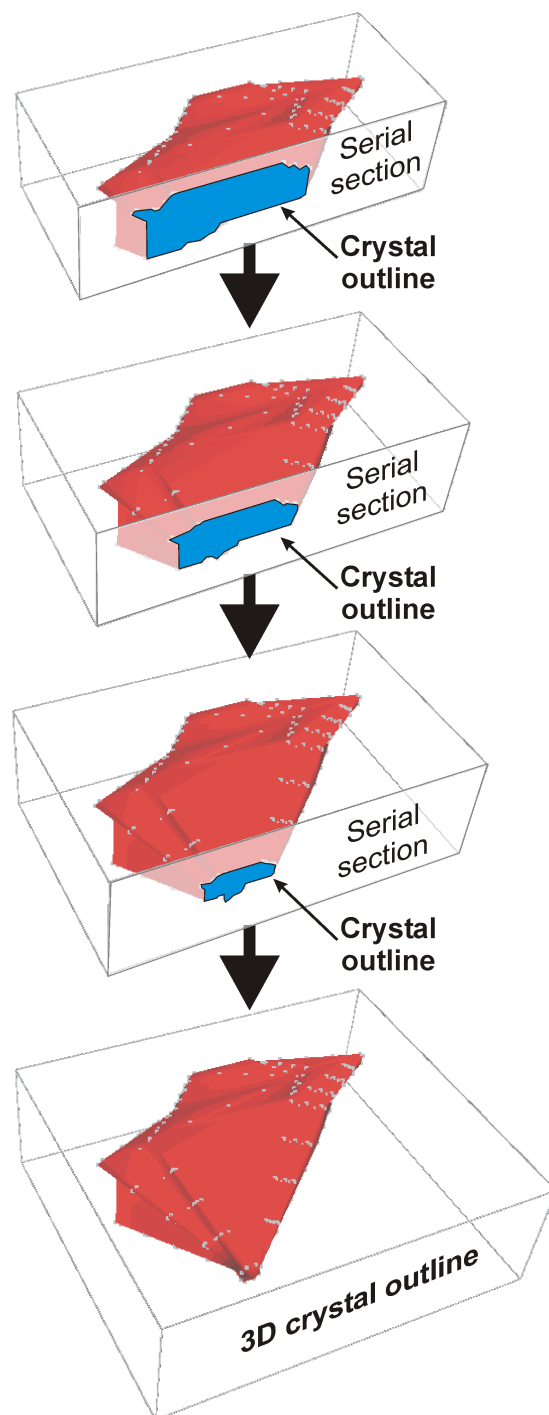


Fig. 4. Crystals are reconstructed by linking their outlines between different sections and then rendered to a 3D surface.

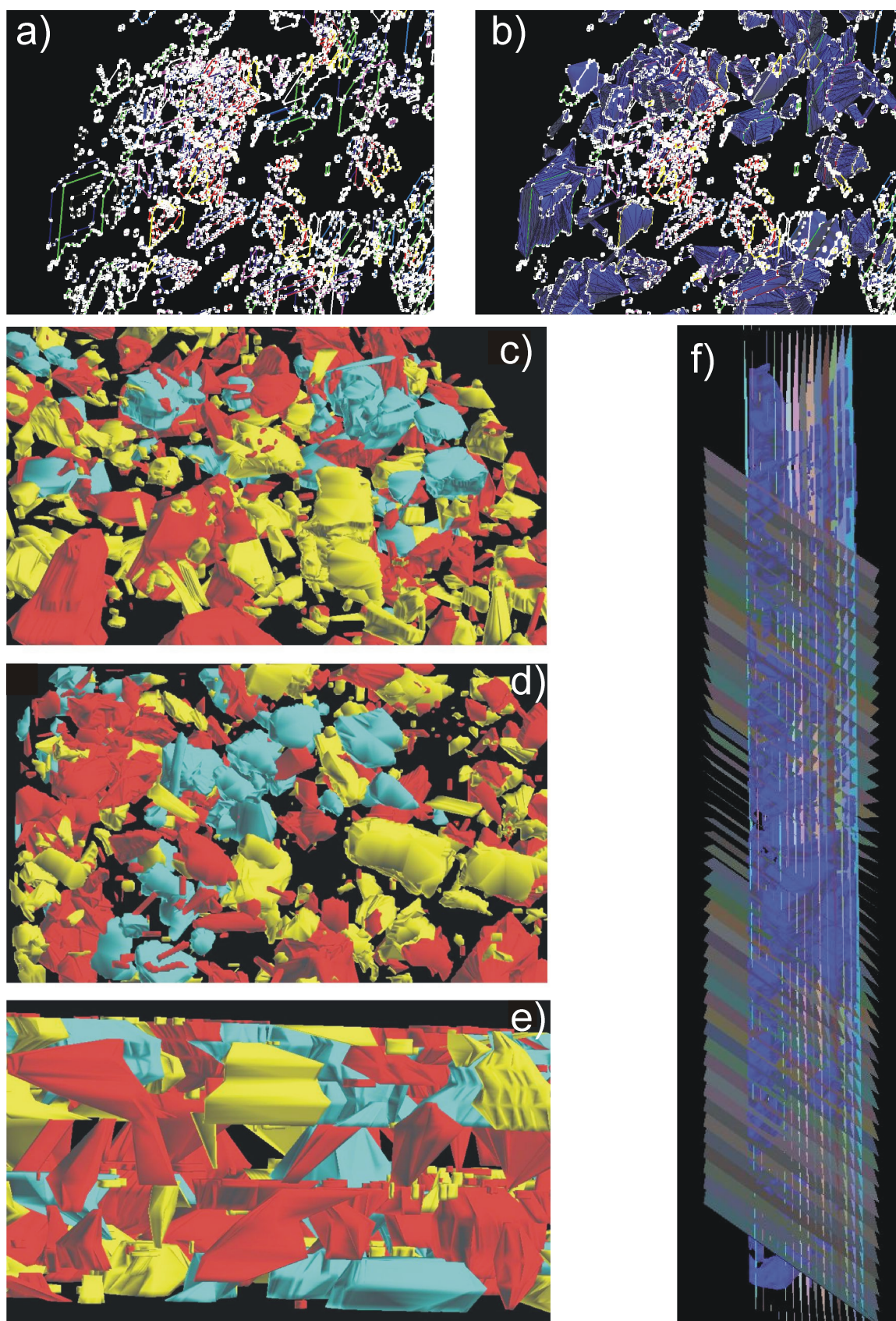


Fig. 5. Three-dimensional reconstruction of felsic phenocrysts. a) Polygons from real sections through the sample. b) Linking polygons belonging to one phenocryst to closed surfaces. c-e) 217 reconstructed phenocrysts in a small sample volume ([animation1](#)), yellow: plagioclase; red (dark blue in animation): K-feldspar; light blue: quartz. Oblique (top), top down (centre) and side (bottom) views. f) Virtual sections through K-feldspar phenocrysts; high angle sections have too few intersections for statistically significant CSD image analysis.

Inspection of Figs. 5, 6, 7 and animations reveals a variety of shapes of KF existing in the sample. Fig. 7 shows representative shapes for 8 phenocrysts with their grain size (length) and their aspect ratios as calculated using the best fit ellipse function in GOCAD. Shapes vary considerably from tabular shapes of 1.7:1.5:1 to very acicular shapes up to 8.7:1.9:1. The complex arrangement of shapes is not re-stricted to size in terms of crystal length, but may be restricted by overall crystal volume, how-ever, smaller volume phenocrysts display both tabular and acicular shapes. This raises issues re-garding conditions of crystal growth and interpretation of CSD patterns produced (discussed later).

Modelling results with equant shapes

As previously stated, CSDs from 2D sections are corrected to 3D distributions [17]. In such techniques, 2D size distribution is stereologically converted into 3D size distribution with the assumption of an ideal crystal shape. Shapes used for this purpose are usually spheres, bi- or triaxial ellipsoids with variable aspect ratios and rectangular solids with aspect ratios between very equant shapes and acicular ones. Correction factors are also applied to take fabrics (i.e. preferred orientations arising from acicular crystals) into account [17, 21]. For comparative purposes, we model 3D size distributions with volume data from 3D crystals. A linear measure of size was determined from volumes as (1) diameter of an equal volume sphere, (2) long axis of an equal volume triaxial ellipsoid with axial ratios of 1:2:3 and (3) diagonal length of an equal volume rectangular solid with aspect ratios of 1:2:3. These aspect ratios have been used in stereological corrections of 2D size distribution data from individual slabs used for serial sectioning [Fig. 10, 17]. Equations used are (V = volume):

$$d_{sphere} = 2 \cdot \sqrt[3]{\frac{3V}{4\pi}} \quad (01)$$

$$c_{ellipsoid} = 2 \cdot \sqrt[3]{\frac{27V}{8\pi}} \quad (02)$$

$$l_{rect.sol.} = \sqrt{2 \cdot \sqrt[3]{\frac{9}{2}V}} \quad (03)$$

The three dimensional model of KF phenocrysts was also cut by 14 surfaces oriented at a low angle to the eroded plane to create sample sections that could be analysed accordingly and compared with results from original sample sections (Fig. 10). The analysing procedure of these virtual sections was the same as for real sections. Virtual sections with too high an angle

(compare Fig. 5f) did not contain enough sections of phenocrysts for a statistically significant size distribution analysis.

Testing reproducibility of CSD at different sample volumes

Representative sample size is an important question in conjunction with the quantification of crystal populations, i.e., at what sample size is the texture of the sample characteristic of a larger portion of the rock. Additionally, the sample must be large enough to obtain a statistically valid quantification of the crystal population. This is especially important when small scale variations in rock texture are to be quantified. Spatial distribution pattern (SDP) of rock textures has been investigated and it has been shown that SDPs are highly variable in sample populations <300 [45]. Additionally, 3D sphere models of different size distributions have been developed which can be sectioned to produce reference textures in 2D [46, 47].

Grain size distributions measured on these models and similar models of low to medium aspect ratio prisms produce accurate results when >300 individuals are measured [46]. As a comparison to the previous studies based on synthetic 3D models, the large sample size of the 3D model presented in this study is ideal to test the minimum sample size required to correctly measure true 3D CSD. Fig. 9 shows CSD plots for different sample volumes of the model. CSDs start to break down between $9/64$ (0.141) and $1/9$ (0.111) of original sample size relating to between 224 and 178 crystals. This suggests that sample sizes of greater than ~200 are required to accurately reproduce the CSD in this study and will act as a guide for other studies using CSD data.

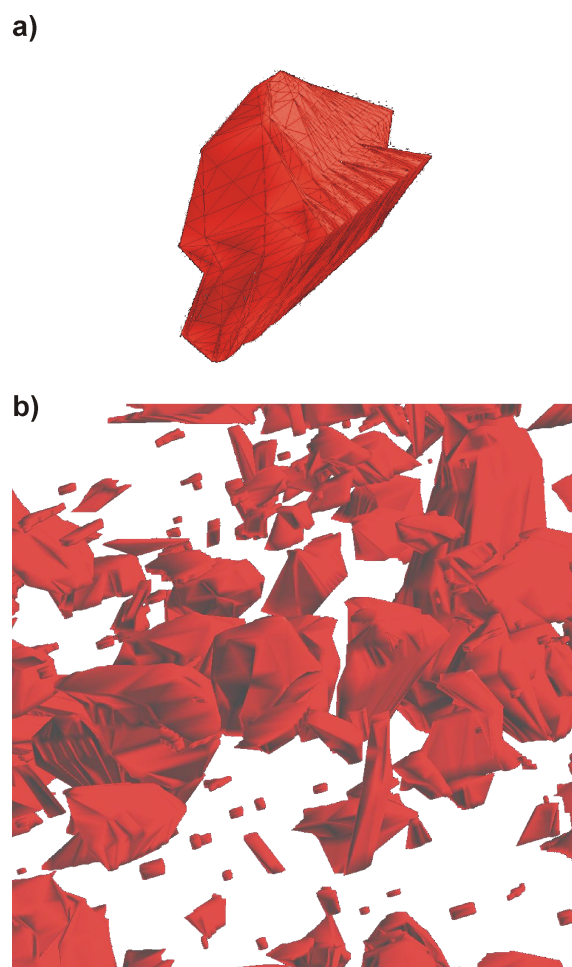


Fig. 6. a) Single reconstructed K-feldspar phenocryst with complex shape ([animation2](#)). Triangles of closed surface are visible. b) 3D-model of around 1599 K-feldspar phenocrysts ([animation3](#)).

Comparing 3D and 2D CSDs

Fig. 3 shows the classified images of all 11 sections. The 3D-model (Fig. 5 and animation) shows that phenocrysts do not form a touching framework. More importantly, individual crystals modelled from more than one intersection exhibit complicated irregular shapes (Fig. 6). These deviate considerably from crystal shapes expected when phenocrysts grow freely in a melt and they also deviate from ideal geometrical shapes so far employed in stereological CSD corrections.

CSDs' characteristic lengths straddle 0.6 mm (Fig. 10). According to standard errors, variation in modal abundance seems to be larger than variation in characteristic lengths (Fig. 10). In Fig. 10 and 11, three slabs cut from sample 90499 of Mock et al. [38] are also shown (blue squares). Standard errors of these sample slabs are calculated from the whole sample set [38]. These slabs have higher characteristic lengths and modal abundances than the serial sections, but characteristic length of the 3D model agrees very well with these three slabs. Modal abundance of the 3D model is slightly higher than the three slabs of [38], but still falls well into the range of the sections. It was determined in two ways: the long axis data was calculated into volumes according to eq. 03 assuming rectangular solids with an aspect ratio of 1:2:3 giving a sum of KF volumes of 534.6 mm³ (3D real length in Fig. 10); the volumes of crystals were taken as such giving a sum of KF volumes of 381.9 mm³ (3D real volume in Fig. 10); both sets of volumes were summed up and related to sample volume calculated from maximum and minimum coordinates of crystals. Histograms of the two volume distributions also show slight differences (Fig. 11). CSDs of the 3D model and individual sections are compared in Figs. 10 and 11. Real and virtual sections display a considerable spread in characteristic length vs. modal abundance (Fig. 10). This convincingly illustrates the variation of quantitative textural parameters due to section effects (see below). Variation due to different shape models in stereology is demonstrated in Fig. 11 by CSDs for sphere, ellipsoid and rectangular solid models for volumes of the KF phenocrysts in comparison to length data determined from coordinates of the crystals' nodes (see above). The sphere model in Fig. 11 clearly has markedly different CSD parameters than the other models. This observation clarifies that too simple a model for stereological correction of CSDs yields misleading results. The CSD of the lengths falls in between CSDs of triaxial model shapes for the volume data and CSDs for the larger sample determined stereologically (Fig. 11a). Their characteristic lengths are very similar around 0.95 ± 0.1 mm. Intercepts on the other hand vary from +0.4 to -3.

Virtual sections through the model of KF phenocrysts are analysed and plotted in Fig. 10. They show a considerably larger spread than real sections. They have smaller characteristic lengths, especially. Compared to samples from the whole HVC (Fig. 10c), serial sections occupy the lower part of the sample cloud. They reach to much lower modal abundances and characteristic lengths.

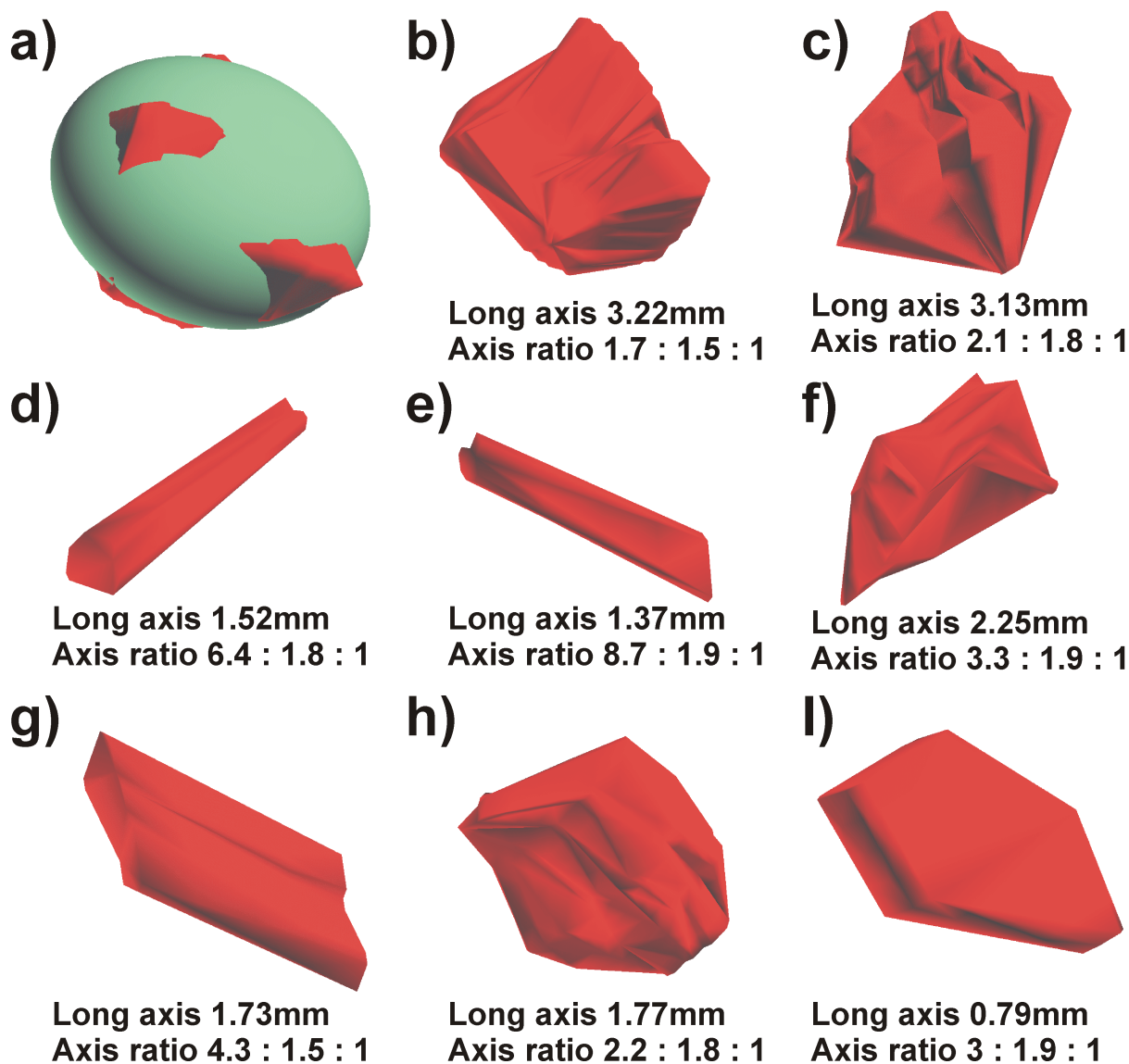


Fig. 7. Examples of shape variation displayed by KF phenocrysts in the 3D model. a) Shape characteristics are determined by the best fit ellipsoid function in GOCAD. b-i) Eight examples of phenocrysts showing maximum dimension and principle axes of their best fit ellipsoid.

Discussion

Variability within the sample cube

Virtually cut sections through the 3D model show a much larger variation in CSD parameters than real sections (Fig. 10). Real sections fall into two groups: one with a low variation of CSD and modal abundance and one with a larger variation. Members of these groups are not distributed uniformly through the sectioned sample volume. This might stem from abundance of flow structures manifest in zones of higher phenocryst content and larger size alternating with zones of less and smaller phenocrysts. Spacing of sections considered, this becomes less likely, because characteristic size of phenocrysts is larger than section spacing. The variation might also stem from section effects (see below). If a crystal is cut along its largest diameter, there is a large size in section 1. The next section necessarily cuts through a level of the crystal with a smaller diameter. In section 2, then, the section of the same crystal yields a smaller size that might even fall into the next smaller size bin, thus influencing the CSD and modal abundance, due to smaller area in the section. A systematic variation of that kind throughout the 11 sections would advocate a layered distribution of crystals in the rock according to their size. A random distribution of crystals would not lead to pronounced variation of textural parameters in sections. Complex shape of grains might also influence variation in CSD data of different sections.

Most importantly, 3D characteristic size in Fig. 10 falls into the same size range determined on three slabs of the larger original sample. 11 real sections used for 3D-reconstruction, on the other hand, give a lower characteristic size and data are more scattered than sections from the larger sample used for comparison. The same applies to the 14 virtual sections, these being even more scattered. In sectioning the sample, many smaller sections of larger crystals in 3D are incorporated into the CSD determined from one section. Although the correction algorithm takes section effects into account, sizes are still found in smaller size bins than in 3D size distribution. By joining many small sections to form large crystals by volume, these do not appear in small size bins of the distribution, but do participate in large crystals and, thus, populate large size bins in the 3D distribution – hence the larger characteristic size of the 3D model than of its individual sections. The original sample on the other hand provides better statistics due to larger number of crystals, thus, correction for the section effects works better.

a) 3D texture model

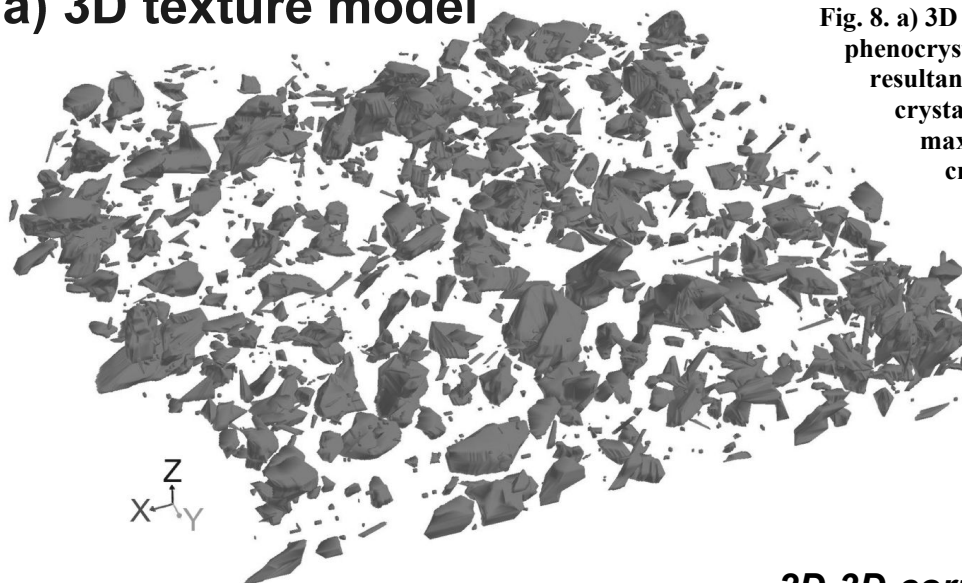
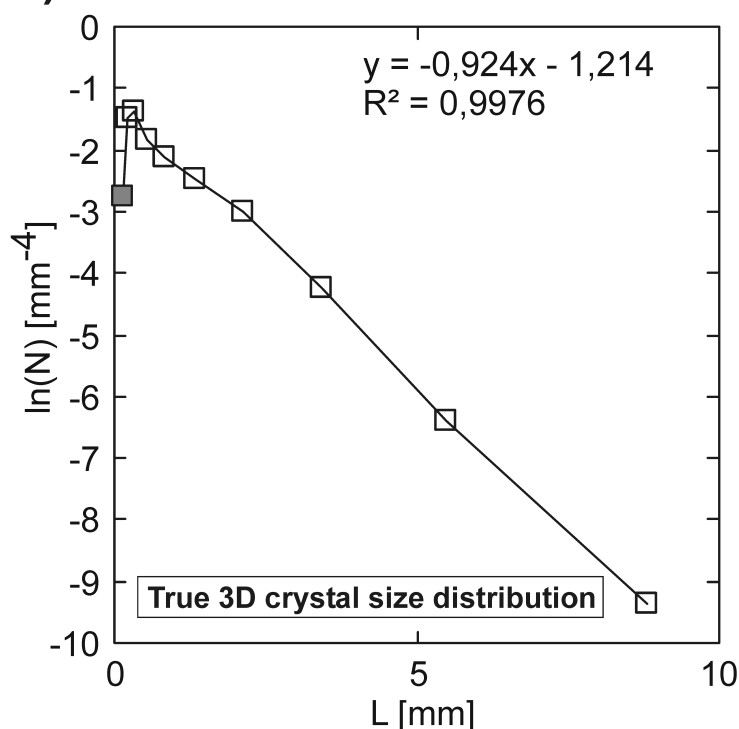


Fig. 8. a) 3D reconstruction of KF phenocrysts with 1599 crystals. b) resultant true 3D CSD plot of crystal population using maximum dimension of crystals.

b) 3D CSD



2D-3D-correction

A measure of size of any 3D-object in 2D is never its true size. The only real size of a three dimensional macroscopic object is its volume or an axis determined in three dimensions. In correction of 2D size distributions to 3D ones, there are three principle problems: First – according to Peterson [37] – the *dimension shift problem*: size distributions in random sections through a body of rock do not equal true 3D size distributions in the rock. Secondly, the *shape problem*: the shape of a grain – or a

crystal – is different when cut through corners or edges. And thirdly, the *orientation problem*: apparent size distribution is a function of orientation of the crystals. Elongate or platy crystals are not cut in sections parallel to lineation or foliation, whereas sections would exist, were these crystals spheres with equal size.

These problems might be reduced to the *cut section effect* and the *intersection probability effect (big grain effect)* [17, 45]. The most complete and vigorous examination of stereology of converting 2D distributions into their 3D equivalents has been achieved by Sahagian and Prousevitch [21] and Higgins [17] continuing from previous work by others (see references

therein). The problem of more complicated shapes than spheres, simple prolate and oblate ellipsoids or rectangular solids with varying aspect ratios, however, has not been solved analytically, yet. Any mathematical correction has to assume such ideal geometry of objects to be analysed. An important result of this study is that crystals in rocks, even when they are assumed to grow freely from a melt, do not possess these ideal shapes. This study has also highlighted problems of having crystal populations with markedly different 3D shapes within the same population. Furthermore, phenocrysts in this study do not form a shape fabric by alignment of acicular or platy crystals. Hence, the orientation problem does not occur in this case and orientation of sections through the sample is not primarily important.

In this study, stereologically corrected CSDs reproduce a true 3D CSD within reasonable error ($\sim 10\%$ for characteristic lengths, $\sim 20\%$ for maximum lengths and higher variability for intercepts; Fig. 11). Thus, even in the presence of non-crystallographic shapes, application of stereological correction methods for CSD analysis seems justified to a first approximation. Overall complicated shapes of reconstructed crystals, however, have severe implications for assumed models of crystal growth, especially in the light of simple straight CSDs.

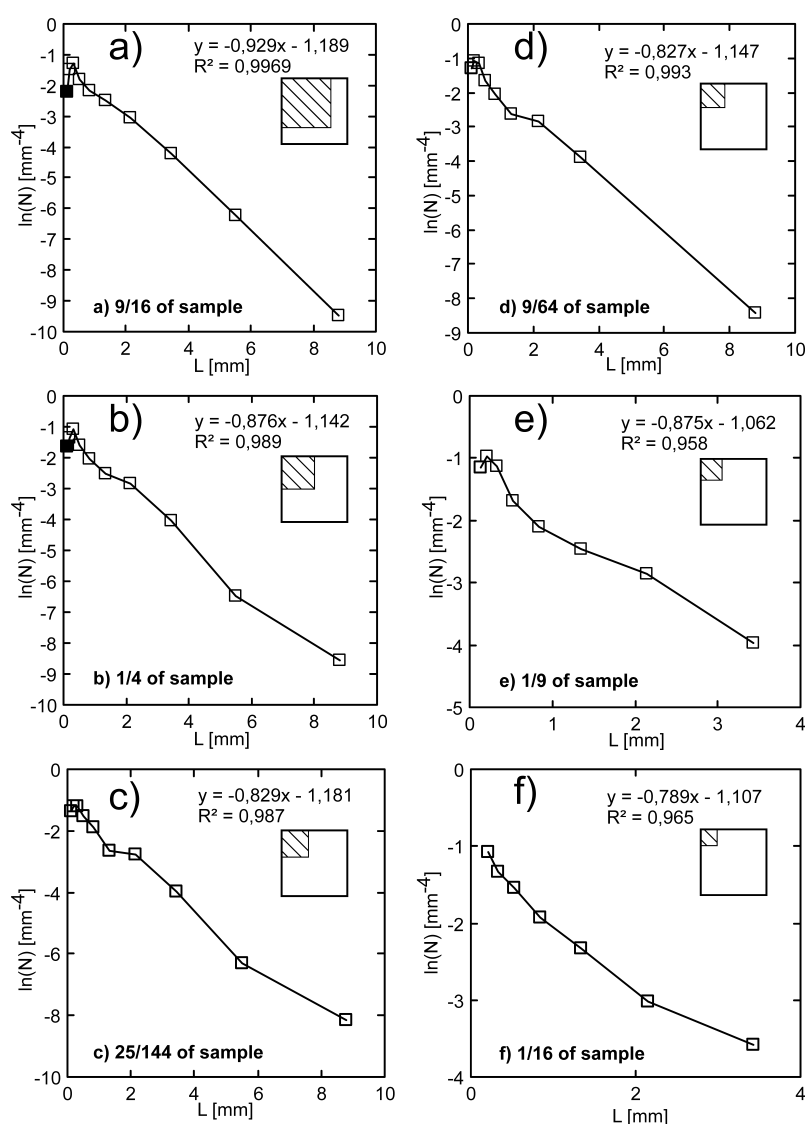


Fig. 9. Testing the sample size vs. robustness of CSD. a) CSD of 9/16 of original sample volume (905 crystals). b) CSD of 1/4 of original volume (424 crystals). c) CSD of 25/144 of original volume (287 crystals). d) CSD of 6/64 of original volume (224 crystals). e) CSD of 1/9 of original volume (178 crystals). f) CSD of 1/16 of original volume (88 crystals).

Crystal growth and crystal shapes

Growth processes in petrology have been modelled extensively [48-50], although comprehensive models for complex multicomponent systems of silicate magmas have not been developed. Qualitative results and order of magnitude calculations accounting for differences between volcanic and plutonic textures are available. Nevertheless, size distributions expected during simple crystallization of magma have been shown [32].

In general, there are two crystal growth laws: size-dependent (proportionate) and size-independent (disproportionate) growth. In proportionate growth, the relative size difference among crystals remains constant, in disproportionation growth, it is the absolute distance. For example: a crystal twice as large as another will stay twice as large when both have grown (proportionate) and a crystal 2 μm larger than another will stay 2 μm larger after they have grown (disproportionate), respectively [51]. Proportionate growth produces log-normal CSDs frequently found in natural systems. Conventional models for CSD often assume disproportionation growth models not confirmed in experiments [51]. On the other hand, reactant supply by advection (stirred solution in crystal growth experiments) has been found to control proportionate growth, whereas disproportionation growth is controlled by diffusive reactant supply in the unstirred crystal growth experiments mentioned above. In felsic magmas, advection should not play an important role in supplying reactants to growing crystals because of very high magma viscosities. Especially in later stages of crystallization, diffusive control of growth is the preferred mechanism. Thus, by draining away nutrients from the vicinity of phenocrysts, ideal crystallographic shapes might develop into complex shapes by differential (phase dependent) anisotropic (direction dependent) overgrowth and resorption. Furthermore, controlling mechanisms on crystal growth are more complex in natural systems than in experiments. Other parameters influence crystal growth [52], such as

- abundance of suitable sites for attachment of molecules on crystal faces,
- twins providing re-entrant angles, favourable sites for attachment of new molecules,
- diffusion of reactants towards and heat away from the crystal,
- adsorption of foreign atoms inhibiting growth,
- overall growth mechanism being interface-controlled vs. diffusion- or heat-controlled growth or continuous vs. layer growth controlled by abundance and rates of surface nucleation, twins, screw dislocations etc.

In a magma of sufficient yield strength (see below), movement is achieved by shearing along discrete shear bands [53, 54]. These might generate a differential diffusivity in the otherwise isotropic magmatic “liquid”, thus, supplying some crystal faces with nutrients more easily than others, essentially leading to irregular shapes such as the ones observed here.

Resorption is an important mechanism to produce complex crystal shapes. In theory, crystal shapes resulting from resorption are expected to be more equant than ideal ones. Resorption is governed ultimately by the same laws as crystal growth with a negative sign. Irregular, often equant shapes in the 3D model advocate a degree of differential anisotropic resorption (Fig. 3, 4).

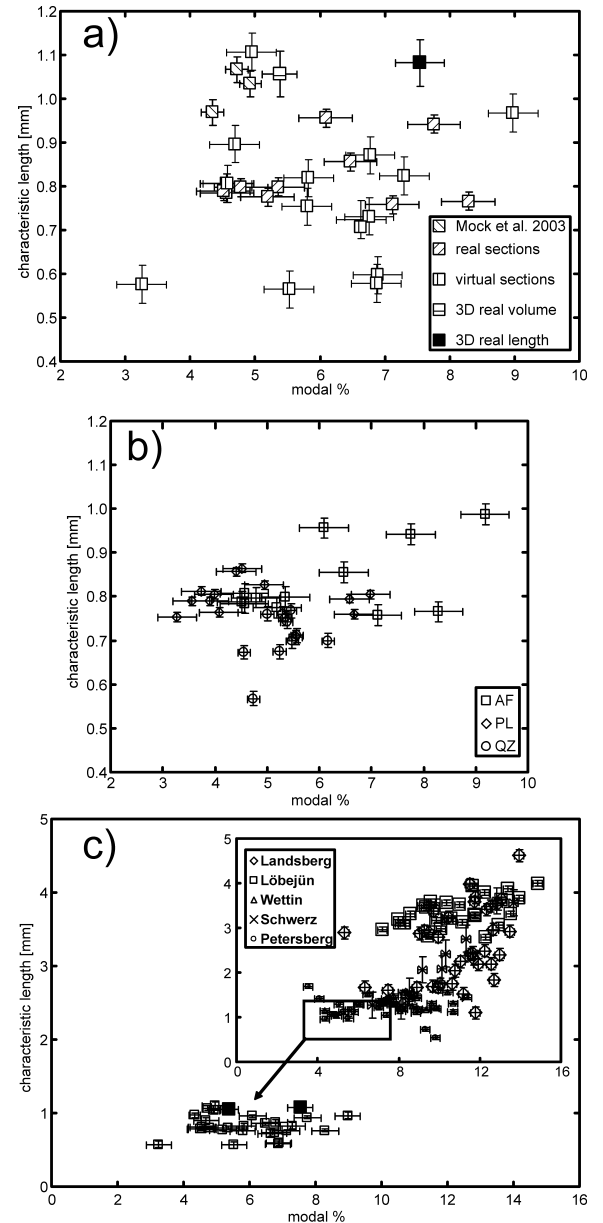


Fig. 10. a) Characteristic length vs. modal abundance plot of serial sections for K-feldspar phenocrysts. Data from actual 2D sections corrected after [17], 15 virtual sections through the 3D model itself (linear size calculated from coordinates of nodes and from volumes as diagonal length of equal volume rectangular solid) and three sample slabs from [38]. **b)** CSD and modal abundance for felsic phenocrysts from serial sections. **c)** Comparison of serial sections with CSDs from the whole laccolith complex [Mock, unpublished data]. Error bars are standard errors (SE) calculated after:

$$SE = \sqrt{\frac{\sum_{s=1}^m \sum_{i=1}^n y_{is}^2}{(n_y - 1)(n_y)}} \quad (04)$$

with y_{is} = i th datum in dataset s and n_y = number of data points in dataset s .

Moreover, phenocrysts, especially QZ, in the Halle rhyolite are often broken, slightly rotated and annealed. Fracturing of feldspar phenocrysts is sometimes more obvious because fragments are slightly further apart (Fig. 3). Nevertheless, fragments have hardly been moved at all from the original phenocryst, so that original phenocrysts could be restored in the 3D model. Thus, in spite of fracturing being an important process in the evolution of the phenocryst population, it is of no major influence on the reconstruction of phenocryst textures in this study, but might produce reduced grain sizes in correction of size distributions of individual sections.

In summary, the complex shapes found in the 3D model of felsic phenocrysts stem from a complex interplay of anisotropic growth mechanisms in connection with most probably complex growth laws, resorption and fracturing of crystals, whereas CSDs as an integration of these processes do not indicate complexity (Fig. 7,).

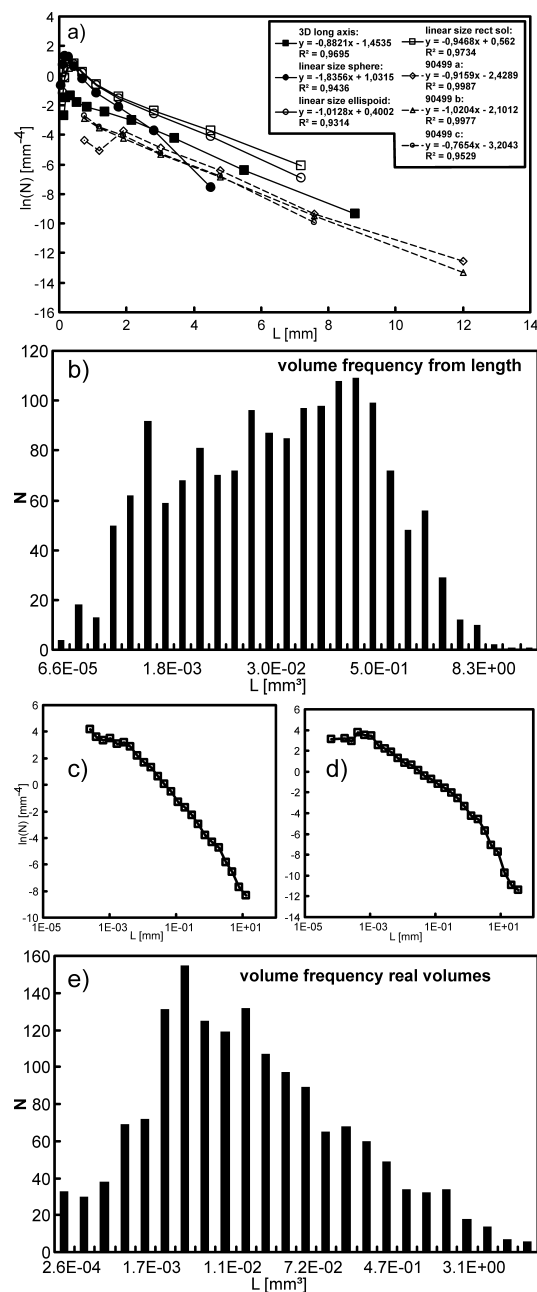


Fig. 11. a) CSD plots of linear sizes calculated from coordinates and from volumes of KF phenocrysts in the 3D model (diameter of equal volume sphere, long axis of equal volume ellipsoid, diagonal length of equal volume rectangular solid with dimensions 1:2:3) and comparison to three sample slabs of the same sample from [38]. b-e) Crystal volume distribution of KF of the 3D-model. b) Histogram of volume frequency calculated from lengths according to eq. 03. c) CSD plot from b). d) CSD plot of e) Histogram of volume frequency calculated from measured volumes (compute_volume function of GOCAD).

Touching frameworks and magma rheology

Numerical simulations of 3D arrangement of rectangular solids have shown a critical value of crystal fraction ϕ , when objects form an interlocking structure or touching framework (so-called backbone) linking opposite sides of a sample volume and thus generating a yield strength τ_y [53]. In suspensions, τ_y may be created by friction, lubrication forces, or electrostatic repulsion between individual particles [55]. In addition, crystal-melt suspensions may provide τ_y by solid connections of intergrown crystals. This is expected to occur at lower ϕ and provide larger τ_y than friction [53]. The value of ϕ_{crit} was found to be rather low at around $\phi_{\text{crit}} = 0.22 \pm 0.01$ for the most equant shapes [53]. Quantification of spatial distribution patterns of crystals in comparison with modal abundance can also highlight the threshold for touching vs. non touching crystal populations [56]. A similar threshold value to that of [53] for formation of a touching framework of phenocrysts has been shown by melting experiments of basalts [57]. Moreover, clusters of crystals can be viewed as essential building blocks of any igneous rock. These crystal clusters are much more likely to connect into a 3D touching framework at lower crystal abundances than individual crystals [56]. In contrast, phenocrysts in the Halle rhyolite are generally randomly distributed, do not form crystal clusters [38] and clearly do not form a touching framework in 3D as shown by the 3D model. Additionally, many of the aspect ratios of phenocrysts modelled in this study are not very acicular and modal abundance of phenocrysts just reaches the critical values found in models of Saar et al. [53]. Thus, the 3D model of this study suggests that phenocrysts, especially in silicic magmas, can sustain non-touching frameworks up to a slightly higher volume fraction due to a higher strength of the rhyolitic melt enabling phenocrysts to be suspended without interconnection.

Conclusions and outlook

This study has investigated the true 3D size, shape and spatial distribution of felsic phenocrysts from a highly porphyritic laccolith from the Halle igneous complex, Germany. Rigorous 3D reconstruction of felsic crystal populations using serial grinding techniques along with quantification of textures using 3D visualisation software has allowed the following conclusions and recommendations:

- 3D size distribution data meets well with stereologically corrected size distributions determined from 2D sections for a larger sample volume (area), but individual sections used for reconstruction show considerable scatter in their 2D size distributions.

- The spatial characteristics of the 3D population indicate a non-touching framework which confirms previous interpretations based on 2D spatial distribution analysis [38, 56]. The threshold established for formation of touching frameworks by numerical models might be higher in natural – especially silicic – rocks.
- 3D reconstruction of this phenocryst population shows a marked difference in shape characteristics of crystals of different sizes within the population. This indicates changing crystallization conditions during growth of the crystal population. This information is not mirrored in relatively straight CSD patterns which would normally be interpreted as indicating a simple nucleation and growth history. This advocates complex growth histories of phenocrysts in spite of their very simple and straight CSDs. Possible factors influencing crystal growth are inhomogeneous distribution of nutrients in the silicate liquid, anisotropies due to shear during magma flow, complex crystal growth mechanisms, resorption and fracturing of crystals.
- Tests on the 3D model show that CSD data can be robustly reproduced from sample sizes greater than ~200.
- 3D reconstruction and visualization of geological materials is on the way to becoming a standard technique even for materials with complex optical properties. In conjunction with feasible models for crystal growth, these would enable the 3D numerical modelling of the evolution of complex crystal textures in igneous rocks.

Acknowledgements

B.-C. Ehling and the Landesamt für Geologie und Bergwesen Sachsen-Anhalt are thanked for providing to the core depository to retrieve the sample. M. Magnus is thanked for preparation of the sample and assistance with technicalities of serial erosion. J. Neff, T. Lohr and other student assistants at TUBA Freiberg are thanked for help with image classification. C. Bauer helped converting classified images into shape files. M. Apel, G. van den Boogaart and R. Single are thanked for help with GOCAD. C. Breitzkreuz gave insightful and helpful comments on earlier versions of the manuscript. Reviewers. This paper was conceived while AM was employed within a Deutsche Forschungsgemeinschaft project granted to C. Breitzkreuz (Br 997/18-1,2).

References

- 1 A. Renzulli and P. Santi, Sub-volcanic crystallization at Stromboli (Aeolian Islands, southern Italy) preceding the Sciara del Fuoco sector collapse: evidence from monzonite lithic suite, *Bulletin of Volcanology* 59, 10-20, 1997.
- 2 J.V. Smith, Interpretation of domainal groundmass textures in basalt lavas of the southern Lamington Volcanics, eastern Australia, *Journal of Geophysical Research* 103(B11), 27383-27391, 1998.
- 3 J.E. Hammer, K.V. Cashman, R.P. Hoblitt and S. Newman, Degassing and microlite crystallization during pre-climactic events of the 1991 eruption of Mt. Pinatubo, Philippines, *Bulletin of Volcanology* 60(5), 355-380, 1999.
- 4 M. Polacci, K.V. Cashman and J.P. Kauahikaua, Textural characterization of the pahoehoe-aa transition in Hawaiian basalt, *Bulletin of Volcanology* 60, 595-609, 1999.
- 5 U. Schreiber, D. Anders and J. Koppen, Mixing and chemical interdiffusion of trachytic and latitic magma in a subvolcanic complex of the Tertiary Westerwald, Germany, *Lithos* 46(4), 695-714, 1999.
- 6 R.F. Weinberg and M.P. Searle, Volatile-assisted intrusion and autometasomatism of leucogranites in the Khumbu Himalaya, Nepal, *Journal of Geology* 107(1), 27-48, 1999.
- 7 J.E. Hammer, K.V. Cashman and B. Voight, Magmatic processes revealed by textural and compositional trends in Merapi dome lavas, *Journal of Volcanology and Geothermal Research* 100(1-4), 165-192, 2000.
- 8 G.G. Kuscü and P.A. Floyd, Mineral compositional and textural evidence for magma mingling in the Saraykent volcanics, *Lithos* 56(2-3), 207-230, 2001.
- 9 S. Couch, R.S.J. Sparks and M.R. Carroll, The kinetics of degassing-induced crystallization at Soufrière Hills volcano, Montserrat, *Journal of Petrology* 44(8), 1477-1502, 2003.
- 10 W. Müller, Strengthening the link between geochronology, textures and petrology, *Earth and Planetary Science Letters* 206, 237-251, 2003.
- 11 D.A. Jerram and M.J. Cheadle, On the cluster analysis of grains and crystals in rocks, *American Mineralogist* 85, 47-67, 2000.
- 12 M.D. Higgins and J. Roberge, Crystal Size Distribution of Plagioclase and Amphibole from Soufrière Hills Volcano, Montserrat: Evidence for Dynamic

- Crystallization-Textural Coarsening Cycles, *Journal of Petrology* 44(8), 1401-1411, 2003.
- 13 R.G. Resmini and B.D. Marsh, Steady-state volcanism, paleoeffusion rates, and magma system volume from plagioclase crystal size distributions in mafic lavas: Dome Mountain, Nevada, *Journal of Volcanology and Geothermal Research* 68, 273-296, 1995.
- 14 A. Tomiya and E. Takahashi, Reconstruction of an Evolving Magma Chamber beneath Usu Volcano since the 1663 Eruption, *Journal of Petrology* 36(3), 617-636, 1995.
- 15 M.A. Delesse, Procédé mécanique pour déterminer la composition des roches, *Annales des Mines* 13, 379-388, 1848.
- 16 M.D. Higgins, Closure in crystal size distribution (CSD), verification of CSD calculations and the significance of CSD fans, *American Mineralogist* 87, 160-164, 2002.
- 17 M.D. Higgins, Measurement of crystal size distributions, *American Mineralogist* 85(9), 1105-1116, 2000.
- 18 B.D. Marsh, Crystal size distribution (CSD) in rocks and the kinetics and dynamics of crystallization; I, Theory, *Contributions to Mineralogy and Petrology* 99(3), 277-291, 1988.
- 19 E.E. Underwood, *Quantitative Stereology*, 274 pp., Addison-Wesley, Reading, Massachusetts, 1970.
- 20 H. Elias and D.M. Hyde, *A Guide to Practical Stereology*, Karger, Basel, 1983.
- 21 D.L. Sahagian and A.A. Proussevitch, 3D particle size distributions from 2D observations; stereology for natural applications, *Journal of Volcanology and Geothermal Research* 84(3-4), 173-196, 1998.
- 22 C. Denison and W.D. Carlson, Three-dimensional quantitative textural analysis of metamorphic rocks using high-resolution computed X-ray tomography; Part II, Application to natural samples, *Journal of Metamorphic Geology* 15(1), 45-57, 1997.
- 23 C. Denison, W.D. Carlson and R.A. Ketcham, Three-dimensional quantitative textural analysis of metamorphic rocks using high-resolution computed X-ray tomography; Part I, Methods and techniques, *Journal of Metamorphic Geology* 15(1), 29-44, 1997.

-
- 24 R.A. Ketcham and W.D. Carlson, Acquisition, optimization and interpretation of X-ray computed tomographic imagery: applications to the geosciences, *Computers & Geosciences* 27(4), 381-400, 2001.
- 25 N. Petford, G. Davidson and J.A. Miller, Investigation of the petrophysical properties of a porous sandstone sample using confocal scanning laser microscopy, *Petroleum Geoscience* 7(2), 99-105, 2001.
- 26 J.M. Castro, K.V. Cashman and M. Manga, A technique for measuring 3D crystal-size distributions of prismatic microlites in obsidian, *American Mineralogist* 88(8-9), 1230-1240, 2003.
- 27 D.N. Bryon, M.P. Atherton and R.H. Hunter, The interpretation of granitic textures from serial thin sectioning, image analysis and three-dimensional reconstruction, *Mineralogical Magazine* 59(2), 203-211, 1995.
- 28 M.R. Cooper and R.H. Hunter, Precision serial lapping, imaging and three-dimensional reconstruction of minus-cement and post-cementation intergranular pore-systems in the Penrith Sandstone of north-western England, *Mineralogical Magazine* 59(2), 213-220, 1995.
- 29 R. Marschallinger, A method for three-dimensional reconstruction of macroscopic features in geological materials, *Computers & Geosciences* 24(9), 875-883, 1998.
- 30 M.J. Herbert and C.B. Jones, Contour correspondence for serial section reconstruction: complex scenarios in palaeontology, *Computers & Geosciences* 27(4), 427-440, 2001.
- 31 K.V. Cashman and B.D. Marsh, Crystal Size Distribution (CSD) in rocks and the kinetics and dynamics of crystallization II: Makaopuhi lava lake., *Contributions to Mineralogy and Petrology* 99, 292-305, 1988.
- 32 B.D. Marsh, On the interpretation of crystal size distributions in magmatic systems, *Journal of Petrology* 39(4), 553-599, 1998.
- 33 A.D. Randolph and M.A. Larson, *Theory of Particulate Processes*, 369 pp., Academic Press, New York, 1988.
- 34 K.M. Cooper and M.R. Reid, Re-examination of crystal ages in recent Mount St. Helens lavas: implications for magma reservoir processes, *Earth and Planetary Science Letters* 213, 149-167, 2003.

- 35 M.D. Higgins, Magma dynamics beneath Kameni Volcano, Thera, Greece, as revealed by crystal size and shape measurements, *Journal of Volcanology and Geothermal Research* 70(1-2), 37-48, 1996.
- 36 G.F. Zellmer, S. Blake, D. Vance, C. Hawkesworth and S. Turner, Plagioclase residence times at two island arc volcanoes (Kameni Islands, Santorini, and Soufriere, St. Vincent) determined by Sr diffusion systematics, *Contributions to Mineralogy and Petrology* 136, 345-357, 1999.
- 37 T.D. Peterson, A refined technique for measuring crystal size distribution in thin section, *Contributions to Mineralogy and Petrology* 124, 395-405, 1996.
- 38 A. Mock, D.A. Jerram and C. Breitzkreuz, Using quantitative textural analysis to understand the emplacement of shallow level rhyolitic laccoliths - a case study from the Halle volcanic complex, Germany, *Journal of Petrology* 44(5), 833-849, 2003.
- 39 F. Eigenfeld and M. Schwab, Zur geotektonischen Stellung des permosilesischen subsequenten Vulkanismus in Mitteleuropa, *Zeitschrift für Geologische Wissenschaften* 2(2), 115-137, 1974.
- 40 V. Lorenz and I.A. Nicholls, Plate and intraplate processes of Hercynian Europe during the Late Paleozoic, *Tectonophysics* 107, 25-56, 1984.
- 41 A. Kampe and W. Remy, Mitteilungen zur Stratigraphie im Raume des Petersberges bei Halle, *Montanwissenschaftliche Berichte - Deutsche Akademie der Wissenschaften, Berlin* 2, 364-374, 1960.
- 42 W. Knoth, U. Kriebel, K.-H. Radzinski and M. Thomae, Die geologischen Verhältnisse von Halle und Umgebung, *Hallesches Jahrbuch für Geowissenschaften B(Beiheft 4)*, 7-34, 1998.
- 43 C. Breitzkreuz and A. Kennedy, Magmatic flare-up at the Carboniferous/Permian boundary in the NE German Basin revealed by SHRIMP zircon ages, *Tectonophysics* 302(3-4), 307-326, 1999.
- 44 J.-L. Mallet, Discrete Smooth Interpolation in Geometric modelling, *Computer Aided Design* 24(4), 178-191, 1992.
- 45 D.A. Jerram, M.J. Cheadle, R.H. Hunter and M.T. Elliott, The spatial distribution of grains and crystals in rocks, *Contributions to Mineralogy and Petrology* 125, 60-74, 1996.
- 46 D.A. Jerram, The development and application of detailed textural analysis techniques. A case study: the origin of komatiite cumulates, PhD, University of Liverpool, 1996.

-
- 47 D.A. Jerram, Visual comparators for degree of grain-size sorting in two and three-dimensions, *Computers & Geosciences* 27(4), 485-492, 2001.
- 48 A. Toramaru, A numerical experiment of crystallization for a binary eutectic system with application to igneous textures, *Journal of Geophysical Research* 106(B3), 4037-4060, 2001.
- 49 T. Spohn, M. Hort and H. Fischer, Numerical simulation of the crystallization of multicomponent melts in thin dikes or sills - 1. The liquidus phase, *Journal of Geophysical Research* 93(B5), 4880-4894, 1988.
- 50 M. Hort and T. Spohn, Numerical Simulation of the crystallization of multicomponent melts in thin dikes or sills - 2. Effects of heterocatalytic nucleation and composition, *Journal of Geophysical Research* 96(B1), 485-499, 1991.
- 51 D.E. Kile and D.D. Eberl, On the origin of size-dependent and size-independent crystal growth: Influence of advection and diffusion, *American Mineralogist* 88(10), 1514-1521, 2003.
- 52 E. Dowty, Crystal growth and nucleation theory and the numerical simulation of igneous crystallization, in: *The Physics of Magmatic Processes.*, R.B. Hargraves, ed., pp. 419-485, Princeton University Press, Princeton, 1980.
- 53 M.O. Saar, M. Manga, K.V. Cashman and S. Fremouw, Numerical models of the onset of yield strength in crystal-melt suspensions, *Earth and Planetary Science Letters* 187, 367-379, 2001.
- 54 J.V. Smith, Structural analysis of flow-related textures in lavas, *Earth-Science Reviews* 57, 279-297, 2002.
- 55 R.G. Larson, *The structure and rheology of complex fluids*, 663 pp., Oxford University Press, Oxford, 1999.
- 56 D.A. Jerram, M.C. Cheadle and A.R. Philpotts, Quantifying the Building Blocks of Igneous Rocks: Are Clustered Crystal Frameworks the Foundation?, *Journal of Petrology* 44(11), 2033-2051, 2003.
- 57 A.R. Philpotts, J.Y. Shi and C.M. Brustman, Role of plagioclase crystal chains in the differentiation of partly crystallized basaltic magma, *Nature* 395, 343-346, 1998.

Part IV

Are laccolith complexes characteristic of transtensional basin systems? – Examples from Permocarboniferous Central Europe

Christoph Breitkreuz and Alexander Mock

in press in a Geological Society of London Special Publication

Table of contents

Abstract.....	2
Laccoliths and magmatism in strike slip settings	3
Geotectonic setting of Central Europe at the Carboniferous-Permian transition	5
Variscan intramontane strike slip basins with prominent laccolith complexes.....	5
Types of laccolith complexes	14
Discussion: Strike slip control on the evolution of laccolith complexes.....	17
Conclusions	21
Acknowledgement	22
References	22

Abstract

Comparing felsic laccolith complexes prominent in the Late Palaeozoic Ilfeld-, Saar-Nahe-, and Saale basins in Germany, a characteristic pattern related to transtensional tectonics is revealed. In contrast to central magma feeding systems recognized so far for laccolith complexes, individual units of the Late Palaeozoic Central European complexes apparently were fed synchronously by numerous feeder systems arranged laterally in a systematic pattern.

The Ilfeld basin is a small strike slip pull apart basin in the SE of the Hartz Mountains cogenetical with a neighbouring rhomb horst – the Kyffhäuser. The Ilfeld basin represents a “frozen-in” early stage of laccolith complex evolution with small isolated intrusions and domes emplaced within a common level at the intersections of intra-basinal Riedel shears. In the Saar-Nahe basin, numerous medium-sized felsic subvolcanic to subaerial complexes emplaced at a common level have been recognized (Donnersberg type laccolith complex). The magmatic evolution of the Halle Volcanic Complex in the Saale basin culminated in the ± synchronous emplacement of voluminous porphyritic laccoliths within different levels of a thick pile of Late Carboniferous sediments (Halle type laccolith complex). Laccoliths in the Halle area might consist of several laccoliths typical for the Saar-Nahe Basin according to outcrop pattern and host sediment distribution.

These three post-Variscan Central European basins are characterized by a dextral transtensional tectonic regime leading to a model for laccolith complex evolution: i) Initial lithosphere-wide faulting forms pathways for magma ascent. ii) Supracrustal pull-apart leads to the formation of a transtensional basin. iii) Continued transtension gives way to decompressional melting of the mantle lithosphere, especially if fertilized by previous magmatic activity as in the Variscan orogen. The mantle melts rise into the lower crust to differentiate, mingle or cause anatexis. iv) They homogenize and start crystallizing in a mid- to upper crustal magma chamber tapped during tectonic episodes. v) Resulting SiO₂-rich magmas ascend along major transtensional faults into thick sedimentary basin fill. The amount of transtension and the amount of melt rising from the lithospheric mantle have major influence on type and size of the laccolith complex to be formed. Additionally, the presence of a mid- to upper crustal magma chamber is a prerequisite for the formation of the Donnerberg and Halle type laccolith complexes. End of abstract

Based on a detailed study of one laccolith complex (i.e. the Halle laccolith complex, HLC) and a literature review on other laccolith complexes in Permocarboniferous Central Europe, we attempt to explain the tectonic controls on the formation of laccolith complexes in continental strike slip systems. This contribution should serve as a base for discussion about the definition of new types of laccoliths beyond the classic mechanical spectrum defined by Corry (1988) with a punch to Christmas tree geometry.

Laccoliths and magmatism in strike slip settings

Laccoliths are intrusive bodies with a flat lower and a curved upper contact. They are common features of intrusive mafic and felsic intracontinental magmatic provinces (Corry 1988; Friedman & Huffman 1998). Several aspects of their emplacement and geometry are not well understood. The classic approach of Gilbert (1877) in the Tertiary Henry Mountains in Utah has been developed further by Corry (1988) with finite element modelling and thorough field investigations (Johnson & Pollard 1973; see also: Jackson & Pollard 1988; and Kerr & Pollard 1998 for recent numerical modelling approaches). Corry postulated that the level of neutral buoyancy of magma and country rock is the major controlling factor for the initiation of laccolith formation. However, other parameters are important such as the presence of fluids, the stress field in the host rock, and dynamic features of the rising magma (crystallization, viscosity, magma driving pressure, transport rate). According to analogue modelling, laccolith emplacement also requires the presence of a weak layer, e.g. a sole thrust or a less competent lithology, near the level of emplacement (Roman Berdiel et al. 1995). There, the orientation of magma flow changes from vertical to horizontal. A sill of ~ 30 m thickness forms first and inflates upon reaching a critical expanse determined by the effective thickness of the overburden (Johnson & Pollard 1973; Pollard & Johnson 1973), given that the supply of magma is sufficient.

Recent studies suggest that laccolith-like mechanisms play a major part in the emplacement even of large plutonic bodies (e.g. Vigneresse et al. 1999). Furthermore, the magma chamber below many caldera complexes has a laccolithic geometry ("lacco-caldera" according to Henry et al. 1997). Depending on the surrounding geology and tectonic setting, laccolith geometries might become much more complex than the simple mechanical models suggested (Morgan et al. 1998).

Before turning to the laccoliths in the strike slip pull-apart basins of Permocarboniferous Central Europe, as a means of comparison, we would like to introduce some examples of

similar tectonic environments showing different styles of magmatism. They represent different styles of deformation and magmatic activity ranging from ancient plutonic emplacement to recent volcanic features.

In the north-western corner of the Arabian plate, near the triple junction of Anatolia, Arabia and Africa, Late Cenozoic elongate volcanoes, volcanic ridges and linear clusters of adjacent volcanic vents are rooted on tension fractures, which are a kilometre or several kilometres in length and show similar development in depth. Non-volcanic tension fractures are also common (Adiyaman & Chorowicz 2002).

Late Jurassic strike slip intra-arc basins formed along the axis of earlier Early to Middle Jurassic extensional intra-arc basins in western North America. Volcanism occurred only in releasing bends in the Late Jurassic arc, producing more episodic and localized eruptions than in the extensional arc, where volcanism was voluminous and widespread (Busby 2002).

The Ollo de Sapo domain of the northern part of the Variscan belt of Spain contains Precambrian and Ordovician metamorphic rocks intruded by the Guitiriz granite. The domain is bounded by two N-S transcurrent shear zones. Plutonism occurred in three steps: (1) development of N-S trending structural and magnetic fabrics; (2) concordant structures in granites and country rocks; and (3) development of shear zones along the eastern and western granite margins. The proposed emplacement model involves the northwards tectonic escape of a crustal wedge – the Ollo de Sapo Domain – bounded by two shear zones acting as conjugate strike slip zones (Aranguren et al. 1996).

The island of Vulcano is composed of four main volcanoes which date from about 120 ka to historical times. The time-space evolution of the volcanism indicates a shifting of the activity from the southeastern sectors towards the northwest. Two main systems of NW-SE-trending right-lateral strike slip faults affect the island. NE-SW- and N-S-trending normal faults are also present. This system of discontinuity is related to the stress field acting in the southern sector of the Aeolian Archipelago. Volcanological and geochronological data are also consistent with the opening of a pull-apart basin (Ventura 1994).

These examples show that a strike slip tectonic environment can produce very different styles of magmatism. In the next section, the focus will turn on some specific examples from the Carboniferous-Permian transition in Central Europe. They will be compared to the well investigated classic examples of the Tertiary Colorado Plateau in the Western US.

Geotectonic setting of Central Europe at the Carboniferous-Permian transition

A number of rift related basin systems with pronounced magmatic activity developed in the wane of the Variscan orogenesis in the foreland and on the cratonic blocks of former Baltica (Arthaud & Matte 1977). Among these are the Oslo graben, Norway, the Whin Sill region, Northern England, the North Sea graben systems Central and Horngraben – the former dominated by tholeiitic flood basalts, the latter with chemically varied magmatism – and the central NE German Basin. The latter contains about 48,000 km³ of volcanic rocks with subordinate SiO₂-poor lavas, but dominantly (~70%) SiO₂-rich, calc-alkaline, subaerial ignimbrites and lava domes (Fig. 1, Benek et al. 1996; Breitzkreuz & Kennedy 1999).

The decaying Variscan Orogen itself, on the contrary, was characterized by gravitational collapse and dextral strike slip (Henk 1997). A number of basins developed within this tectonic framework in the later Alpine region, the Pyrenees, the Sudetic Mountains, the Thuringian Forest, SW Germany, and – focussed on in this study – the basins Saar-Nahe, Saale, and Ilfeld (Fig. 1). Sedimentation in the latter basins started early (Namurian, Westfalian, and Stephanian, respectively), the onset of volcanism took place at a later stage. A longstanding volcanic evolution with a climax at around 300 Ma as in other areas is recorded. Also, subvolcanic SiO₂-rich complexes are prominent here. For these Central European systems, a complex magma genesis has been assumed involving mantle derived melts which experienced differentiation and mixing with anatectic crustal melts (Arz 1996; Büthe 1996; Romer et al. 2001). The intrusive complexes in the Saar-Nahe, Saale, and Ilfeld basins will be discussed in detail in the next section.

Variscan intramontane strike slip basins with prominent laccolith complexes

The Ilfeld Basin is a small strike slip pull apart basin that formed cogenetically with a neighbouring rhomb horst – the Kyffhäuser – in the SE of the Hartz Mountains, Germany (Fig. 2). It is characterized by subalkaline high-K magmatic rocks: pyroclastics, lavas, and minor subvolcanic intrusions. The sedimentary basin fill spans from the Stephanian to Saxonian with mainly alluvial fan deposits (conglomerates and coarse, poorly sorted partly cross bedded sandstones), some coal bearing fine grained sediments, and an interlayering of clay-bearing siltstones and cross-bedded sandstones. Partly, silicified limestone beds occur. Compositions of the volcanic rocks cover the range of latitic-andesitic, andesitic, rhyodacitic,

and rhyolitic. They formed pyroclastic flow deposits (partly ignimbrites), lavas, and ash tuffs. Radiometric dating of dykes and a rhyolite conglomerate revealed ages from 289 to 298.6 ± 1.6 Ma (Büthe 1996). The volume of intrusive/lava dome material has been estimated at about 15 km^3 , the total amount of magmatic material (extrusive andesitic pyroclastics and rhyolitic lavas with a non-quantifiable amount of rhyolitic dykes) is about 24 km^3 .

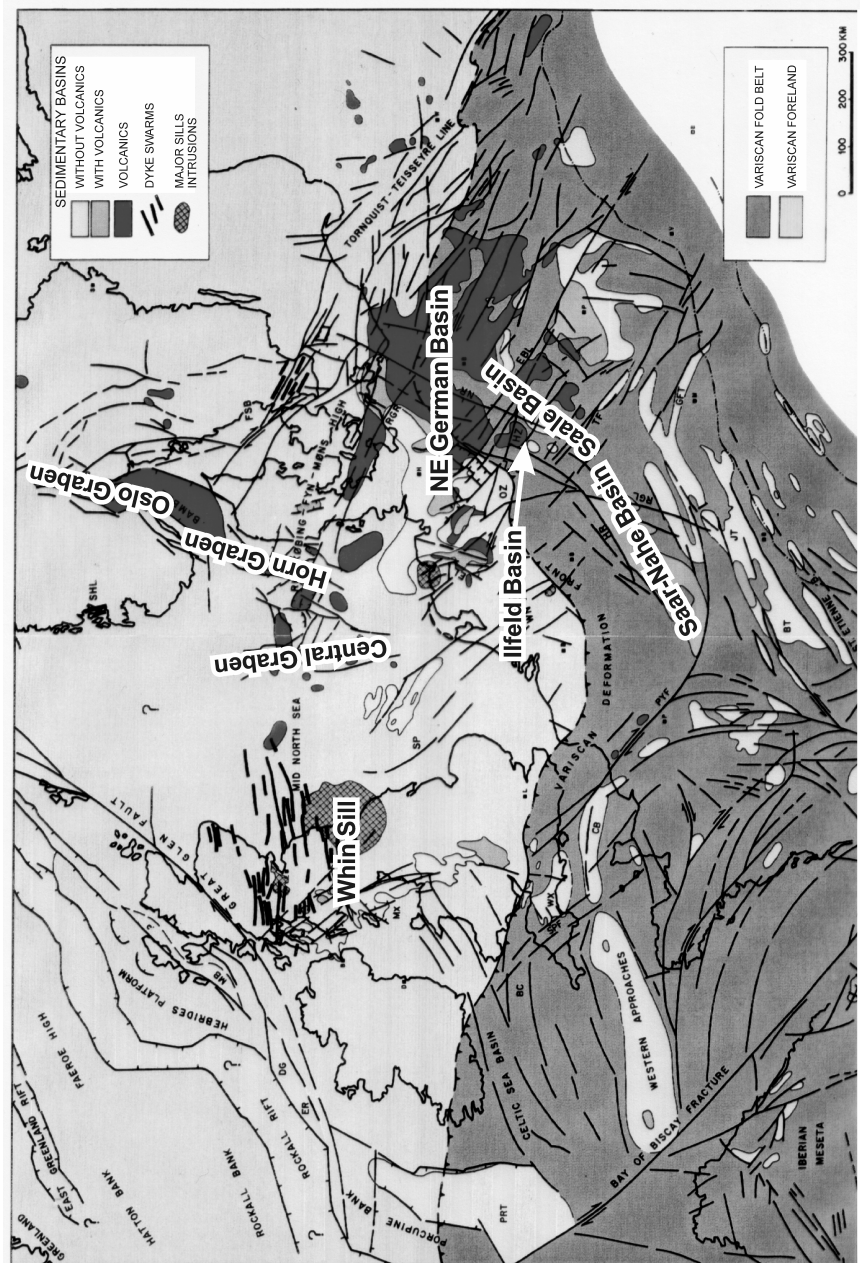


Fig. 1. Palaeogeographical map of Central Europe at Late Palaeozoic times after Ziegler (1990). The main regions of volcano-tectonic activity are indicated as well as the basins focussed on in this study.

In the Ilfeld basin, small isolated felsic intrusions and domes emplaced and extruded within a common stratigraphic level at the intersections of intra-basinal syn- and antithetic Riedel shears (Fig. 2, Büthe & Wachendorf 1997). Some rhyolitic domes crop out at the margin of the basin, but most magmatic centres are inferred from gravimetric and geomagnetic surveys (Büthe 1996). The emplacement character of the domes has not been shown unambiguously, but they are believed to be mainly extrusive.

The Ilfeld Basin in the Hartz Mts.

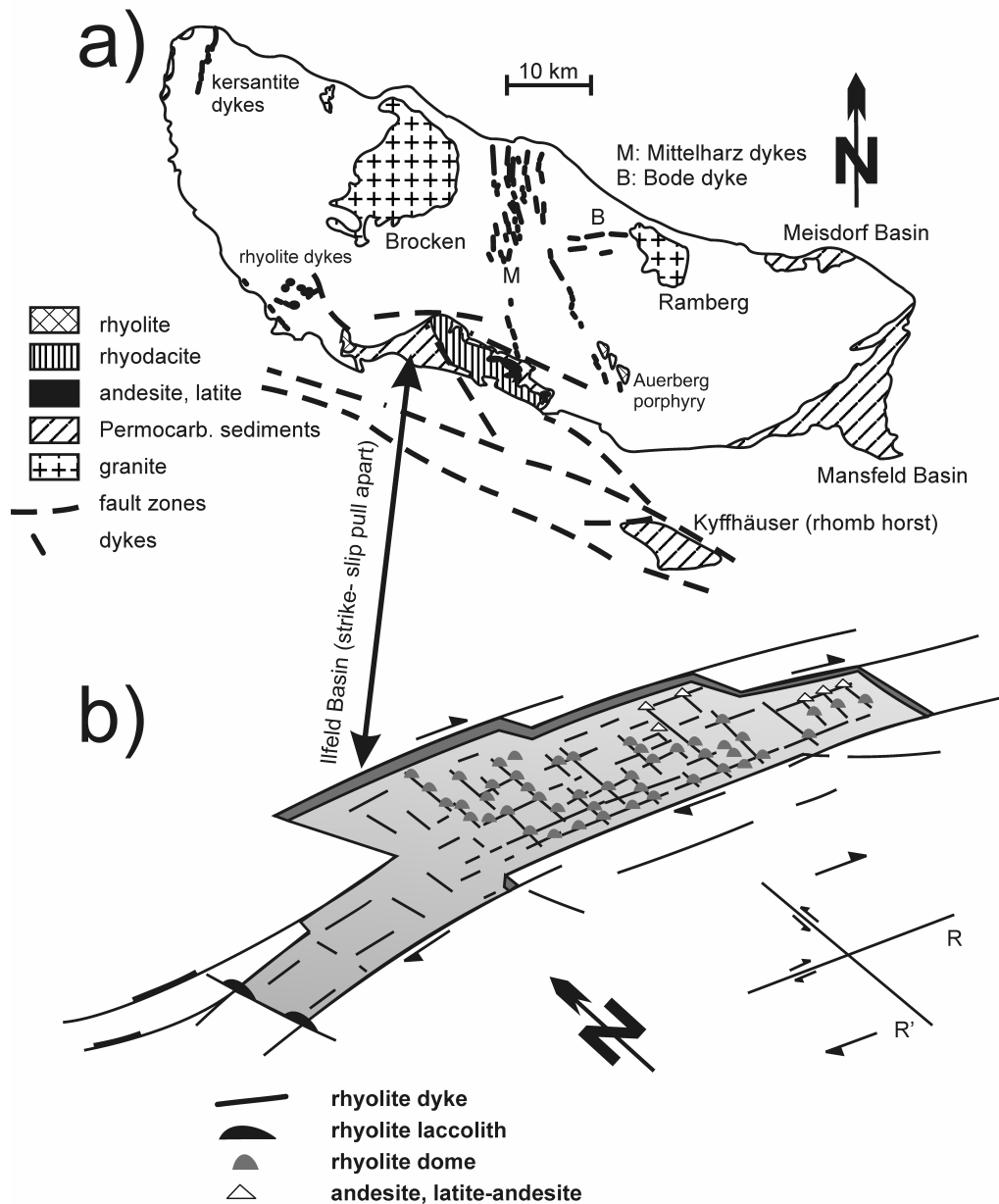


Fig.2. (a) The Ilfeld basin south of the Hartz Mountains (location see Fig. 1) and its connection to the Kyffhäuser crystalline rise as a strike slip pull-apart structure with a rhomb horst. (b) Structure and spatial pattern of intrusive bodies in the Ilfeld basin. The correlation between points of intersecting complementary Riedel shears and magmatic activity becomes evident (modified after Büthe 1996).

The Saar-Nahe basin is filled by lacustrine, deltaic, fluvial, and alluvial fan deposits (Stollhofen & Stanistreet 1994). Predominant lithologies are grey shales with minor coal horizons, conglomerates, and sandstones interrupted by phases of volcanic activity (effusive basaltic to andesitic and rhyolitic deposits of pyroclastic flows from phreatoplinitic eruptions). Four main tectono-stratigraphic phases can be recognized: (1) initial proto-rift, (2) prevolcanic syn-rift, (3) volcanic syn-rift, and (4) final post-rift phases. The intrusive activity

mainly took place in the volcanic syn-rift phase of basin evolution. In the Saar-Nahe basin, around 230 km³ of medium-sized felsic subvolcanic to subaerial complexes have been recognized (Bad Kreuznach, Donnersberg, Kuhkopf, Nohfelden etc. Fig. 3; see Lorenz & Haneke this volume). In the Saar-Nahe basin, there are abundant contemporaneous pyroclastic deposits related to the formation of the laccolith/dome complexes. Events of volcanic activity are closely related to tectonic events in the basin history (Stollhofen et al. 1999).

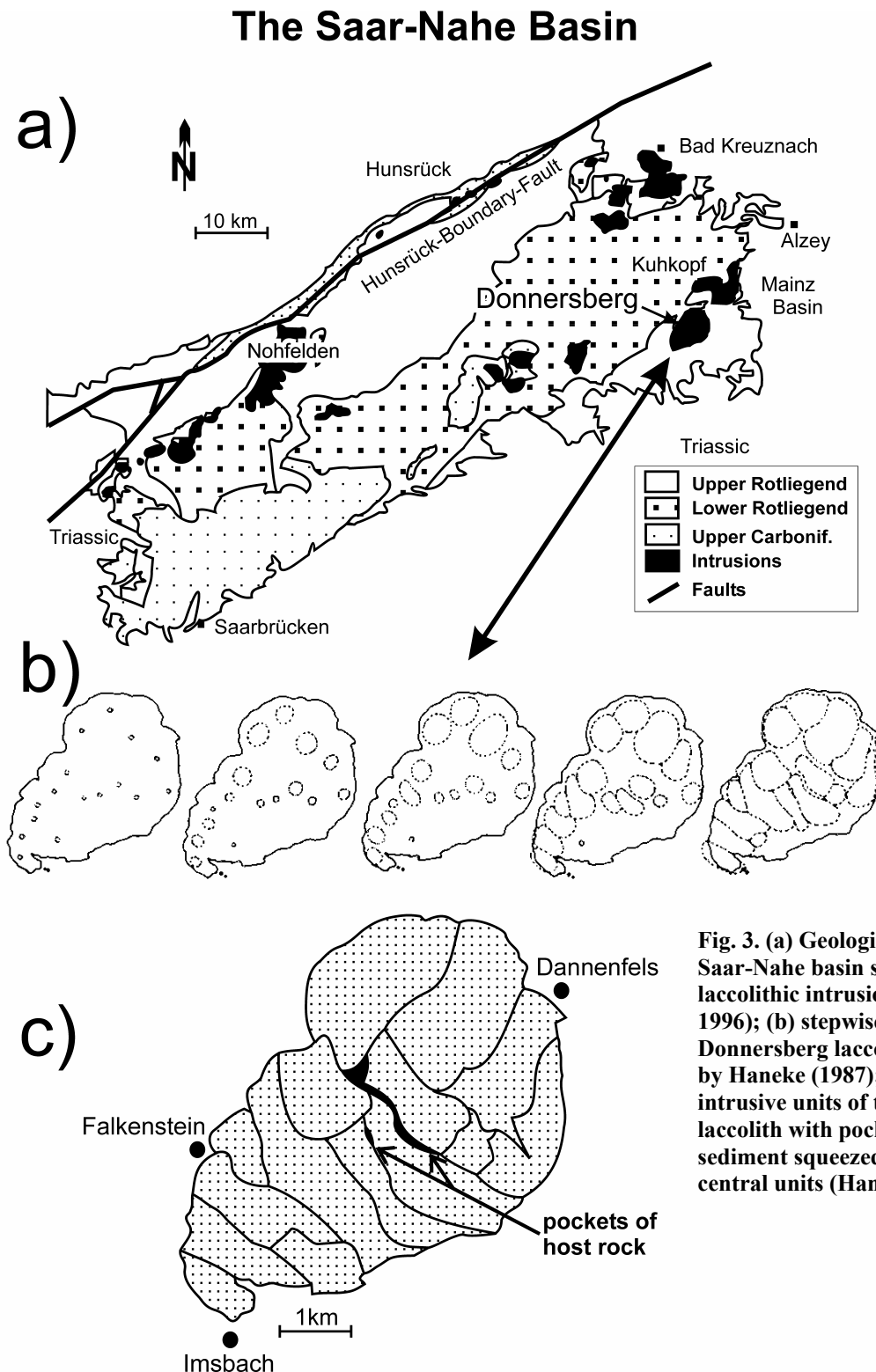
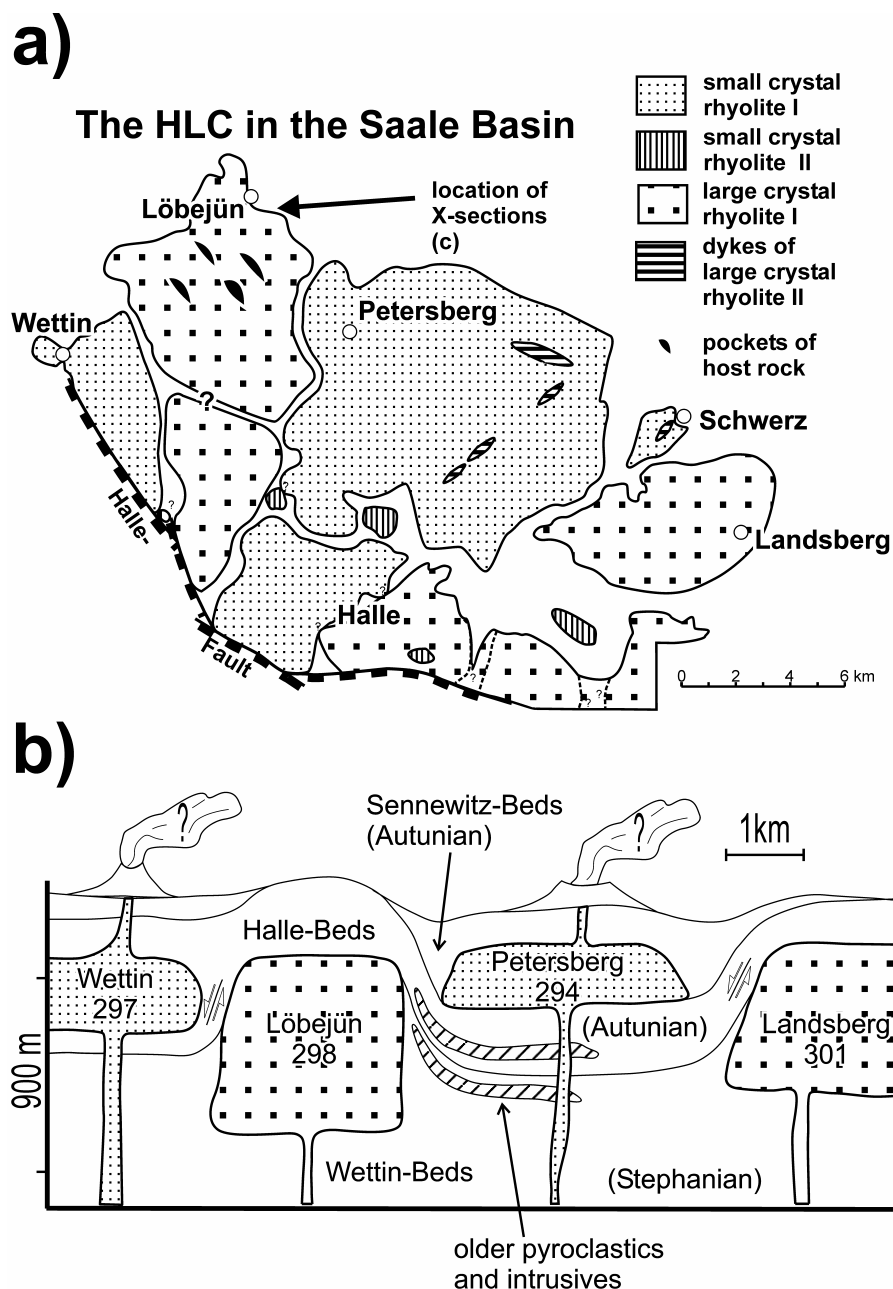


Fig. 3. (a) Geological map of the Saar-Nahe basin showing the main laccolithic intrusions (black Arz 1996); (b) stepwise intrusion of the Donnersberg laccolith as envisioned by Haneke (1987); (c) different intrusive units of the Donnersberg laccolith with pockets of host rock squeezed in between some central units (Haneke 1987).

The Donnersberg laccolith complex might represent a continuation of the Ilfeld like scenario. Flow foliation measurements led Haneke (1987) to distinguish 15 units emplaced in lateral contact with each other within the same stratigraphic level – like balloons inflated in a box. Abundant mafic sills and dykes occur in the Donnersberg area. The rhyolite dome intruded in a very shallow level. It was exposed rapidly and deposited its own debris apron during and shortly after emplacement. A deep seated intrusion preceded the shallow intrusion of the Donnersberg massive. It was inferred from seismic exploration of the area and has been postulated because the pre-Donnersberg sediments are less thick in the area surrounding the Donnersberg than elsewhere in the generally subsiding Saar-Nahe basin. Rocks equivalent to the Donnersberg rhyolite have been dated with Rb/Sr to 280 Ma and with Ar/Ar to 295-300 Ma. Arikas (1986) subdivided the Donnersberg complex into 4 different units according to their geochemical characteristics. The volume of the Donnersberg was estimated at around 40 km³.

The magmatic evolution of the Halle Volcanic Complex in the Saale basin culminated in the ± synchronous formation of > 200 km³ of porphyritic rhyolitic laccoliths which emplaced in different levels of the thick pile of Late Carboniferous sediments (i.e. the Halle laccolith complex (HLC), Fig. 4, Schwab 1965; Kunert 1978; Breitkreuz & Kennedy 1999). Romer et al. (2001) reported the remarkably homogeneous composition of the laccolith complex. The main laccolith units (Wettin, Löbejün, Petersberg, Landsberg) are separated by tilted host sediments (Fig. 4, Kampe et al. 1965). These consist of a succession of grey silt- and mudstones with several fine sandstone beds and coal seams, and a fluvio-limnic succession of reddish-grey conglomerates, siltstones, clays, and sandstones with abundant volcanoclastics (Kampe & Remy 1960; Knoth et al. 1998). The large thicknesses, very thin contact aureoles and lacking or very thin chill zones within the laccoliths indicate the intrusive character of the rhyolitic intrusions (Schwab 1962; Mock et al. 1999). The coarsely porphyritic units (Löbejün, Landsberg; phenocryst content up to 35%) are thicker (>1000 m) than the finely and generally less porphyritic units (Petersberg ≤ 500m, Wettin, < 300 m, Fig. 4), and they emplaced at deeper levels.

Fig. 4. (a) Map of the HLC, after B.-C. Ehling, LGBSA, Halle (pers. comm.); (b) sketch cross E-W through the HLC. Numbers in the sketch cross section refer to U/Pb-SHRIMP (Sensitive High Resolution Ion Microprobe) ages from Breitzkreuz & Kennedy (1999).



Bowl-shaped flow banding geometries have been observed in SiO₂-rich lavas and lava domes (e.g. Fink 1987). In contrast, intrusions develop an onion-like closed flow banding with cupola-shapes in the upper part and bowl-shapes in the lower part

(Nickel et al. 1967; Fink 1987). In the Halle laccoliths, flow structures are present only in the small-crystal units. Flow banding structures show complexly cupola- and bowl-shaped geometries, inferring erosion to the upper or lower part, respectively; sometimes flow banding indicates feeder systems (Mock et al. 1999). The flow structures of the Wettin laccolith, the style of the out- and subcrop of the Löbejün laccolith, and the occurrence of at least four pockets of host sediment trapped during the emplacement at the top of the Löbejün laccolith suggest that individual Halle type laccoliths may consist of several Donnersberg type units (see Figs. 4, 6, and next section). Size distributions and the spatial arrangement of the felsic phenocrysts in the Petersberg laccolith put forward that the intrusion formed by several magma batches without major cooling in between (Fig. 4 and Mock et al. 2003). Only minor

pyroclastic activity associated with the intrusion of the laccoliths took place in the HLC (Büchner & Kunert 1997). Instead, the topographical heights created during laccolith intrusion led to more pronounced erosion and subsequent exhumation of each laccolith. Abundant clasts of the porphyritic rhyolite of the laccoliths can be found in the alluvial fan deposits filling the valleys between the laccolith hills.

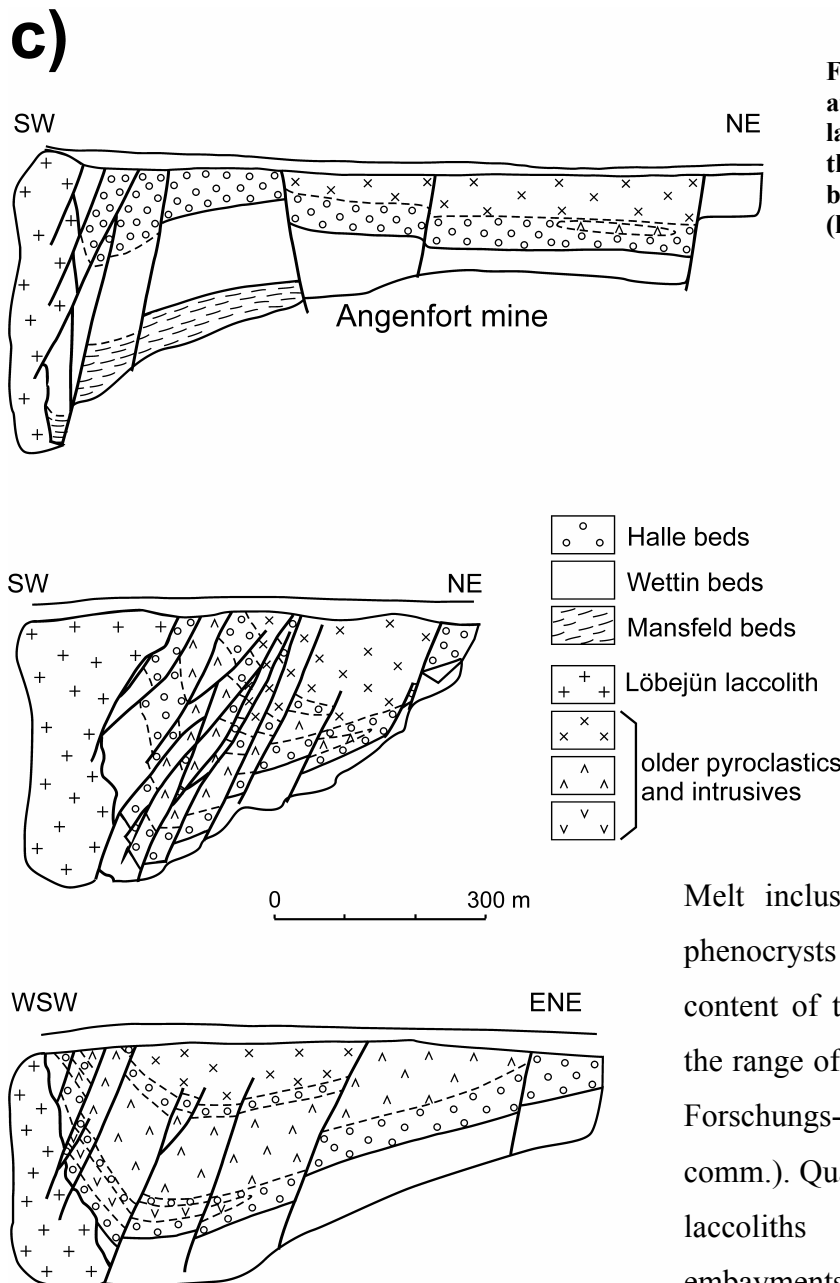


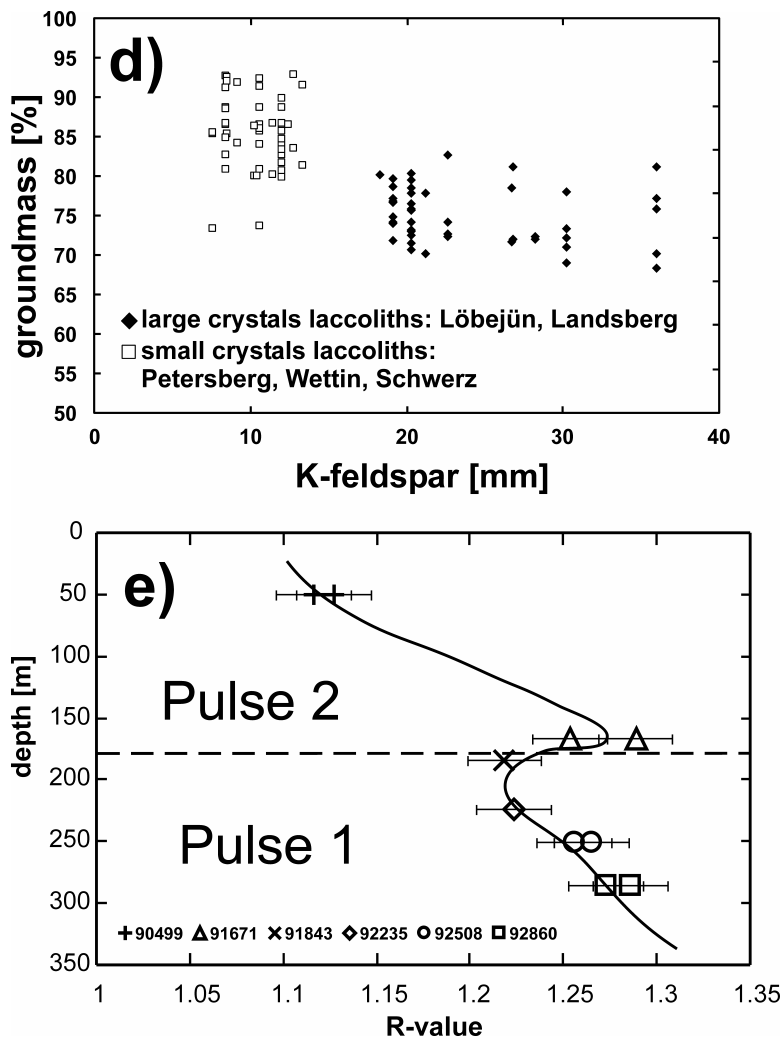
Fig. 4 cont. (c) three cross sections at the margin of the Löbejün laccolith after Kampe (1965) show the host rock deformation caused by the emplacing laccolith (location see a).

Melt inclusion compositions in quartz phenocrysts indicate that the H_2O -content of the magma was originally in the range of 2-3% (Rainer Thomas, Geo-Forschungs-Zentrum, Potsdam, pers. comm.). Quartz pheno-crysts in the Halle laccoliths are often broken along embayments, the fragments slightly rotated and annealed (Fig. 5).

Presumably, the rising magma vesiculated upon decompression in some 3-4 km depth (Eichelberger et al. 1986); vesiculation inside the embayments led to the fragmentation of quartz phenocrysts (Best & Christiansen 1997). Thus, volatile loss into the unconsolidated

sediments of the Saale basin was possible. As a result, the volatile-poor magma was emplaced as laccolith or lava, instead of erupting explosively. However, the exact conditions determining effusive (lava) or intrusive (laccolith) emplacement are still contentious.

Saar-Nahe and Saale basin are associated with major lineaments of the late Variscan orogenesis; the Hunsrück fault and the Northern Hartz boundary fault. Early in their history, these basins show only minor evidence of intrusive activity, but volcanism was eruptive. The Iffeld basin represents such an early stage of basin evolution. The inferred magmatic centres (Fig. 2) led mainly to the formation of domes and to eruptive activity. In the Saar-Nahe basin, like in the Iffeld basin, a relation between eruptive centres and the pattern of strike slip faults and Riedel shears can be shown (Stollhofen et al. 1999).



The size of these three basins has been estimated from maps or cited from the references given (Tab. 1). The volume of laccolithic intrusions or domes respectively has been estimated from the subcrop and outcrop maps (Figs. 2 to 4). The areas of out- and subcrop have been multiplied by the exposed thickness or the true thickness prior to erosion where indicators provide a present level of erosion (see above). The values such obtained are minimum values.

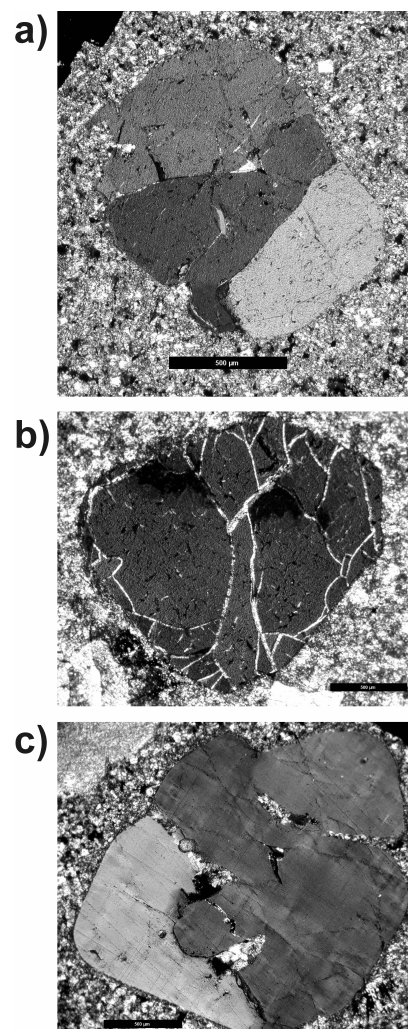
Fig. 4 cont. (d) plot of groundmass content vs. size of K-feldspar phenocrysts for 99 samples from the porphyritic rhyolitic laccoliths of the HLC showing the clear distinction between the large and small crystal varieties; **(e)** R-value vs. depth plot of six samples from a drill core through the Petersberg laccolith suggesting the intrusion of the laccolith by at least two batches of magma. For details on the R-value method see Jerram et al. (1996) and Mock et al. (2003).

Table 1. Comparison of three Variscan intra-montane basins and the dominant laccolith complexes

Basin, laccolith province*	Size	volume of SiO ₂ -rich Magma as laccoliths	Styles of magmatism	Tectonic setting	References
Ilfeld (900 m)	120 km ²	~ 15 km ³	Dominantly felsic subalkaline, pyroclastics, lava flows and domes	Strike-slip pull-apart	Büthe (1996)
Saale Basin (~3000 m)	>1000 km ² (cut off by faults)	~ 210 km ³ (HLC only)	Dominantly felsic, calc-alkaline, laccoliths, lava flows and domes, and pyroclastics	Orogenic collapse associated with overall dextral strike slip	Romer <i>et al.</i> (2001) Schneider <i>et al.</i> (1994) Schneider <i>et al.</i> (1998)
Saar-Nahe (>10000 m)	4800 – 6000 km ²	~ 230 km ³ (Donnersberg: 40 km ³)	Bimodal calc-alkaline, pyroclastic and extrusive, laccoliths becoming cryptodomes	Orogenic collapse associated with overall dextral strike slip	Haneke (1987) Stollhofen (1999)

*First column in brackets: cumulative thickness of sedimentary basin fill.

Fig. 5. Broken quartz phenocrysts from the rhyolitic laccoliths of the HLC; (a) sample HA 1-55 from the drill core situated in the Landsberg laccolith (Fig. 4); (b) sample HA 5-9 from the Schwerz quarry near Landsberg (Fig. 4); (c) sample 28/8/97/4 from a quarry at the Quetzer Berg, NE of the Schwerz quarry. For approximate locations see Fig. 4. Scale bars are 500 µm.



Types of laccolith complexes

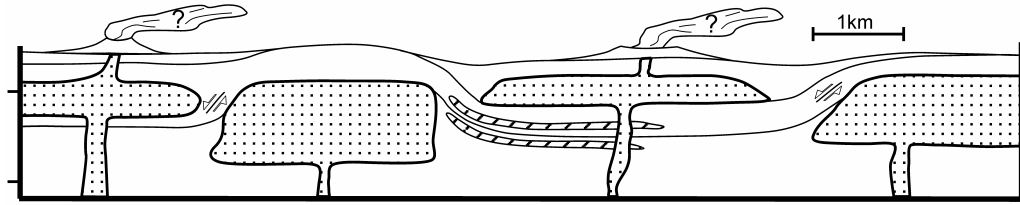
The types of basins and associated laccolith complexes from the previous chapter shall now be compared with the classic concept developed for laccoliths. Corry (1988) suggested a spectrum of laccolith types and shapes with two end-member geometries: Punch and Christmas tree. These are fed by central single-conduit plumbing systems. In contrast, the individual units of the Late Palaeozoic Central European laccolith complexes, apparently, were fed synchronously by numerous feeder systems laterally arranged in a systematic pattern (Fig. 6):

- the Donnersberg type (Saar-Nahe basin, Haneke 1987): a group of intrusions (each about 500 – 1000 m in diameter) with discrete conduits, emplaced simultaneously at \pm the same stratigraphic level. In the course of emplacement, the intrusive bodies get in contact with and sometimes penetrate each other. According to Lorenz and Haneke, (this volume) some of the very shallow-level intrusions breached their roofs forming dome complexes.
- the Halle type (Saale basin, Kunert 1978; Mock et al. 1999): \pm synchronous emplacement of laccolith units (several km in diameter, several hundreds to (?) more than a thousand meters thick) into different stratigraphic levels by sub-sequent magma batches with no intermittent cooling, resulting in the laccolith units being separated by host rock sediments. Individual Halle type laccoliths might consist of several Donnersberg type units (Fig. 6, see also Fig. 4 and previous section).

The above mentioned laccolith complexes can be envisioned as fully developed. The small strike slip pull apart basin of Ilfeld on the southern flank of the Hartz Mountains, Germany, contains a large number of small scale intrusive centres. They indicate the tectonic control on magma ascent and emplacement in these transtensional settings and might even be pictured as early stages of the magmatic evolution in these basin types (see next section and Fig. 2).

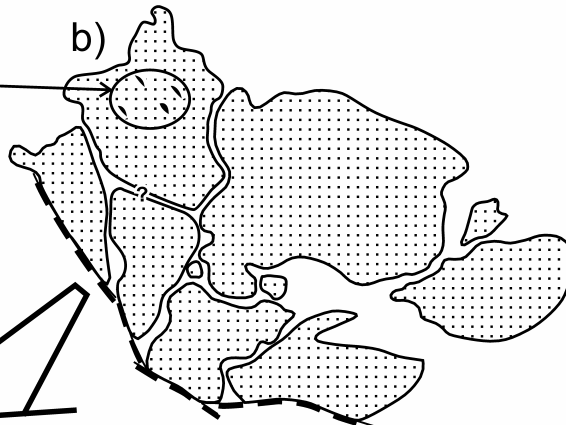
The laccolith complexes of the Halle and Donnersberg type formed in Late Palaeozoic basin systems which have been controlled by continent-scale dextral strike slip (Arthaud & Matte 1977). The Tertiary laccolith complexes in the Paradox Basin in Utah – the classic sites of laccolith research (see above) – are the product of extensional basin and range tectonics (Tab. 2, Huffman & Taylor 1998). The complexes are slightly offset from the intersection points of major lineaments. The basin is an order of magnitude larger than the Palaeozoic basins described above.

a) Halle type



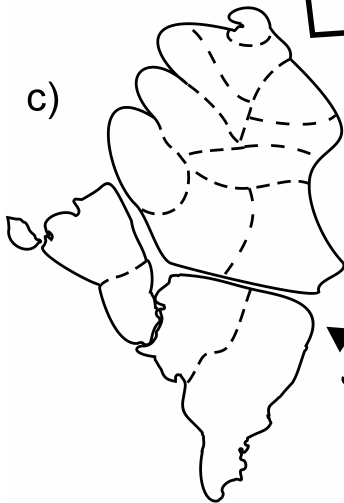
sediments as
pockets between
intrusive bodies

b)

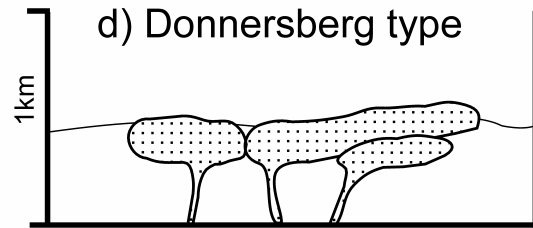


10 km

c)



d) Donnersberg type



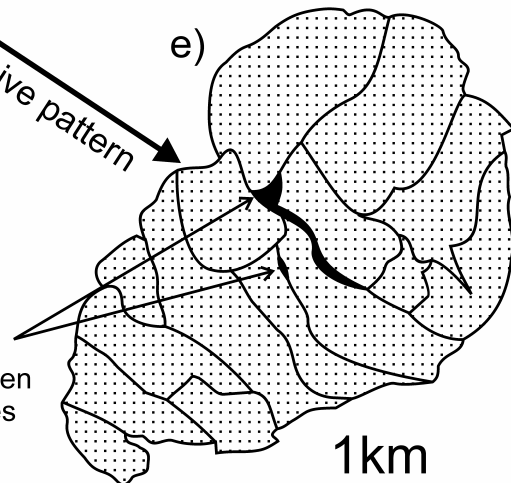
1km

similar intrusive pattern

☐ intrusive bodies

sediments as
pockets between
intrusive bodies

e)



1km

Fig. 6. Comparison of laccolith types in Tertiary Utah and Permocarboneous Central Europe (Breitkreuz & Mock 2001); (a) sketch cross section of the HLC after Breitkreuz & Kennedy (1999) showing the main laccoliths and different stratigraphic units which they intruded into (compare with Fig. 4); (b) subcrop map of the porphyritic rhyolites of the HLC; (c) possible intrusive pattern of the Löbejün and Wettin laccoliths (enlargement from (b), not stippled for clarity) for comparison with the Donnersberg type; (d) cross section of the Donnersberg laccolith of the Saar-Nahe basin (Haneke 1987). It intruded into one stratigraphic level, the Nahe Subgroup (Autunian/Saxonian, 290-272? Ma (German-Stratigraphic-Commission 2002), compare with Fig. 3); (e) map of the Donnersberg laccolith with distinct intrusive bodies (Fig. 3, Haneke 1987).

f) Location map
SW USA

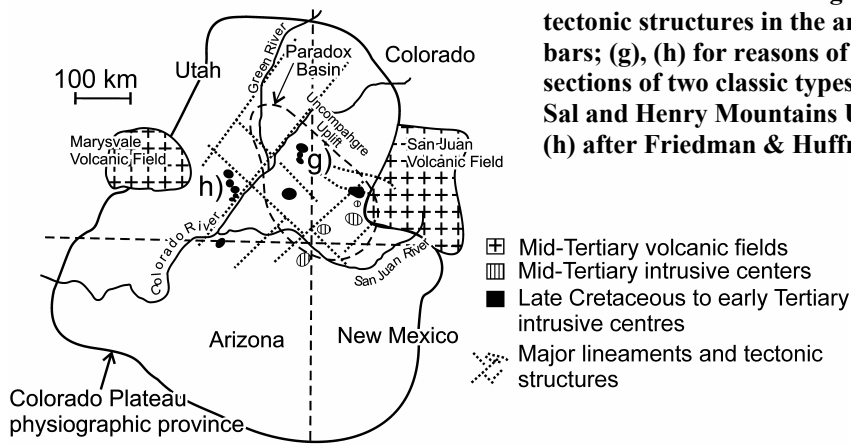
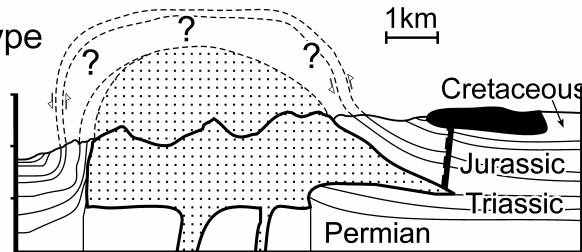


Fig. 6 cont. (f) location of the Utah laccoliths on the Colorado Plateau showing their relation to major tectonic structures in the area. Note the different scale bars; (g), (h) for reasons of comparison, the cross sections of two classic types of laccoliths from the La Sal and Henry Mountains Utah/USA are given. (f), (g), (h) after Friedman & Huffman (1998).

g) Punch type



h) Christmas tree type

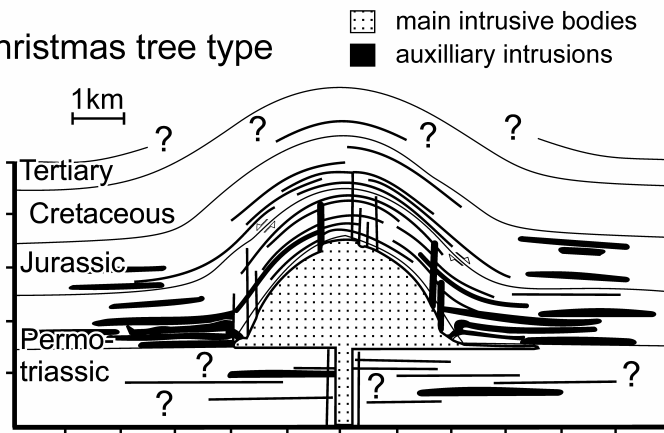


Table 2. Features of the laccolith complexes in the Colorado Plateau region

Basin, laccolith province	Size	Magma volume as laccoliths	Volume of pyroclastics	Styles of magmatism	Tectonic setting	References
Colorado plateau (e.g. Paradox Basin)	42000 km ²	139 km ³	unknown	Dominantly mafic	Subduction related crustal extension, uplift	Friedman & Huffman (1998)

Discussion: Strike slip control on the evolution of laccolith complexes

The laccoliths of Permocarboneferous Europe differ from those first described from the Western United States in a number of significant ways. Some ideas on the tectono-magmatic control of basin evolution that might account for these differences are presented in this section. As discussed below, the controlling parameters for the formation of the Central European laccolith complexes are active in different levels of the lithosphere affected by intra-continental strike slip tectonics (Fig. 7).

Amount and rate of magmatism is related to the rate and amount of strike slip, but also to the (pre-)conditions (temperature, composition) of the mantle which undergoes partial melting. Magma generation in intra-continental (trans)tensional systems is related to decompressional melting of the asthenospheric and/or lithospheric mantle. ~10% of melt are generated on average with every GPa of lithostatic pressure released during upwelling (corresponding to an uplift of ~35 km Asimov 2000). In the case of melt generation in the asthenosphere, large amounts of lithospheric stretching are required (Harry & Leeman 1995) and magmatism of asthenospheric origin would occur relatively late during strike slip basin evolution. In contrast, early magmatism, prominent during the initial stages of transtension, is characteristic of decompression of lithospheric mantle which has been fertilized with magma and fluids during previous plate tectonic processes, such as subduction. This model has been developed for initial magmatism in the Tertiary Basin and Range Province (Harry & Leeman 1995; Hawkesworth 1995).

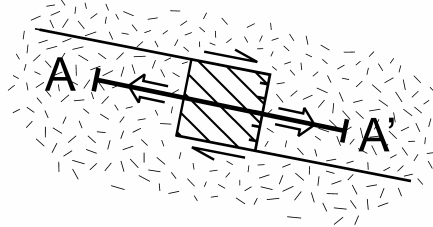
Applying simple models for the structure of mantle and crust under transtension (e.g. from Turcotte & Schubert 2002 p. 75), a melt percentage may be calculated considering the above mentioned relation of melt percentage to the lithostatic pressure release. The thickness of the subcontinental lithosphere after stretching is then:

$$h_{stretched} = h_{unstretched} \left(\frac{\rho_m - \rho_l}{\rho_m - \rho_s} \right) \left(1 - \frac{1}{\beta} \right) + \frac{h_{unstretched}}{\beta}, \quad (01)$$

with β = stretching factor, ρ_m = density of the asthenosphere, ρ_l = density of the lithosphere, ρ_s = density of the sedimentary basin fill and h = thickness. Assuming reasonable mean densities ($\rho_m = 4500 \text{ kgm}^{-3}$, $\rho_l = 3200 \text{ kgm}^{-3}$, $\rho_s = 2200 \text{ kgm}^{-3}$), a stretching factor $\beta = 1.5$, and an initial continental lithosphere of ~120 km (Henk 1997), the resulting thickness amounts to

~100 km. This corresponds to a lithostatic pressure release of ~0.6 GPa at the base of the lithosphere and thus to a melt percentage of ~6% (Asimov 2000). Higher temperatures in the mantle, as discussed for post-Variscan Europe (Henk 1997; Ziegler & Stampfli 2001), would result in a slightly higher percentage of melt (Harry & Leeman 1995).

a) map view:



b) lithosphere wide cross section:

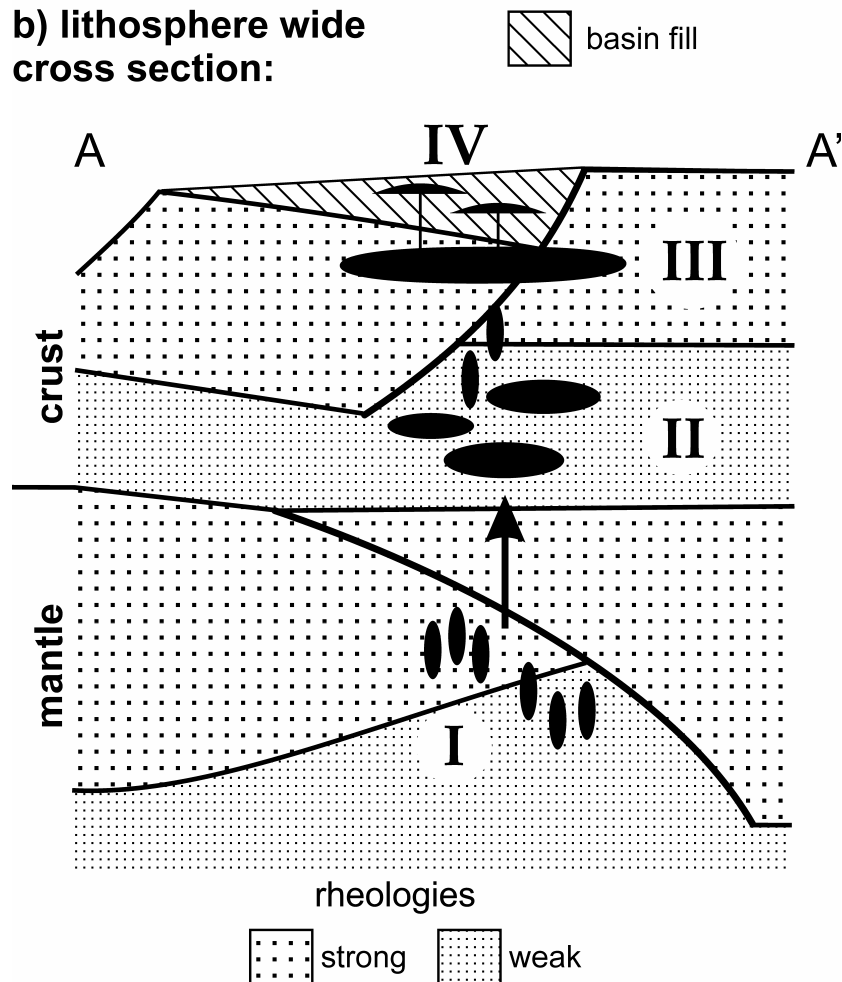


Fig. 7. Simple model of a strike slip pull-apart basin in (a) map and (b) lithosphere wide section view; different rheologies and sites of magma generation, ponding, and emplacement are shown. I: decompressional melting in the lithospheric and/or asthenospheric mantle; II: magma differentiation, anatexis, and magma mingling in the lower crust; III: magma chamber in the mid- to upper crust; IV: emplacement of laccolith complexes in the un- to semi-consolidated basin fill. See text for further explanation. Partly after Eisbacher (1996) and Reston (1990).

Following this concept, the late start of magmatism in the Saar-Nahe, Saale, and Ilfeld basins points to a certain asthenospheric melt contribution, the amount of which has not been fully constrained, yet (see Arz 1996; Büthe 1996 for contributions on magma genesis; Romer et al. 2001). In comparison, the strong initial magmatism in the NE German Basin reflects melt generation in the lithospheric mantle (Marx et al. 1995; Benek et al. 1996; Breitzkreuz & Kennedy 1999).

The formation of laccolith complexes requires evolved viscous magmas. Principally, these SiO₂-rich magmas can form by differentiation of mantle melt, by anatexis of continental crust due to magmatic underplating, and by mixing and mingling of mantle derived with crustal melts. Presumably, these processes take place at the crust-mantle boundary or in the lower crust (Fig. 7). The amount of melt generated by mantle decompression and the rate of melt generation may have a strong influence on subsequent magma differentiation, anatexis and assimilation. Also, the composition of the lower crust which is affected by anatexis influences the physical characteristics of the resulting SiO₂-rich melts. For example, the H₂O content strongly influences both the degree of melting and melt viscosity. Thus, the size and type of the laccolith complex depends on physical processes in both the mantle and the lower crust.

The presence of a pluton ca. 3 km below the Donnersberg Laccolith Complex has been inferred from seismic sections (Haneke 1987). Similarly, the 230 km³ HLC displays a remarkably homogeneous composition (Romer et al. 2001), which could be explained best with the presence of a large magma chamber feeding the laccolith units. Thus, it appears that during evolution of the Late Palaeozoic European intra-continental strike slip systems mid- to upper crustal magma chambers formed which collected and homogenized the magma ascending from the lower crust. The size difference between the HLC on one hand and the Donnersberg and other Saar-Nahe rhyolitic complexes on the other (Table 1) is presumably related to the size of the mid-crustal magma chamber, which itself is controlled by lower crustal and mantle processes (see above). The site of this large magma store is constrained by numerous factors which include the level of neutral buoyancy, the magma driving pressure, the structural state of the crust, the stress field, the presence of fluids, and magma viscosity.

During renewed strike slip activity conduits open and tap the magma chamber. The timing of the tapping event relative to the cooling and crystallization of the magma chamber may vary. Apparently, the Donnersberg magma chamber was tapped early as inferred from the low phenocryst content of the laccolith units (3 to 9 vol %, Haneke 1987). Tapping of the chamber beneath the HLC presumably occurred late with respect to the state of its crystallization as

indicated by its high phenocryst content (Fig. 4d). The different phenocryst contents of the Halle laccolith units might either stem from simultaneous tapping of different levels of a magma chamber zoned according to phenocryst size and content, or from differing durations of ascent and emplacement. As a consequence, the presence of a mid- to upper crustal magma chamber is a prerequisite for the formation of the Donnerberg and Halle type laccolith complexes with their multi-feeder systems. Laccolith complex formation is restricted to the time lapse between the filling of the magma chamber and its advanced crystallization.

The viscous magma rises from the magma chamber through the sediments of the strike slip basin along conduits arranged in a spatial pattern determined by the array of intra-basinal faults. The intramontane basins such as Saar-Nahe, Saale, and Ilfeld contained a thick pile of un- to semi-consolidated sediments when intrusive activity commenced, so that magma emplacement might have been decoupled from the regional stress regime and largely controlled by neutral buoyancy. Perhaps, in the stress-coupled environment (e.g. in the NE German basin, see above) the formation of lavas prevails, in the stress decoupled environment it is laccoliths and sills.

The volatile-rich magma vesiculates in a depth of less than 4 km releasing H₂O and other volatiles into the unconsolidated sediments. Apparently, the rising magma batches which formed the Donnersberg Laccolith Complex possessed common physical properties since they are geochemically and texturally indistinguishable and emplaced in one stratigraphic level (Fig. 6d). In contrast, it is presumed that the emplacement of the geochemically homogeneous HLC into different levels of the sedimentary succession was controlled by different viscosities and densities caused by different phenocryst sizes and contents. Different amounts of microlites in the groundmass would cause similar or additional effects (Cashman et al. 1999: pahoehoe-Aa transition in basalts; Stevenson et al. 2001: effective viscosity as a function of microlite content in rhyolites). However, this cannot be verified in the case of the Halle samples.

Thus, it is speculated that the evolution of laccolith complexes in strike slip systems is controlled by a number of parameters, acting in different levels of the affected continental lithosphere. The presence of melts may also have a secondary feedback effect on the strike slip system by acting as a lubricant and, thus, enhancing tectonic activity. As such, they form part of the tectonic system and should be described and treated like tectonic objects such as faults and folds (Vigneresse 1999).

Conclusions

On the base of the authors' own and literature studies from Permocarboniferous strike slip systems in Central Europe, two types of laccolith complexes are defined with multi-feeder systems leading to large, closely spaced laccoliths (Donnersberg and Halle type). In the USA, basin and range tectonics with regional uplift, on the other hand, led to widely spaced laccolith complexes with single feeder systems and punch and Christmas tree geometries developing off the intersections of major regional tectonic lineaments. The evolution of the laccolith complexes is strongly dependent on the tectono-magmatic environment (Fig. 7). It appears that transtension in continental lithosphere controls all major phases of laccolith complex formation:

- Initial lithosphere-wide faulting provides pathways for magma ascent.
- Supracrustal pull-apart leads to the formation of a transtensional basin with a thick pile of unconsolidated sediments.
- Continued transtension gives way to decompressional melting of the mantle lithosphere and possibly the asthenosphere, especially, as it occurred in the Variscan orogen, if fertilized by previous magmatic activity. The mantle melts rise into the lower crust to differentiate, mingle, or cause anatexis.
- At mid- to upper crustal levels, the magmas form large magma chambers that are chemically homogenized and start to crystallize to a varying degree. These chambers are tapped during episodes of tectonic activity, necessarily before complete crystallization, and
- the resulting SiO₂-rich magmas ascend along major transtensional faults into the thick sedimentary basin fill, where vesiculation and de-volatilization of the magma takes place.

Conjugate intra-basinal faults (Riedel shears) provide a sieve-like system of pathways for magma ascent approximately in the upper 4 km of the crust, however, the stress field in the emplacement level might be uncoupled from the regional stress field. The amount of transtension and the amount of melt rising from the lithospheric mantle have a major influence on the type and size of the laccolith complex to be formed, as has the formation of

an upper crustal magma chamber. Laccolith complex evolution depends on local and regional conditions in the crust and the sedimentary basin it takes place in.

Acknowledgement

Many thanks to all the participants of the LASI workshop for an inspiring and successful meeting. Nick Petford and an anonymous reviewer are thanked for their reviews. These ideas were brought forward during a research grant from the Deutsche Forschungsgemeinschaft to CB (Grant: Br 997/18-1,2).

References

- Adiyaman, O. & Chorowicz, J. (2002): Late Cenozoic tectonics and volcanism in the northwestern corner of the Arabian Plate; a consequence of the strike-slip Dead Sea fault zone and the lateral escape of Anatolia. - *J. Volcan. Geotherm. Res.*, 117(3-4): 327-345.
- Aranguren, A., Tubia, J. M., Bouchez, J. L. & Vigneresse, J. L. (1996): The Guitiriz Granite, Variscan Belt of northern Spain; extension-controlled emplacement of magma during tectonic escape. - *Earth Planet. Sci. Lett.*, 139(1-2): 165-176.
- Arikas, K. (1986): Geochemie und Petrologie der permischen Rhyolithe in Südwestdeutschland (Saar-Nahe-Pfalz-Gebiet, Odenwald, Schwarzwald) und in den Vogesen. - *Pollichia-Buch*, 8, 321 S. Bad Dürkheim (Pfalzmuseum für Naturkunde).
- Arthaud, F. & Matte, P. (1977): Late Paleozoic strike-slip faulting in southern Europe and Northern Africa: results of right-lateral shear zone between the Appalachians and the Urals. - *Geol. Soc. Am. Bull.*, 88: 1305-1320.
- Arz, C. (1996): Origin and petrogenesis of igneous rocks from the Saar-Nahe-Basin (SW-Germany): Isotope, trace element and mineral chemistry. PhD, Bayerische Julius-Maximilians-Universität Würzburg.
- Asimov, P. D. (2000): Melting the Mantle. - *In*: Sigurdsson, H., Houghton, B. F., McNutt, S. R., Rymer, H. & Stix, J. (eds.) *Encyclopedia of Volcanoes*. London (Academic Press) 55-68.
- Benek, R., Kramer, W., McCann, T., Scheck, M., Negendank, J. F. W., Korich, D., Hübscher, H. D. & Bayer, U. (1996): Permo-Carboniferous magmatism of the Northeast German Basin. - *Tectonophysics*, 266: 379-404.

- Best, M. G. & Christiansen, E. H. (1997): Origin of broken phenocrysts in ash-flow tuffs. - *Geol. Soc. Am. Bull.*, 109: 63-73.
- Breitkreuz, C. & Kennedy, A. (1999): Magmatic flare-up at the Carboniferous/ Permian boundary in the NE German Basin revealed by SHRIMP zircon ages. - *Tectonophysics*, 302(3-4): 307-326.
- Breitkreuz, C. & Mock, A. (2001): Laccoliths in Cenozoic Western US and Permocarboneferous Europe: models and problems. *Tektonik & Magma*, Bautzen, Exkursionsführer und Veröffentlichungen der GGW, 30.
- Büchner, C. & Kunert, R. (1997): Pyroklastische Äquivalente der intrusiven Halleschen Rhyolithe. - *Mitt. Geol. Sachsen-Anhalt*, 3: 37-57.
- Busby, C. J. (2002): Climatic and tectonic controls on Jurassic intra-arc basins related to northward drift of North America. - *AAPG Bulletin*, 86(1): 197.
- Büthe, F. (1996): Struktur und Stoffbestand des Ifelder Beckens geodynamische Analyse einer intramontanen Rotliegend-Molasse. - *Braunschweiger Geowissenschaftliche Arbeiten*, 20, 119 S. Braunschweig (Technische Universität Braunschweig).
- Büthe, F. & Wachendorf, H. (1997): Die Rotliegend-Entwicklung des Ifelder Beckens und des Kyffhäusers: Pull-Apart-Becken und Rhomb-Horst. - *Zeitschrift für Geologische Wissenschaften*, 25(3/4): 291-306.
- Cashman, K. V., Thornber, C. & Kauahikaua, J. P. (1999): Cooling and crystallization of lava in open channels, and the transition of Pahoehoe Lava to 'A'a. - *Bull. Volcanol.*, 61(5): 306-323.
- Corry, C. E. (1988): Laccoliths; Mechanics of emplacement and growth. - *Geological Society of America Special Paper*, 220, 110 S. Boulder, Colorado (Geological Society of America).
- Eichelberger, J. C., Carrigan, C. R., Westrich, H. R. & Price, R. H. (1986): Non-explosive silicic volcanism. - *Nature*, 323: 598-602.
- Eisbacher, G. H. (1996): Einführung in die Tektonik. 374 S. Stuttgart (Enke).
- Fink, J. H. (1987): The Emplacement of Silicic Domes and Lava Flows. - *Spec. Pap. Geol. Soc. Amer.*, 212: 103-111.

Friedman, J. D. & Huffman, J., A. C. (1998): Laccolith complexes of southeastern Utah; time of emplacement and tectonic setting; workshop proceedings. - U. S. Geological Survey Bulletin, 292 S. Reston, Virginia (U. S. Geological Survey).

German-Stratigraphic-Commission (2002): Stratigraphic Table of Germany, Deutsche Stratigraphische Kommission.

Gilbert, G. K. (1877): Geology of the Henry Mountains, Utah. - U.S. Geographical and Geological Survey of the Rocky Mountain Region, 170 S. (U.S. Geographical and Geological Survey of the Rocky Mountain Region).

Haneke, J. (1987): Der Donnersberg. - Pollichia-Buch, 10, 147 S. Bad Dürkheim (Pfalzmuseum für Naturkunde).

Harry, D. L. & Leeman, W. P. (1995): Partial melting of melt metasomatized subcontinental mantle and the magma source potential of the lower lithosphere. - J. Geophys. Res., 100(B7): 10255-10269.

Hawkesworth, C., Turner, S., Gallagher, K., Hunter, A., Bradshaw, T., Rogers, N. (1995): Calc-alkaline magmatism, lithospheric thinning and extension in the Basin and Range. - J. Geophys. Res., 100(B7): 10271-10286.

Henk, A. (1997): Gravitational orogenic collapse vs plate-boundary stresses: a numerical modelling approach to the Permo-Carboniferous evolution of Central Europe. - Geol. Rundschau, 86(1): 39-55.

Henry, C. D., Kunk, M. J., Muehlberger, W. R. & McIntosh, W. C. (1997): Igneous evolution of a complex laccolith-caldera, the Solitario, Trans-Pecos Texas; implications for calderas and subjacent plutons. - Geol. Soc. Am. Bull., 109(8): 1036-1054.

Huffman, A. C., Jr. & Taylor, D. J. (1998): Relationship of basement faulting to laccolithic centers of southeastern Utah and vicinity. - *In*: Friedman, J. D. & Huffman, C. J. (eds.) Laccolith complexes of southeastern Utah; time of emplacement and tectonic setting; workshop proceedings. Reston, VA, United States (U. S. Geological Survey) U. S. Geological Survey Bulletin, 41-43.

Jackson, M. D. & Pollard, D. D. (1988): The laccolith-stock controversy; new results from the southern Henry Mountains, Utah. - Geol. Soc. Am. Bull., 100(1): 117-139.

- Jerram, D. A., Cheadle, M. J., Hunter, R. H. & Elliott, M. T. (1996): The spatial distribution of grains and crystals in rocks. - *Contrib. Mineral. Petrol.*, 125: 60-74.
- Johnson, A. M. & Pollard, D. D. (1973): Mechanics of growth of some laccolithic intrusions in the Henry Mountains, Utah; I, Field observations, Gilbert's model, physical properties and flow of the magma. - *Tectonophysics*, 18(3-4): 261-309.
- Kampe, A., Luge, J. & Schwab, M. (1965): Die Lagerungsverhältnisse in der nördlichen Umrandung des Löbejüner Porphyrs bei Halle (Saale). - *Geologie*, 14: 26-46.
- Kampe, A. & Remy, W. (1960): Mitteilungen zur Stratigraphie im Raume des Petersberges bei Halle. - *Montanwissenschaftliche Berichte - Deutsche Akademie der Wissenschaften, Berlin*, 2: 364-374.
- Kerr, A. D. & Pollard, D. D. (1998): Toward more realistic formulations for the analysis of laccoliths. - *J. Struct. Geol.*, 20(12): 1783-1793.
- Knoth, W., Kriebel, U., Radzinski, K.-H. & Thomae, M. (1998): Die geologischen Verhältnisse von Halle und Umgebung. - *Hall. Jb. Geowiss. B(Beiheft 4)*: 7-34.
- Kunert, R. (1978): Zur Platznahme rhyolithischer Laven. - *Zeitschrift für Geologische Wissenschaften*, 6(9): 1145-1160.
- Marx, J., Huebscher, H.-D., Hoth, K., Korich, D. & Kramer, W. (1995): Vulkanostratigraphie und Geochemie der Eruptivkomplexe. - *In: Plein, E. (eds.) Stratigraphie von Deutschland I - Norddeutsches Rotliegendbecken. Frankfurt (Courier Forsch. Senckenberg)* 54-83.
- Mock, A., Exner, M., Lange, D., Breitzkreuz, C., Schwab, M. & Ehling, B.-C. (1999): Räumliche Erfassung des Fließgefüges der kleinporphyrischen Lakkolithe im Halle-Vulkanit-Komplex. - *Mitt. Geol. Sachsen-Anhalt*, 5: 169-175.
- Mock, A., Jerram, D. A. & Breitzkreuz, C. (2003): Using quantitative textural analysis to understand the emplacement of shallow level rhyolitic laccoliths - a case study from the Halle volcanic complex, Germany. - *J. Petrol.*, 44(5): 833-849.
- Morgan, S. S., Law, R. D. & Nyman, M. W. (1998): Laccolith-like emplacement model for the Papoose Flat Pluton based on porphyroblast-matrix analysis. - *Geol. Soc. Am. Bull.*, 110(1): 96-110.

- Nickel, E., Kock, H. & Nungässer, W. (1967): Modellversuche zur Fließregelung in Graniten. - Schweiz. Mineral. Petrgraph. Mitt., 47: 399-497.
- Pollard, D. D. & Johnson, A. M. (1973): Mechanics of growth of some laccolithic intrusions in the Henry Mountains, Utah; II, Bending and failure of overburden layers and sill formation. - Tectonophysics, 18(3-4): 311-354.
- Reston, T. J. (1990): Shear in the lower crust during extension; not so pure and simple. - Tectonophysics, 173(1-4): 175-183.
- Roman Berdiel, T., Gapais, D. & Brun, J. P. (1995): Analogue models of laccolith formation. - J. Struct. Geol., 17(9): 1337-1346.
- Romer, R., Förster, H.-J. & Breitzkreuz, C. (2001): Intracontinental extensional magmatism with a subduction fingerprint: the late Carboniferous Halle Volcanic Complex (Germany). - Contrib. Mineral. Petrol., 141(1): 201-221.
- Schneider, J. W., Rössler, R. & Gaitzsch, B. (1994): Time lines of the Late Variscan volcanism - a holostratigraphic synthesis. - Zbl. Geol. Paläont., 5/6: 477-490.
- Schneider, J. W., Schretzenmayr, S. & Gaitzsch, B. (1998): Excursion Guide Rotliegend Reservoirs at the Margin of the Southern Permian Basin. - Leipzig. Geowiss., 7: 15-44.
- Schwab, M. (1962): Über die Inkohlung der Steinkohlen im Nördlichen Saaletrog bei Halle. - Geologie, 11(8): 917-942.
- Schwab, M. (1965): Tektonische Untersuchungen im Permokarbon nördlich von Halle/Saale. - Freiberg. Forschungsh., C139: 1-109.
- Stevenson, R. J., Dingwell, D. B., Bagdassarov, N. S. & Manley, C. R. (2001): Measurement and implication of "effective" viscosity for rhyolite flow emplacement. - Bull. Volcanol., 63(4): 227-237.
- Stollhofen, H., Frommherz, B. & Stanistreet, I. G. (1999): Volcanic rocks as discriminants in evaluating tectonic versus climatic control on depositional sequences, Permo-Carboniferous continental Saar-Nahe Basin. - In: Pedley, M. & Frostick, L. (eds.) Unravelling tectonic and climatic signals in sedimentary successions. London, United Kingdom (Geological Society of London) Journal of the Geological Society of London, 801-808.

Stollhofen, H. & Stanistreet, I. G. (1994): Interaction between bimodal volcanism, fluvial sedimentation and basin development in the Permo-Carboniferous Saar-Nahe Basin (south-west Germany). - *Basin Res.*, 6: 245-267.

Turcotte, D. L. & Schubert, G. (2002): *Geodynamics*. 456 S. Cambridge (Cambridge University Press).

Ventura, G. (1994): Tectonics, structural evolution and caldera formation on Vulcano Island (Aeolian Archipelago, southern Tyrrhenian Sea). - *J. Volcan. Geotherm. Res.*, 60(3-4): 207-224.

Vigneresse, J. L. (1999): Should felsic magmas be considered as tectonic objects, just like faults or folds? - *J. Struct. Geol.*, 21(8-9): 1125-1130.

Vigneresse, J. L., Tikoff, B. & Ameglio, L. (1999): Modification of the regional stress field by magma intrusion and formation of tabular granitic plutons. - *Tectonophysics*, 302(3-4): 203-224.

Ziegler, P. (1990): *Geological atlas of western and central Europe*. 1-239 S. Den Haag (Shell Internationale Petroleum Maatschappij).

Ziegler, P. A. & Stampfli, G. M. (2001): Late Palaeozoic-Early Mesozoic plate boundary reorganization: Collapse of the Variscan orogen and opening of neotethys. - *In*: Cassinis, G. (eds.) *Permian continental deposits of Europe and other areas. Regional and Correlations*. Brescia (Museo Civico di Scienze Naturali di Brescia) *Monografie di "Natura Bresciana"*, 17-34.

Part V

Inherited correlation in crystal size distribution: Comment and Reply

COMMENT

Helmut Schaeben*

K. Gerald van den Boogaart

Alexander Mock

Christoph Breitzkreuz

Institut für Geologie, TU Bergakademie Freiberg, Germany

The crystal size distribution model that is now in frequent use in the geosciences was first introduced by Marsh (1988) and by Cashman and Marsh (1988). In a recent paper, however, Pan (2001) questioned the validity of this model and concluded that there is an inherited correlation of $-3 \ln(L)$ versus L , which predominates, and which flaws the analysis to the extent that the parameters controlling crystal growth cannot be correctly inferred. In this comment we re-examine the mathematical treatment of Pan (2001) and find that his conclusions are erroneous, and thus that there are no new grounds to call into question the application of the crystal size distribution model.

Pan's (2001) concern is his equation 1 (p. 227)

$$n = \frac{w}{k_v \rho L^3 \Delta L}, \quad (1)$$

(Randolph and Larson, 1988) where w is mass per unit volume of the system, k_v is shape factor, ρ is density, L is average crystal size, and ΔL is window size, and the interpretation of equation 1 in terms of the crystal growth law (cf. Marsh, 1988 [p. 280, eq. 16]) is

$$n = n_0 \exp\left(-\frac{L}{G\tau}\right), \quad (2)$$

where n_0 is initial number of nuclei, G is growth rate, and τ average crystallization time. Rearranging equation 1 and substituting n according to equation 2 yields

$$w = nk_v \rho L^3 \Delta L = n_0 \exp\left(-\frac{L}{G\tau}\right) k_v \rho L^3 \Delta L \quad (3)$$

and reveals that the mass w per unit volume of the system actually depends on L , or, more specifically, on L and ΔL as L is binned according to the window size ΔL in practical applications. Thus, equation 1 correctly restated should be

$$n = \frac{w(L; \Delta L)}{k_v \rho L^3 \Delta L}. \quad (4)$$

The mass $w(L; \Delta L)$ per unit volume of the system is not the same for all size bins; if $w(L; \Delta L)$ was generally (almost) constant, then why should it be measured experimentally? Hence, according to the crystal growth law, equation 2, we derive the following

$$\begin{aligned} \ln(n) &= \ln\left(\frac{w(L; \Delta L)}{k_v \rho L^3 \Delta L}\right) = \ln\left(\frac{n_0 \exp\left(-\frac{1}{G\tau}\right) k_v \rho L^3 \Delta L}{k_v \rho L^3 \Delta L}\right) \\ &= \ln(n_0) - \frac{1}{G\tau} L \end{aligned} \quad (5)$$

and note that there is indeed a linear relationship in the $\ln(n)$ versus L plot. Equation 5 is the basis for the slope analysis to estimate the growth parameter $-1/G\tau$ since an $\ln(n)$ versus L scatter plot would provide this linear relationship between $\ln(n)$ and L .

Pan (2001) neglects the dependence $w = w(L; \Delta L)$ and is therefore incorrect in stating that the dominating term L^3 in equation 1 must be removed to allow for valid inferences regarding nucleation and growth, and that a new or additional (p. 230) relationship of crystal mass and shape to nucleation and growth is required for inferences to be valid (p. 227).

In this comment we demonstrate that Pan's (2001) examples and arguments are based upon the false assumption that the mass per unit volume, w , is (almost) constant, contradictory to equation 3, the corollary of the crystal growth law.

In the following, Pan (2001) correctly considered ρ , ΔL , and for the sake of simplicity, k_v , all to be constant (p. 227), and argued that w is the only term with significance for nucleation and growth (p. 227).

Following Pan (2001) and additionally assuming that $w(L; \Delta L) = w = \text{constant}$, then Pan's (2001) equation 1 can be rewritten as

$$n = \frac{w}{k_v \rho \Delta L} \frac{1}{L^3}$$

and after taking logarithms as

$$\ln(n) = \ln\left(\frac{w}{k_v \rho \Delta L}\right) - 3 \ln(L),$$

with slope

$$\frac{\partial \ln(n)}{\partial L} = -\frac{3}{L}.$$

This describes the sole dependence of the total number of crystals with respect to window size (i.e., the log density of crystals by number $\ln(n)$), upon the average crystal size L . Since w is assumed to be constant and therefore independent of L and ΔL , this dependence is logistically interpreted as the decrease of the log number density $\ln(n)$ with increasing average crystal size L .

Next, Pan (2001) models (p. 227) the mass $w = w(L; \Delta L)$ per unit volume of the system using an identical uniform distribution for each size bin independent of $(L; \Delta L)$. Now the expected mass per unit volume is constant, which is sufficient to cause a clear dependence of $\ln(n)$ on L ; the log number density $\ln(n)$ decreases with increasing average crystal size L , and the fit is better the smaller the standard deviation.

Pan's (2001) implicit false assumption of constant mass or constant expected mass per unit volume for each size bin leads to a false interpretation of the implication (in this case accurate) that the log number density $\ln(n)$ decreases solely with increasing average crystal size L (p. 228).

This situation basically remains the same as long as the expected mass per unit volume is constant and the variance is sufficiently small, e.g., for a normal distribution with sufficiently small standard deviation.

If this assumption is abandoned and $w = w(L; \Delta L)$ is considered, then

$$\ln(n) = \ln\left(\frac{w(L; \Delta L)}{k_v \rho \Delta L}\right) - 3 \ln(L)$$

and

*E-mail: schaeben@geo.tu-freiberg.de.

$$\frac{\partial \ln(n)}{\partial L} = \frac{\frac{\partial w(L; \Delta L)}{\partial L}}{w(L; \Delta L)} - \frac{3}{L}, \quad (6)$$

which is the slope of the “true” theoretical regression curve and which may be quite different from $-3/L$. For some mathematical functions $w(L; \Delta L)$ which may not necessarily be geologically reasonable, the slope may even be positive as Pan (2001) notices in case of an exponential dependence (p. 228). Nevertheless, the slope of an empirical regression curve $\ln(n)$ versus L still provides an estimation of the unknown “true” slope. Pan’s (2001) conclusion that the $\ln(n)$ versus L scatter plot “is primarily a size versus size plot” (p. 228) is therefore erroneous because the term $\ln w(L; \Delta L)/k_p \Delta L$ is involved in the relationship displayed in the $\ln(n)$ versus L scatter plot. The presence of the term $-3 \ln(L)$ does not put any limitations on the estimation of the slope of the empirical regression curve. The mathematical problem remains to estimate $G\tau$ without bias from equation 6 or its estimation, if the variability (error) of $w(L; \Delta L)$ is large and the correlation in the $\ln(n)$ versus L plot is poor, but this is beyond the scope of this comment.

Thus, Pan’s (2001) conclusion that $-1/G\tau$ cannot be inferred from the $\ln(n)$ versus L scatter plot arises as follows: If crystal growth does not behave according to the crystal growth law, equation 2, but according to $w(L; \Delta L) = \text{constant}$, then the plot $\ln(n)$ versus L actually displays $-3 \ln(L)$ versus L and the unknown parameter $-1/G\tau$ of equation 2 cannot be estimated; or, more emphatically, if the crystal growth law really was $w(L; \Delta L) = \text{constant}$, then the $\ln(n)$ versus L plot would reduce to a $-3 \ln(L)$ versus L plot and would therefore be useless.

However, Pan’s (2001) arguments do not stand when the crystal growth law given by equation 2 is valid. Then the mass $w(L; \Delta L)$ depends explicitly on L as given in equation 3 and the parameter $-1/G\tau$ can be estimated from the slope of the curve in the $\ln(n)$ versus L plot as indicated by equation 5.

In conclusion, the objections raised by Pan (2001) are mathematically unsound and do not call into question crystal size distribution theory and its current practical applications. This is no doubt reassuring for those using the crystal size distribution theory, and who were perhaps troubled by the apparently grave implications of the Pan (2001) paper.

ACKNOWLEDGMENT

The authors would like to thank Michael Edwards, Freiberg, Germany, for his help with the English language.

REFERENCES CITED

- Cashman, K.V., and Marsh, B.D., 1988, CSD (crystal size distribution) in rocks and the kinetics and dynamics of crystallization. II: Makaopuhi lava lake: *Contributions to Mineralogy and Petrology*, v. 99, p. 292–305.
- Marsh, B.D., 1988, CSD (crystal size distribution) in rocks and the kinetics and dynamics of crystallization. I. Theory: *Contributions to Mineralogy and Petrology*, v. 99, 277–291.
- Randolph, A.C., and Larson, M.A., 1988, *Theory of particulate processes* (second edition): New York, Academic Press, 369 p.
- Pan, Y., 2001, Inherited correlation in crystal size distribution: *Geology*, v. 29, p. 227–230.